FutureWater

Water Availability Analysis for the Upper Indus, Ganges, Brahmaputra, Salween and Mekong River Basins

Final Report

September 2013

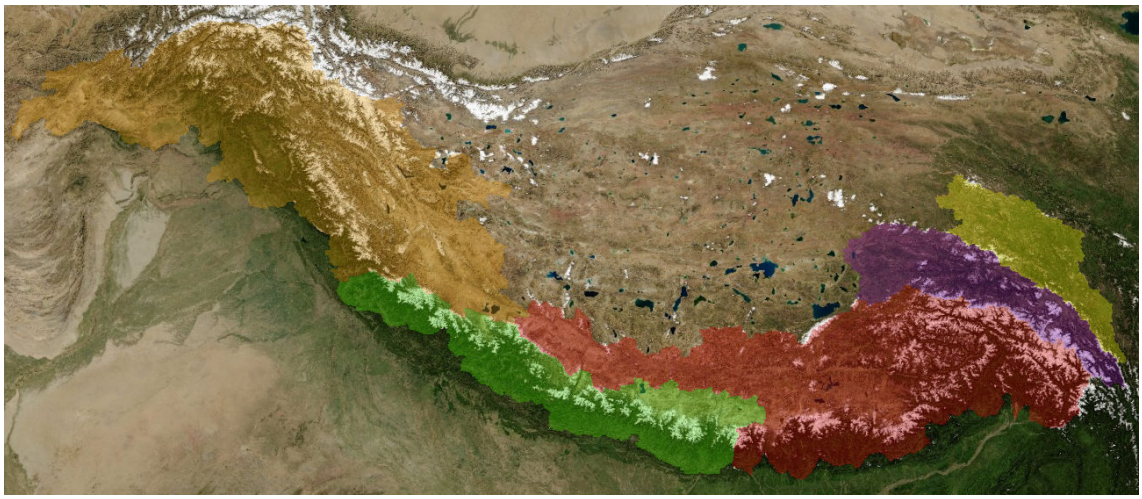

Authors
A.F. Lutz, MSc
Dr. W.W. Immerzeel

Client
International Centre for Integrated Mountain Development (ICIMOD)

Report FutureWater: 127

Water Availability Analysis for the Upper Indus, Ganges, Brahmaputra, Salween and Mekong River Basins

Final Report

September 2013

Authors
A.F. Lutz, MSc
Dr. W.W. Immerzeel

Client
International Centre for Integrated Mountain Development (ICIMOD)

Report FutureWater: 127

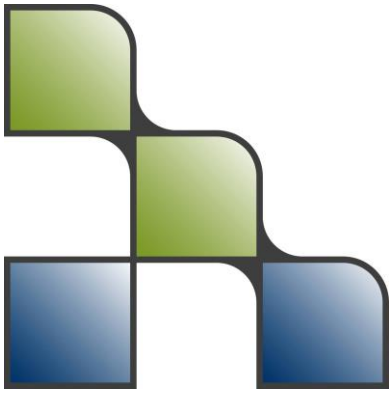

FutureWater
Costerweg 1V
6702 AA Wageningen
The Netherlands

+31 (0)317 460050

info@futurewater.nl

www.futurewater.nl

Preface

ICIMOD is the implementing agency for the Himalayan Climate Change Adaptation Programme (HICAP) that runs from January 2011 to December 2015. HICAP addresses climate change adaptation challenges across different related disciplines such as water resources, ecosystem services, food security, vulnerability and gender. Part of the project is related to the generation of water availability scenarios from upstream river basins that are primarily characterized by snow and glacial melt. ICIMOD has contracted FutureWater to generate these scenarios based on a high resolution hydrological model that FutureWater has developed. The project runs from January 2012 until July 2013. This final report describes the tasks performed by FutureWater, including results of the hydrological modeling.

Dr. W.W. Immerzeel
A.F. Lutz MSc.
Wageningen, September 2013

Summary

ICIMOD is the implementing agency for the Himalayan Climate Change Adaptation Programme (HICAP). This assignment relates to component 2 of the HICAP on Water Availability and Demand Scenarios. With the overall goal to improve our knowledgebase on climate change impact on water availability and demand in the upper parts of the Indus, Ganges and Brahmaputra basins, the specific objectives of the this study are to:

1) Assess climate change scenarios and develop water availability scenarios corresponding to base and future climate scenarios at sub-basin and catchment scales in the three basins;
2) Improve our understanding of the partitioning of runoff contribution from different natural sources (snow, glacier, rainfall and base flow);
3) Detailed analysis of uncertainty of water availability scenarios and assessment of hydropower potential for three pilot catchments.

The key findings regarding runoff composition and future runoff (per basin) are:

- In the upper Indus, stream flow is dominated by glacier melt (~41%) and snow melt (~22%). Rainfall-runoff has minor importance (~27%). Total runoff is likely to change by -5% to +12% by 2050. The share of melt water stays the same, and the changes in total runoff are directly related to changes in precipitation.
- In the upper Ganges, stream flow is dominated by rainfall-runoff (~66%), with ~20% of stream flow contributed by melt water. It is likely that total runoff increases by ~1-27% by 2050. The share of melt water is decreasing and the share of rainfall-runoff in total runoff is increasing.
- The stream flow in the upper Brahmaputra is dominated rainfall-runoff (~59%), and melt water contributes ~25% to total runoff. It is likely that total runoff increases by 2050 (0% to +13%). The share of melt water is decreasing while the share of rainfall-runoff increases.
- In the upper Salween, runoff is dominated by rainfall runoff (~42%), but snow melt is also important (~28%). Glacier melt contributes ~8% to total runoff. It is likely that total runoff changes by -3% to +19% by 2050. The share of glacier melt and snow melt is likely to decrease, while the share rainfall-runoff increases.
- The runoff in the upper Mekong is dominated by rainfall-runoff (44%). Snow melt contributes ~33% and glacier melt contributes ~1% to total runoff. It is likely that the total runoff increases ~2-20% by 2050. The share of melt water is decreasing while the share of rainfall-runoff increases.

A first order assessment of the hydropower potential in the Chitral, Lhasa, Dudh Koshi and Tama Koshi catchments leads to the following conclusions:

- The Chitral catchment has a hydropower potential of ~2350 GWh/yr in the current situation. A projected change to ~2100-2450 GWh/yr is projected for 2041-2050.
- The Lhasa catchment has ~2650 GWh/yr hydropower potential in the current situation. This is expected to stay the same or decrease to ~2650-2150 GWh/yr by 2041-2050.
- The Dudh Koshi and Tama Koshi catchments currently have a hydropower potential of ~1000 GWh/yr each. Future projections suggest that this might decrease by ~0-10% until 2050.

Table of contents

Tables

Figures

1 Introduction

1.1 Himalayan Climate Change Adaptation Programme (HICAP)

The Hindu Kush-Himalayan (HKH) region is highly dynamic as there are many socioeconomic and environmental drivers of change at play, including climate change. The impacts of these changes challenge the resilience of natural and human capacities and environments in the region. Climate change is believed to contribute to extreme weather events and possibly to increase the frequency and magnitude of natural hazards and associated disasters, exacting high economic and social costs. Recent studies have shown that the Himalayan region and the downstream areas that depend on its water supply and ecosystem services, including the Indo-Gangetic plain – 'the grain basket of South Asia' – are particularly vulnerable to climate change.

HICAP's goal is to contribute to enhancement of resilience of mountain communities, particularly women, through improved understanding of vulnerabilities, opportunities, and potentials for adaptation. Women are more vulnerable than men to climate change as they face more social, economic, and political barriers limiting their coping capacity. However, women's responsibilities in households and communities, and as stewards of natural and household resources, position them well to contribute to strategies for adaptation to changing climate and environment.

At the sixteenth Conference of the Parties (COP16) to the United Nations Framework Convention on Climate Change (UNFCCC) in Cancun, Mexico, the Ministry of Foreign Affairs (MFA) Norway announced its support to ICIMOD, the Center for International Climate and Environment Research – Oslo (CICERO), and UNEP/GRID-Arendal to help the Himalayas in view of the rapidly melting glaciers and the need for people to prepare for the challenges of the future. A series of consultations with these and other strategic and operational partners from the region and beyond culminated in the creation of the Himalayan Climate Change Adaptation Programme (HICAP).

Based on the Himalayan Climate Change Impact and Adaptation Assessment (HICIA) feasibility study, additional scoping studies of the Eastern Himalayas, and consultations with strategic partners, seven components were identified to generate policy-relevant knowledge of climate change impacts on natural resources and ecosystem services, and on the communities depending on these resources and services. These seven components are:

1. Climate change scenarios
2. Water availability and demand scenarios
3. Ecosystem services
4. Food security
5. Vulnerability and adaptation
6. Women in adaptation
7. Communications and outreach

HICAP's major objectives are:

- to reduce uncertainty through development of downscaled and customised climate scenarios as well as water availability and demand scenarios for parts of major river basins such as the Indus, Brahmaputra and Ganges;
- to develop knowledge and enhance capacities to assess, monitor, and communicate the impacts of and responses to climate change on natural and socioeconomic environments at local, national, and regional levels;
- to make concrete and actionable proposals for strategies and policies, considering vulnerabilities, opportunities, and potentials for adaptation, with particular reference to strengthening the role of women and local communities.

1.2 Objectives

This assignment relates to component 2 of the HICAP on Water Availability and Demand Scenarios. With the overall goal to improve our knowledgebase on climate change impact on water availability and demand in the upper parts of the Indus, Ganges and Brahmaputra basins, the specific objectives of the proposed study are to:

- Assess climate change scenarios and develop water availability scenarios corresponding to base and future climate scenarios at sub-basin and catchment scales in the three basins;
- Improve our understanding of the partitioning of runoff contribution from different natural sources (snow, glacier, rainfall and base flow);
- Detailed analysis of uncertainty of water availability scenarios and assessment of hydropower potential for three pilot catchments.

This report provides a detailed account of the methodology used and the results.

2 Spatial Extent and Time Frame

Figure 1 shows the extent of the upstream river basins of the Indus, Ganges, Brahmaputra, Salween and Mekong. The hydrological model is set up for these basins. The upper Indus basin covers an area of 437201 km^2, the upper Ganges covers an area of 169162 km^2, the upper Brahmaputra covers an area of 372664 km^2, the upper Salween covers an area of 103497 km^2 and the upper Mekong covers an area of 77696 km^2. The model spatial resolution is 1 km^2 and temporal resolution is one day.

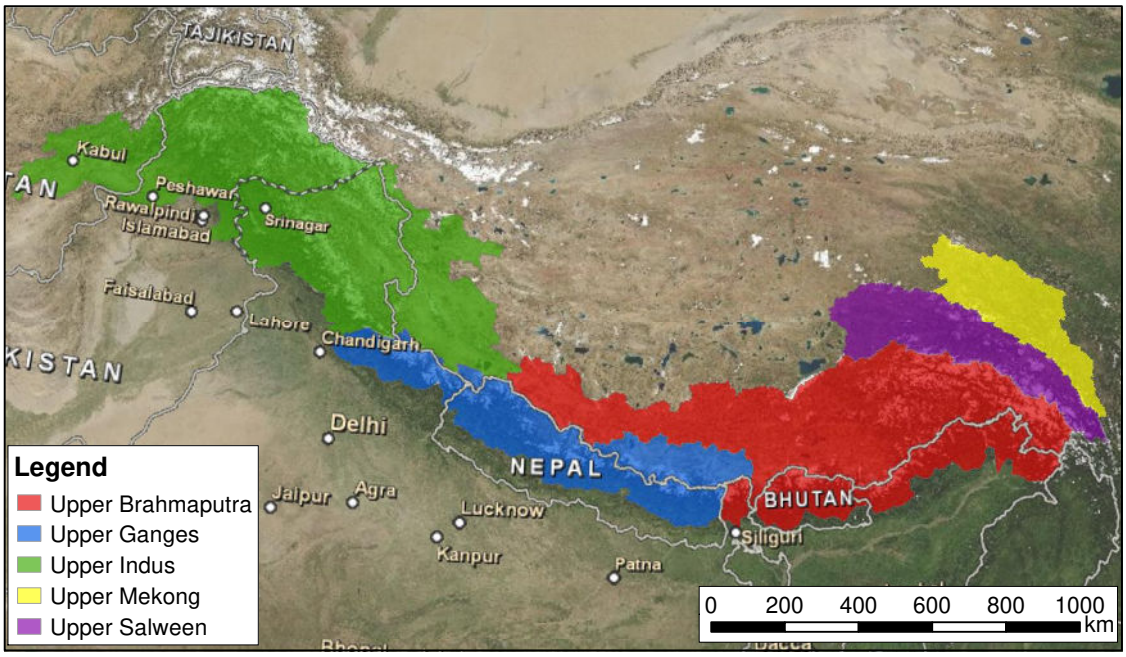

Figure 1: Overview upstream basin boundaries of the Indus, Ganges, Brahmaputra, Salween and Mekong river basins

In Figure 2 detailed maps are presented for the upper Indus, Ganges and Brahmaputra including the location of three catchments where detailed analysis has been conducted. These catchments are the Chitral catchment (22746 km^2), the Tama and Dudh Kosi catchment (13920 km^2) and Lhasa catchment (32589 km^2). These catchment scale analysis are done using the same model as for the entire upper basins but with a specific focus on uncertainty analysis of the water availability scenarios and on hydropower potential.

We distinguish a historic reference period spanning the period from 1998 until 2007 and this period is used as calibration period. This period is further referred to as reference period. Climate change impact is assessed from 2008 until 2050. All simulations are conducted with a daily time step.

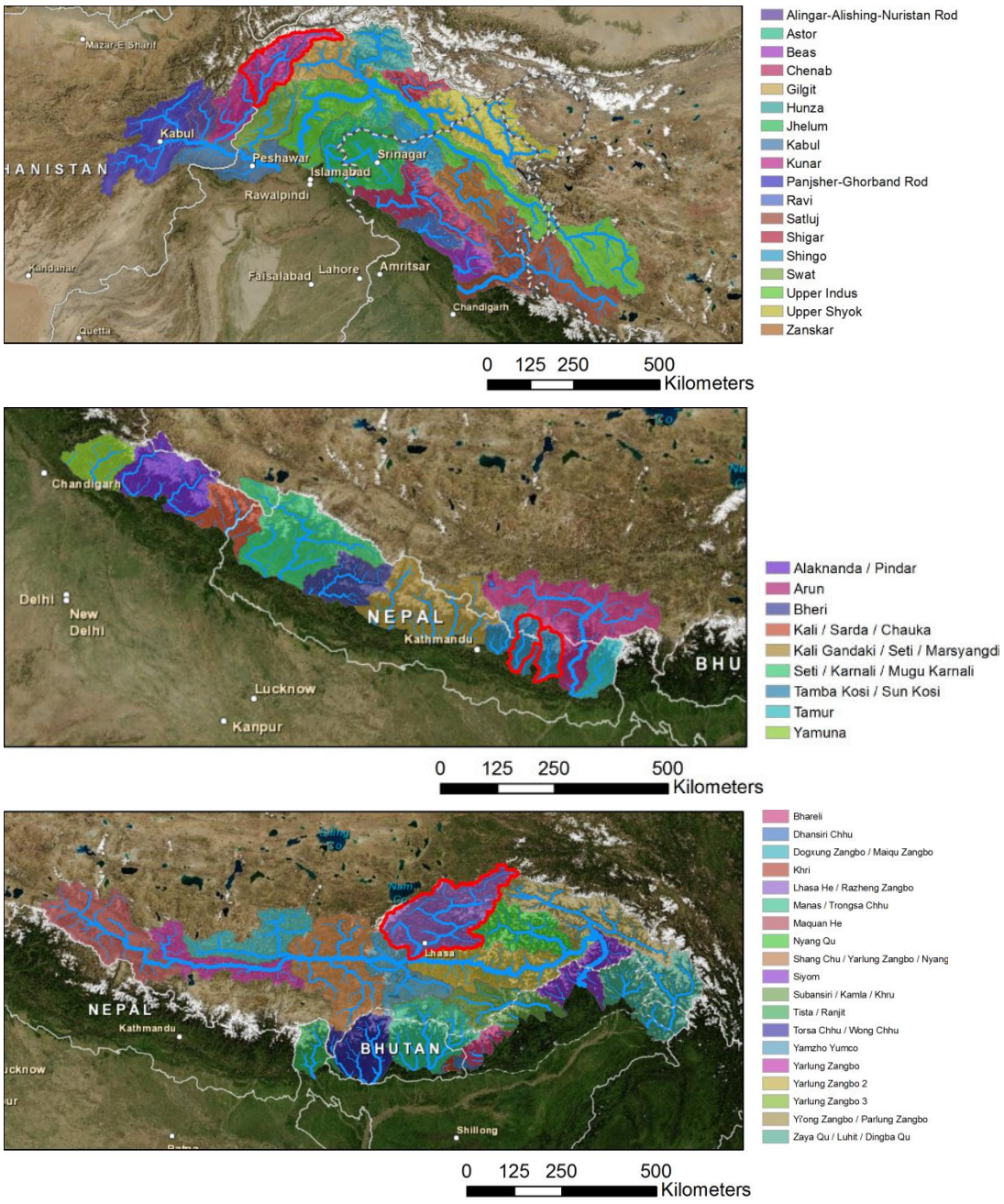

Figure 2: Detailed maps of the upstream river basins of the Indus (top), Ganges (middle) and Brahmaputra (bottom) including sub-basin boundaries and river network. Highlighted in red are the catchments where detailed analysis is conducted (Chitral for Indus, Dudh and Tama Kosi for Ganges and Lhasa river for the Brahmaputra).

3 Description of the Model

3.1 Himalaya Spatial Processes in Hydrology model (HI-SPHY)

In this project FutureWater's Spatial Processes in Hydrology (SPHY) model is used. New components were designed for this project, hence this version of the model is entitled Himalaya Spatial Processes in Hydrology (HI-SPHY). The HI-SPHY model is a raster based highly detailed full distributed cryospheric- hydrological model. The model is based on commonly accepted standards from multiple proven hydrological models and the approach is based on [*Immerzeel et al.*, 2010]. HI-SPHY is created in PCRaster environmental modelling software [*Karssenberg et al.*, 2001]. PCRaster is a spatio-temporal environmental modelling language developed at Utrecht University, the Netherlands. The model runs at 1 x 1 km spatial resolution with daily time steps and incorporates all major hydrological processes as well as cryospheric processes.

The actual runoff which is calculated for each grid cell consists of four contributing factors. These are: runoff originating from rain, runoff originating from snow melt, runoff originating from glacial melt, and base flow, as visualized in Figure 3. With the daily air temperature and daily precipitation per grid cell as input the model evaluates how much precipitation falls and it is disaggregated into either snow or rain based on the air temperature distribution. The model evaluates the amount of glacier melt and snow melt or accumulation and which part of snow and glacier melt is directly transformed to runoff and which part refreezes. Rainfall-runoff processes are evaluated in a soil component in the model. The runoff from all contributing components is routed through the system using the DEM.

Each grid cell is divided in fractions. If a cell is (partly) glacierized, the cell has a glacier fraction between 0 and 1 (0: no glacier cover, 1: complete glacier cover). The other fraction of the grid cell can be either 'snow' or 'rain'. This depends on the presence of snow cover, which is determined by the model. As long as snow cover is present, the snow module is active, while the rain module is active when no snow cover is present.

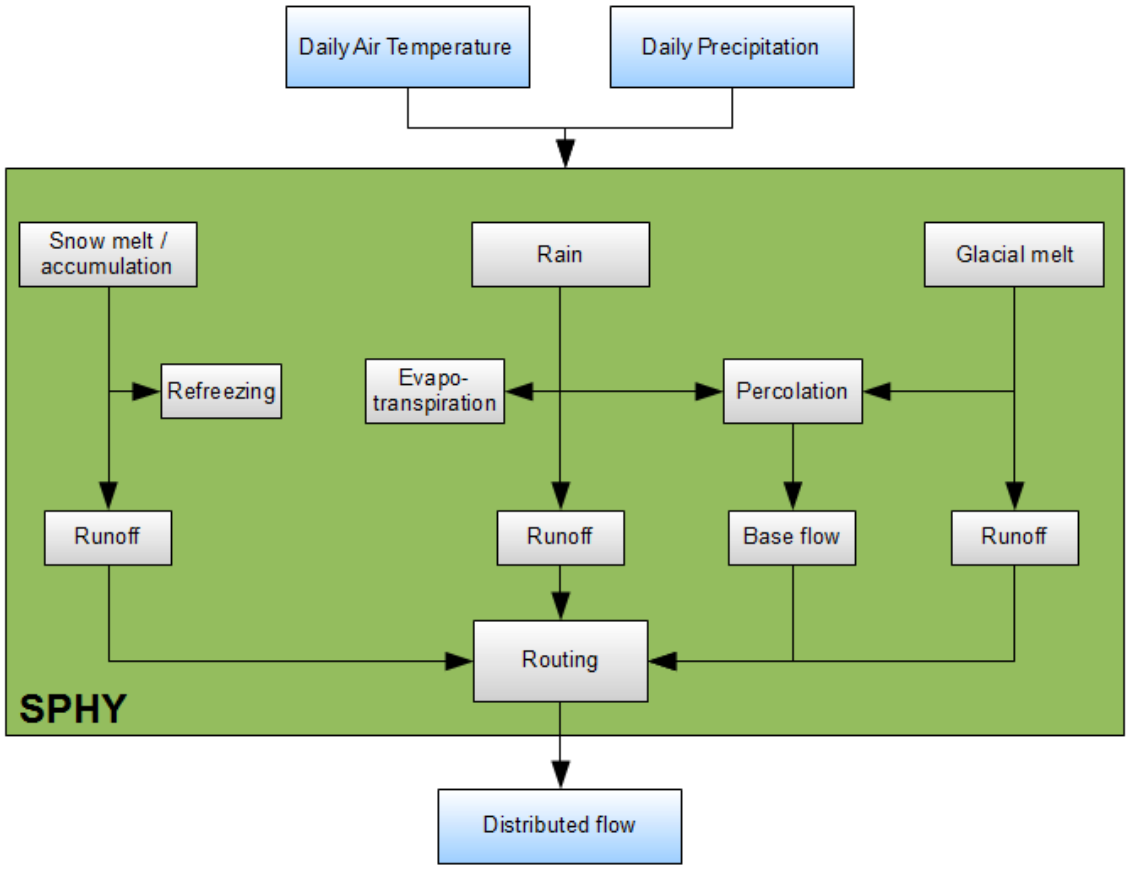

Figure 3: Model structure of SPHY model

3.2 Cryospheric processes

The initial glacier cover is derived from the recently completed inventory by ICIMOD [*Bajracharya and Shrestha*, 2011]. With this dataset the initial glacierised fraction of each grid cell is calculated. Since the model is set up for a 1 x 1 km resolution, the ice cover is described as a fraction varying from 0 (no glacial cover) to 1 (100% glacial cover). In this way, 1 x 1 km grid cells which are partly covered with ice can be simulated. A differentiation is made between clean ice glaciers and debris covered glaciers. Glaciers at lower altitude tend to have more debris cover because of the cumulative accumulation of debris from higher grounds and glacier parts with a small slope have more debris cover compared to steep-sloped parts of the glacier. The differentiation between clean ice glaciers and debris covered glaciers is then re-calculated to fractions of the 1 x 1 km grid cells used in the model. Summing the fractions of clean ice glacier and debris covered glacier will always result in a total fraction of one.

Initial conditions for snow cover are obtained directly from the model. A model run is done simulating several years to develop a balanced snow cover. The snow cover at the end of this model run is used as initial snow cover for further model runs. In the model calculations, the amounts of ice and snow are described as millimeters water equivalent. The modelling of processes involving glaciers is described in a schematic way in Figure 4. Melt from clean ice glaciers is defined as the air temperature (if above 0 °C) multiplied by the degree day factor for clean ice, multiplied by the clean ice fraction of the glacier cover and the cell fraction with glacier cover.

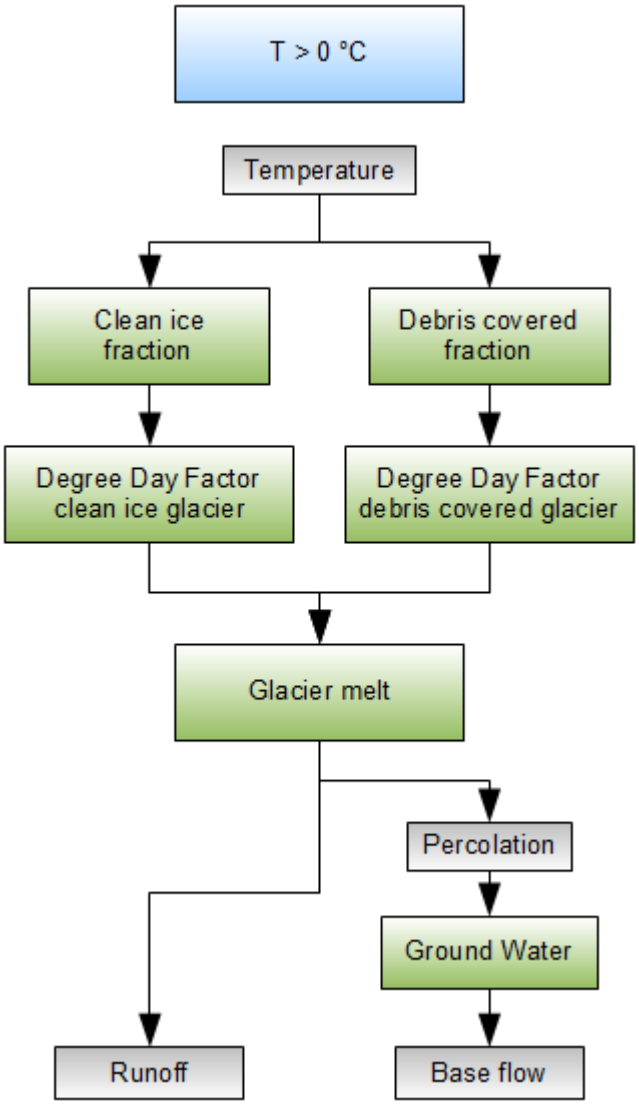

Figure 4: Schematic representation glacier related processes in the HI-SPHY model

For the melt from debris covered glaciers the calculation is similar, although a different degree day factor for debris covered glaciers is specified. Melt rates for debris covered glaciers are lower, since the energy fluxes are partly blocked by the (thick) debris cover.

Degree Day Modeling
The use of temperature index or degree day models is widespread in cryospheric models to estimate ice and snow melt. In these models an empirical relationship between melt and air temperature based on a frequently observed correlation between the two quantities is assumed [*Hock*, 2005]. Degree-day models are easier to set up compared to energy-balance models, and only require air temperature, which is mostly available and relatively easy to interpolate.

The total glacier melt is then calculated by summing the two components from clean ice glacier melt and debris covered glacier melt. A part of glacial melt comes to runoff, while another part percolates to the ground water. This process is controlled by adjusting the glacial runoff factor.

For each cell the model determines if precipitation falls as snow or rain by comparing the actual air temperature to a critical temperature. When air temperature is below or equal to the critical

temperature, precipitation will fall as snow. When air temperature is above the critical temperature, precipitation will fall as rain.

In the model a differentiation is made between the potential snow melt and the actual snow melt (Figure 5). The potential snow melt is defined as the air temperature (if above 0 °C) multiplied by a degree day factor for snow multiplied by the cell fraction covered with snow. The actual snow melt however, is limited by the thickness of the snow pack. No more snow can be melted than the amount of snow which is available at the considered time step. The snow storage is then updated, to be used for the next time step. The snow storage is updated by subtracting the melt and/or adding the freshly fallen snow or rain to the water storage in the snow pack. The updated snow storage is the 'old' snow storage with the fresh snow added and the actual snow melt subtracted.

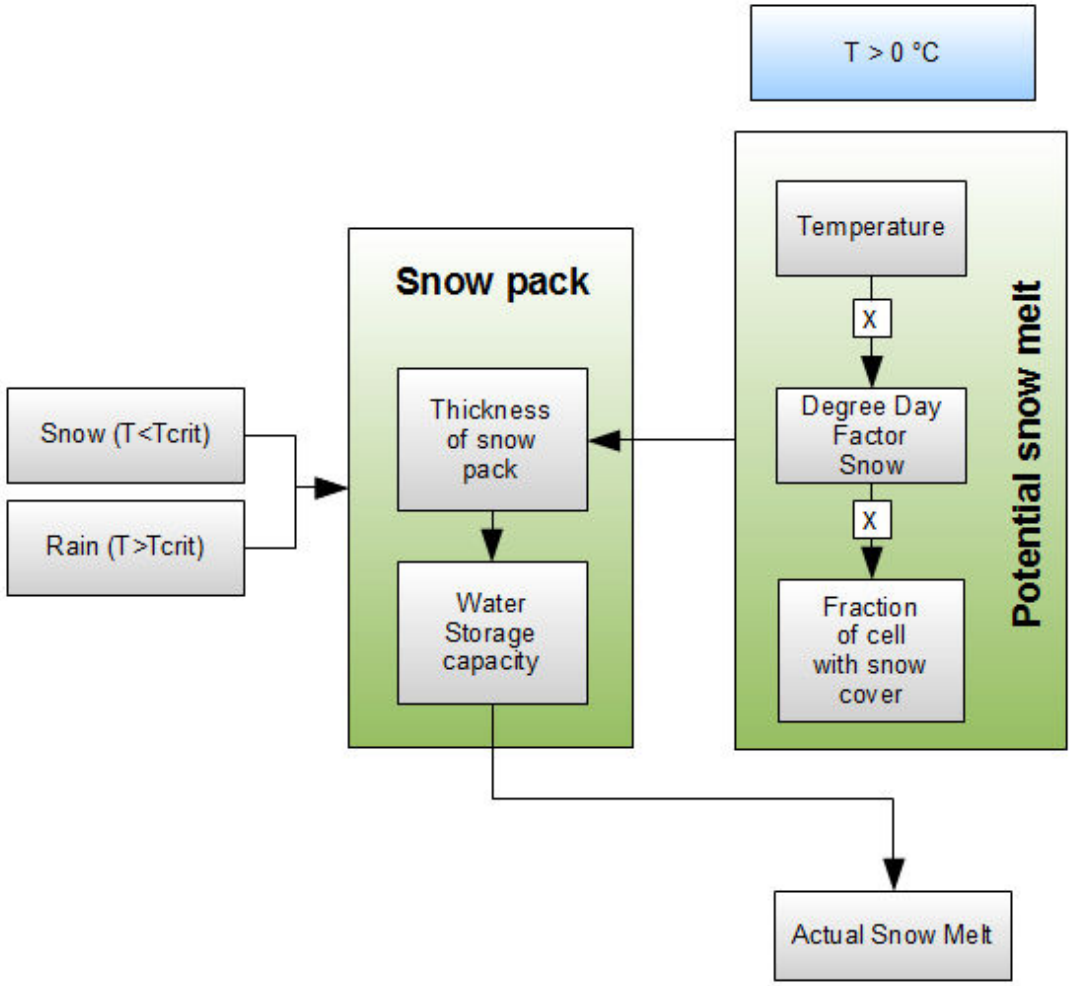

Figure 5 Schematic representation of snow related processes in the HI-SPHY model

The water resulting from snow melt will partially refreeze as it infiltrates the underlying snow pack. The maximum amount of water that can refreeze is defined by the water storage capacity of the snow pack which depends on the thickness of the snow pack present and the storage capacity of snow (e.g. the total millimeters of melt water that can refreeze per millimeter of snow). The actual amount of water that is stored in the snow pack is defined as the water stored in the snow pack during the previous time step summed by the actual snow melt. Snow melt will become actual snow melt when the amount of snow melt exceeds the water storage capacity of the snow pack. When all snow in a grid cell has melted, the snow fraction is set to zero. If snow

falls on a cell which had no snow during the previous time step the snow fraction is updated to 1.

3.3 Rainfall runoff

The modelling steps for rainfall in the HI-SPHY model are represented in Figure 6. Precipitation in the model will fall as rain when the air temperature is above a critical temperature.

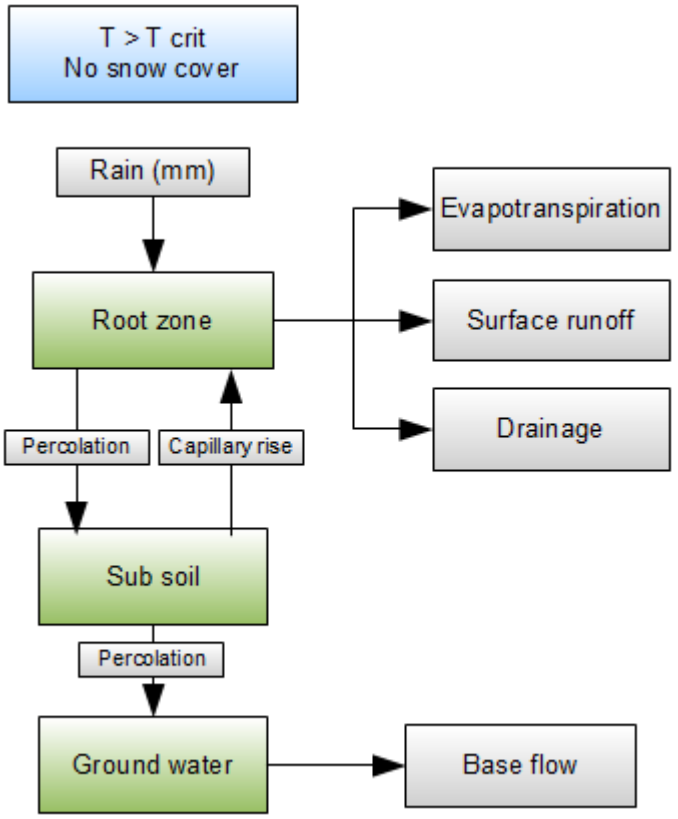

Figure 6: Schematic representation of rainfall-runoff modelling in the HI-SPHY model

A soil module based on the saturation excess overland flow (also known as Hewlettian runoff) concept is incorporated in the HI-SPHY model. The soil layer in the model is divided in a root zone and a sub soil. The thickness of the soil is slope dependent in the model. The soil properties are based on pedotransfer functions, to quantify soil properties for different soil types. The soil properties used in the HI-SPHY model are listed in Table 1. Using these properties, the model evaluates how much water in the rootzone is available for evapotranspiration, surface runoff, lateral drainage and percolation/capillary rise to/from the subsoil.

Table 1: Soil properties used in HI-SPHY model.

Rootzone	Subsoil
Rooting depth (mm)	Subsoil depth (mm)
Saturated water content (mm/mm)	Saturated water content (mm/mm)
Field capacity (mm/mm)	Field capacity (mm/mm)
Wilting point (mm/mm)	Saturated conductivity (mm/day)
Permanent wilting point (mm/mm)	
Saturated conductivity (mm/day)	

The potential evapotranspiration (ET_{pot}) in the model is calculated using the reference evapotranspiration (ET_{ref}) and a crop coefficient (K_c):

$$ET_{pot} = ET_{ref} \cdot K_c$$

The reference evapotranspiration is calculated according to the Modified Hargreaves method [*Droogers and Allen*, 2002]. This method requires average, maximum and minimum air temperature (T_{avg}, T_{max}, T_{min}), the summed precipitation (P) and incoming extraterrestrial radiation (Ra):

$$ET_{ref} = 0.0013 \cdot 0.408Ra \cdot (T_{avg} + 17.0) \cdot ((T_{max}\text{-}T_{min}) - 0.0123P)^{0.76}$$

Based on land use type, each grid cell is assigned a K_c factor to calculate the potential evapotranspiration. The actual evapotranspiration (ET_{act}) is the potential evapotranspiration limited by the water available in the rootzone (e.g. the saturation of the root zone).

Excess water is also leaving the rootzone as surface runoff, lateral drainage or percolation to the sub soil. The occurrence of capillary rise from the sub soil to the root zone or percolation from the root zone to the sub soil depends on differences in water saturation of both soil layers. Water percolates from the sub soil to the ground water.

At the moment a 'rain fraction' is covered with snow, it switches to 'snow fraction'. As long as snow cover is present, the snow module (described in section 3.2) is active. However, the soil component remains active, although no more precipitation is entering the soil and no more water is leaving the soil as surface runoff or evapotranspiration. Percolation to the subsoil and eventually to the ground water remains active.

3.4 Ground water

A ground water reservoir generating base flow is incorporated in the model. During periods with low runoff the streams are fed by processes such as sustained ground water flow and/or slow throughflow through the deeper soil from earlier precipitation events. This is referred to as base flow. The ground water reservoir is active for each entire grid cell. The ground water is fed by percolation from the sub soil and percolation from the glacier fraction of a cell. These two components provide recharge to the ground water reservoir. The ground water recharge is translated into baseflow released from the reservoir with a certain time lag.

3.5 Routing

In the model, the generated runoff is routed through the basin according to a flow direction map based on the DEM. For each cell the local drain direction is defined. The runoff generated per grid cell accumulates with runoff generated in downstream grid cells. Using a linear regression with a regression constant, the time water needs to flow through the reservoir towards the outflow point is simulated.

4 Model Input Data and Preprocessing

4.1 Digital elevation model

We use the NASA Shuttle Radar Topography Mission SRTM digital elevation model that has been corrected to represent drainage patterns consistently for the HydroSHEDS[1] database. HydroSHEDS is a mapping product that provides hydrographic information for regional and global-scale applications in a consistent format. It offers a suite of geo-referenced data sets (vector and raster) at various scales, including river networks, watershed boundaries, drainage directions, and flow accumulations. Figure 7 shows the HydroSHEDS DEM for the model domain at the model resolution (1 km^2) including major streams.

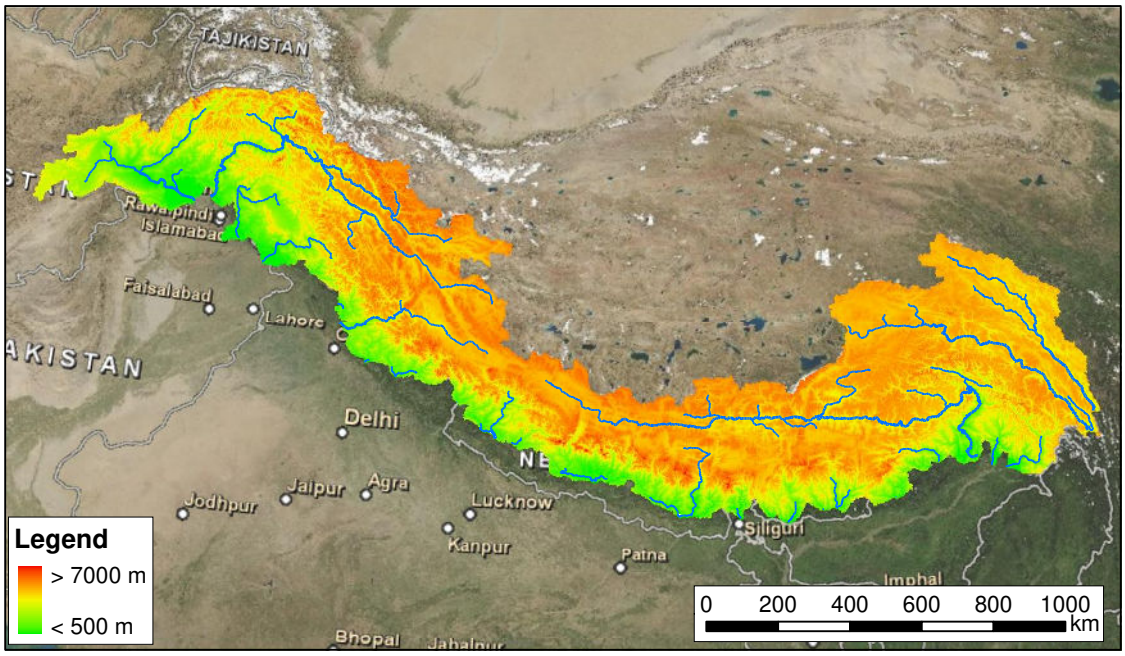

Figure 7: HydroSHEDS DEM for model domain.

4.2 Precipitation data

For the reference period (1998-2007) daily precipitation data are required for the HI-SPHY model. We use the gridded APHRODITE product for daily precipitation input [*Yatagai et al.*, 2012]. APHRODITE is based on rain gauge data and is available at 0.25 x 0.25° spatial resolution and daily temporal resolution. A recent study comparing the TRMM product and the APHRODITE product for estimations of precipitation over Nepal showed that APHRODITE provides more accurate data [*Duncan and Biggs*, 2012]. However, the uncertainty in precipitation forcing datasets remains for the Himalaya remains large [*Palazzi et al.*, 2013], especially for the Karakoram region. The precipitation grids were resampled to model resolution (1 km^2) applying a spline interpolation. In this way an input map series consisting of 3652 precipitation grids was generated. Figure 8 shows the average annual precipitation during the

[1] http://hydrosheds.cr.usgs.gov/

reference period for the model domain and the coefficient of variation (standard deviation of 10 years divided by the average annual precipitation).

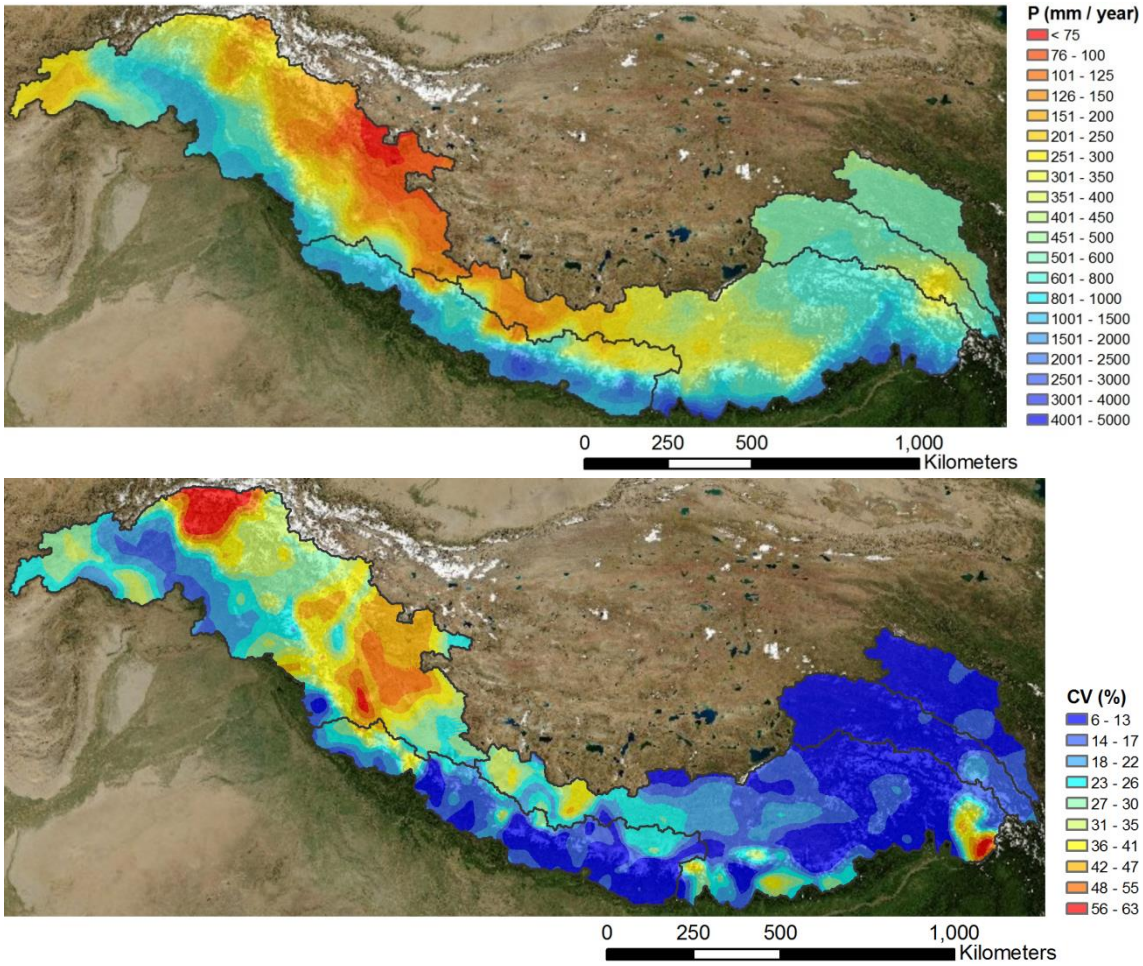

Figure 8: Average annual precipitation and covariance of precipitation for reference period (1998-2007).

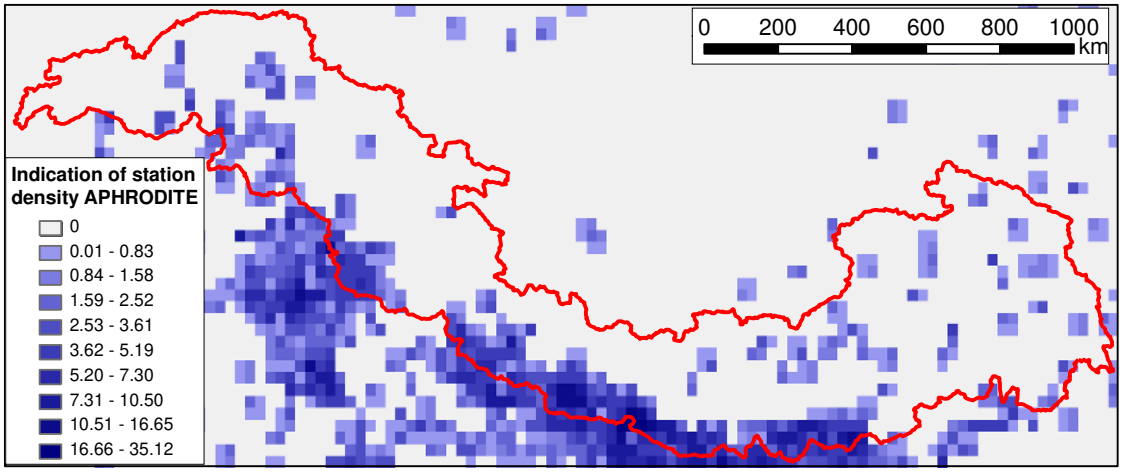

Figure 9: Station density in APHRODITE product. The indicator value is the proportion of 0.05° grid cells with at least one station within a 0.5° grid cell.

Figure 9 shows the spread of APHRODITE stations over the model domain. The large variation in station density over the model domain leads to varying accuracy of the model forcing for precipitation. We validated APHRODITE precipitation data to station data for observed precipitation. Station data were provided by ICIMOD. Five stations spread geographically over the model's horizontal and vertical domain were selected for validation (Figure 10).

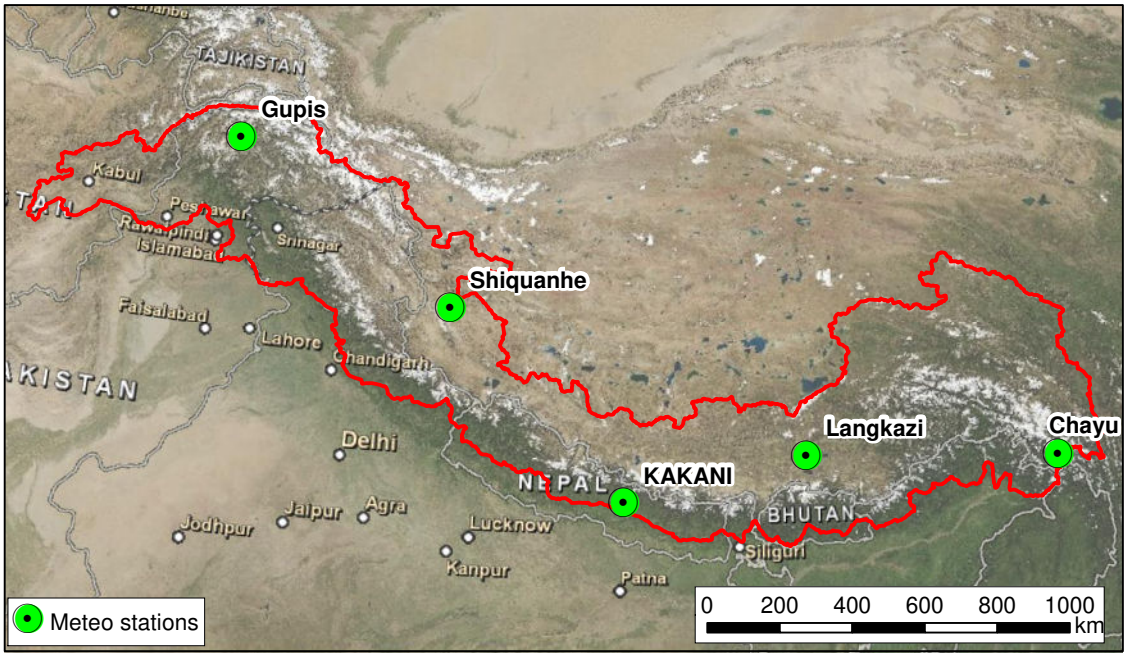

Figure 10: Selected meteo stations for validation of temperature and precipitation products.

Figure 11 shows the measured station data and the data from the APHRODITE product. The precipitation values from APHRODITE correlate very well to the observed precipitation values, leading to the conclusion that the APHRODITE dataset provides precipitation values with sufficient accuracy for this modeling study. However some caution is required in drawing this conclusion as the APHRODITE product is based on gridding observed data. So, if a station is used in generating the gridded dataset, then it is likely that it will show a high correlation. Furthermore, the number of stations used to construct the APHRODITE product shows a high variation over the model domain (Figure 9). The high density of stations over Nepal will yield a more accurate precipitation grid there compared to the low density in stations in the upper Indus basin and the parts of the model domain on the Tibetan Plateau. Moreover, precipitation measurements are subject to large systematic errors that can add up to 30% and even more in those cases in which a significant part of precipitation falls in the form of snow and undercatch prevails [e.g. *Cheema and Bastiaanssen*, 2012]. In addition, valley stations in mountain regions are generally not representative for basin precipitation because of strong vertical precipitation lapse rates, thus leading to an underestimate of high altitude precipitation. Several regional studies show that this is particularly valid for the Karakoram in the upper Indus [*Hewitt*, 2005; *Winiger et al.*, 2005]. We therefore stress the need to develop a bias correction methodology for high altitude precipitation at large scale in a future study.

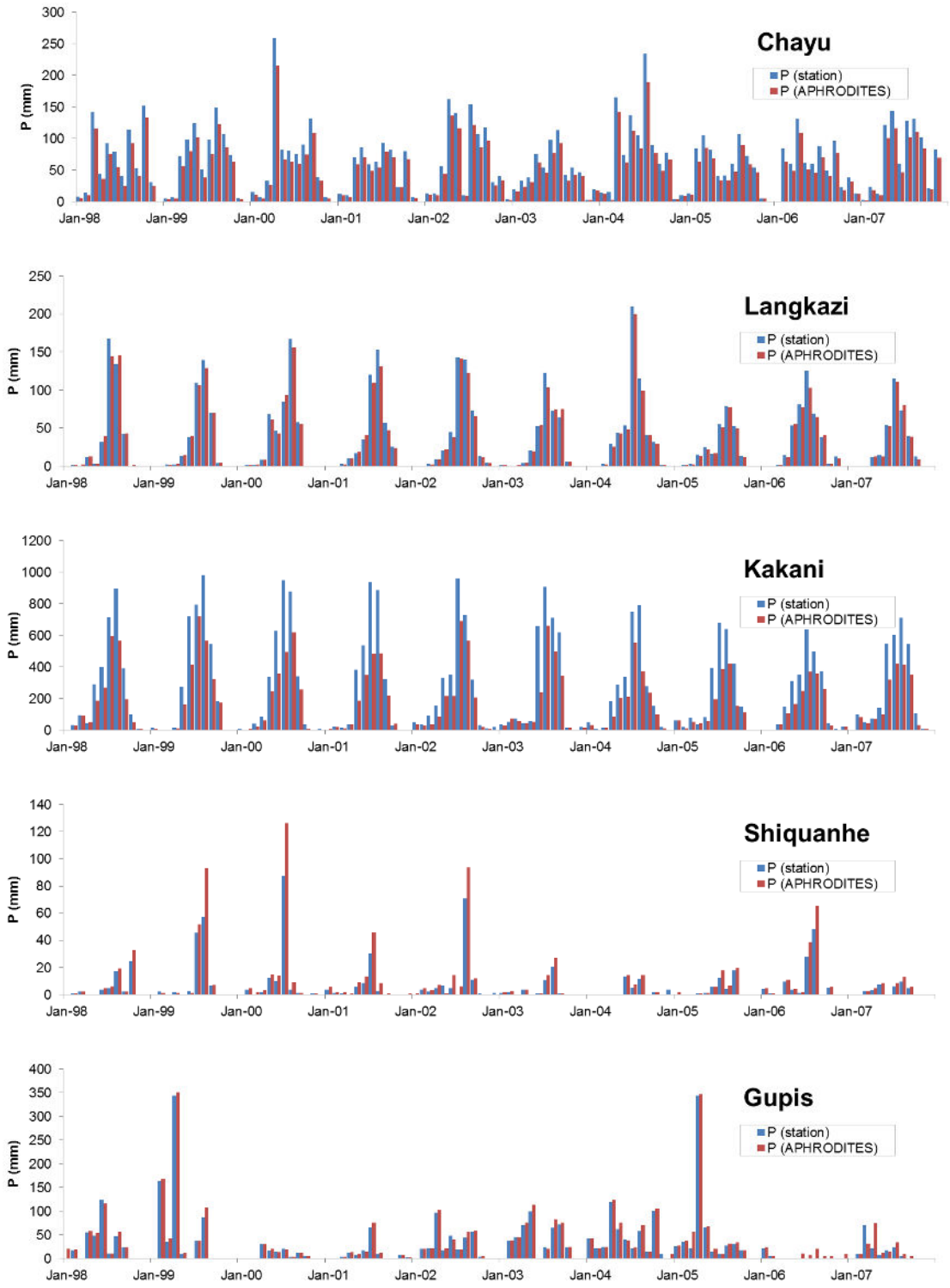

Figure 11: Precipitation station data and APHRODITE precipitation for five locations.

4.3 Temperature data

For the reference period (1998-2007) daily precipitation and daily average, minimum and maximum air temperature data are required for the HI-SPHY model. We use gridded air temperature extracted from the PRINCETON Global Meteorological Forcing Dataset for land surface modelling (PRINCETON) [*Sheffield et al.*, 2006]. The PRINCETON dataset is constructed by combining a suite of global observation-based datasets with the National Centers for Environmental Prediction–National Center for Atmospheric Research (NCEP–NCAR) reanalysis. Daily Average air temperature is available at 0.5° x 0.5° spatial resolution, while daily maximum and minimum temperature are available at 1.0° x 1.0° spatial resolution. The raw gridded data was resampled to model resolution (1km^2) by bilinear interpolation. The resampled grids where corrected
using the SRTM DEM and the moist adiabatic lapse rate, to account for temperature variations with elevation.

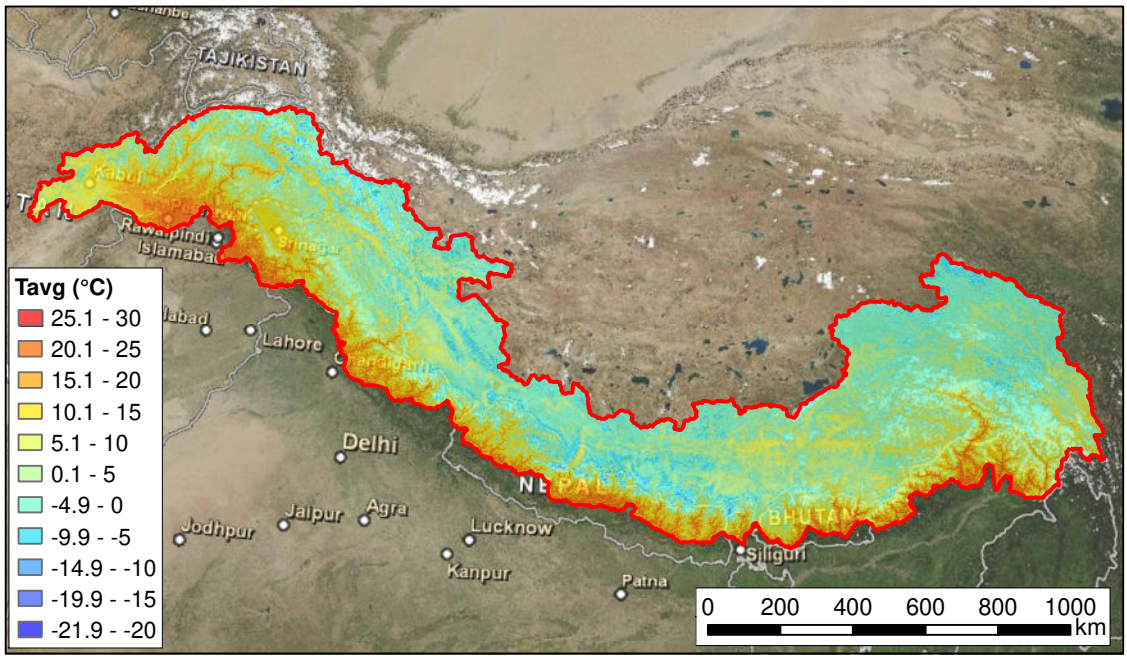

Figure 12: Average temperature for model domain during reference period (1998-2007).

An error was discovered in the PRINCETON dataset for the studied area during the reference period. This error is present during several days in 2005 in a major area (Figure 13). For a number of days during December 2005 this area shows anomalously low temperature values (Figure 14). This error was fixed by the Land Surface Hydrology Research Group at Princeton University.

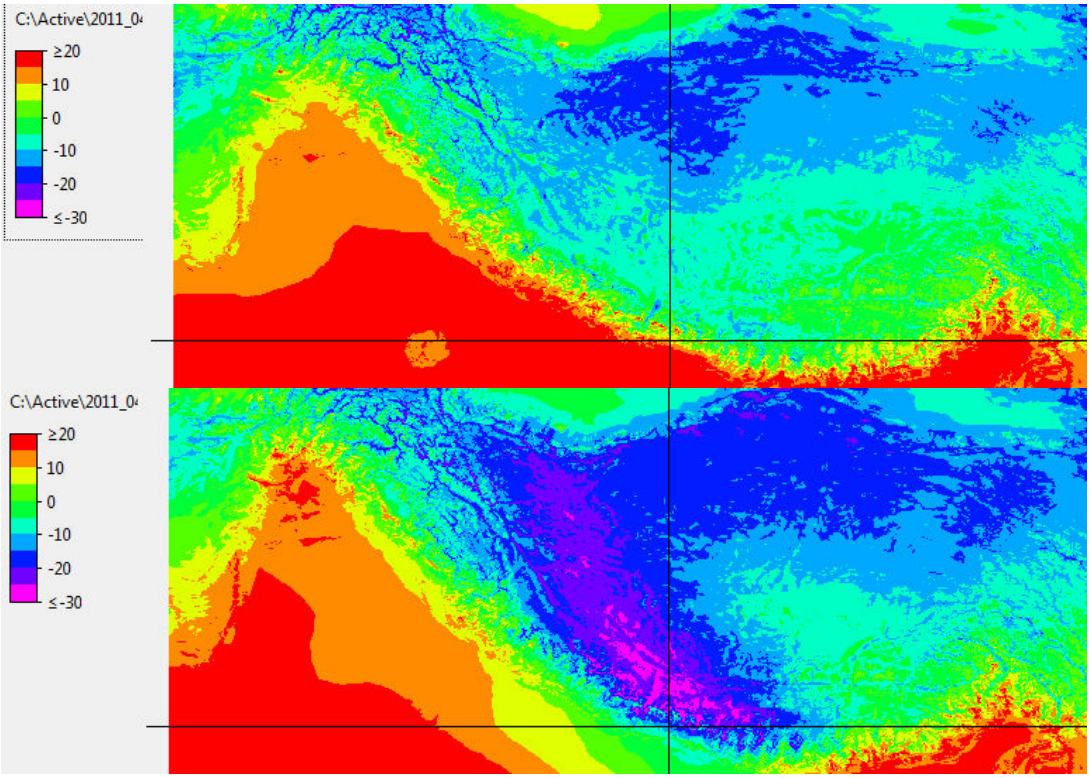

Figure 13: PRINCETON temperature for 1 December 2005 (above) and 2 December 2005 (below).

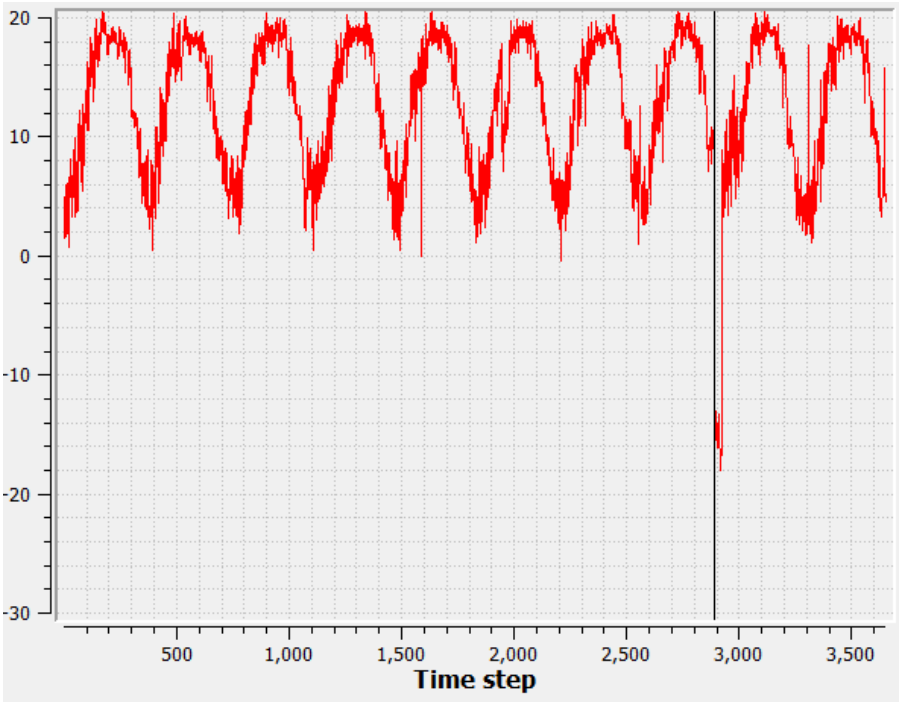

Figure 14: PRINCETON temperature timeseries for reference period at location indicated by crosshair in Figure 13.

Apart from this error, a number of errors lasting just a single time step are present in the dataset. To minimize these errors, all grid cells where the temperature difference with respect to the previous day is larger than 10 °C, where replaced with the average monthly temperature for that particular grid cell.

We validated the resulting average, maximum and minimum temperature datasets using the same meteo stations as for the validation of the precipitation dataset (Figure 10), as far as records of average, maximum or minimum temperature observations where available at the mentioned stations. Observed temperatures and temperatures extracted from the PRINCETON dataset at stations' locations are plotted in Figure 15 - Figure 18.

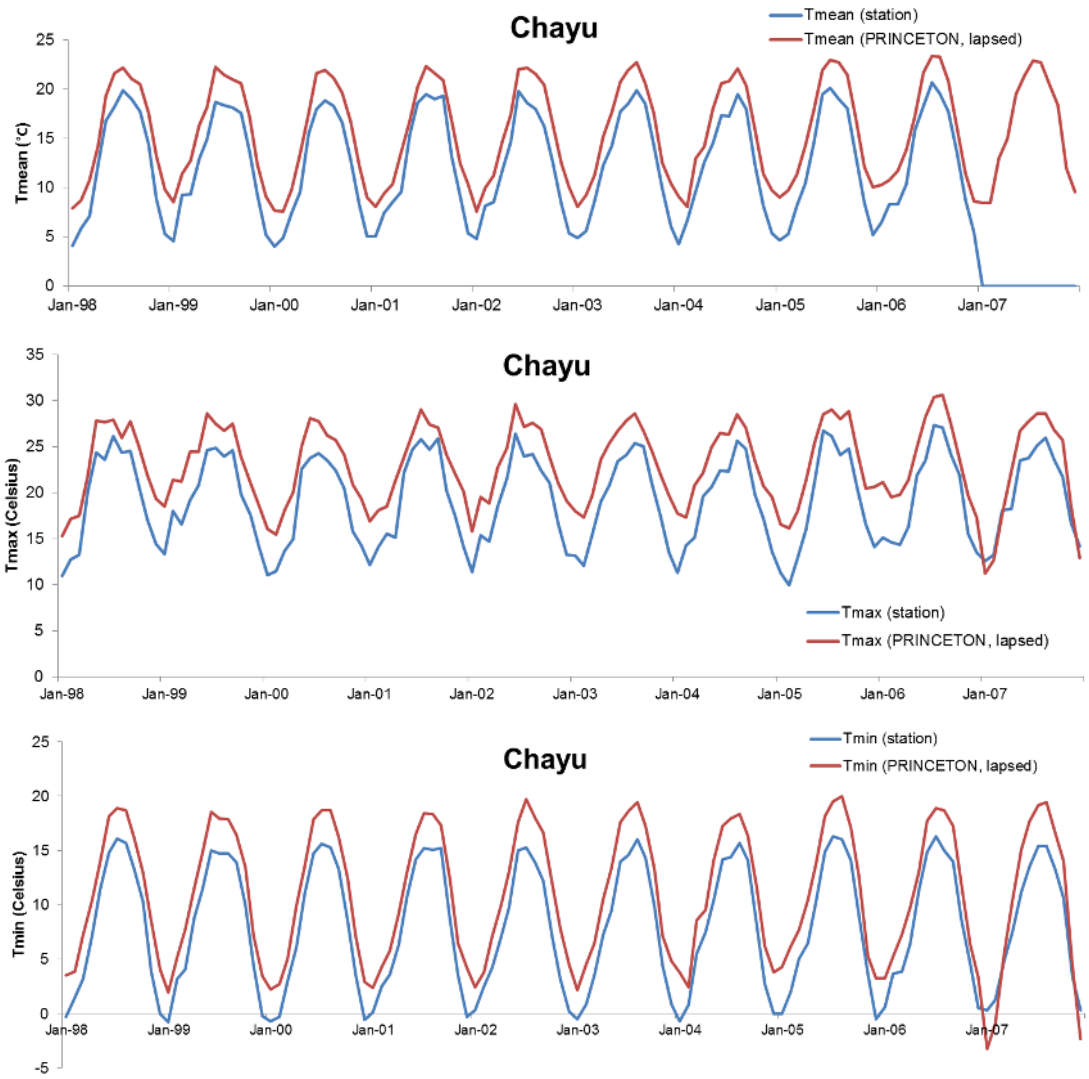

Figure 15: Observed temperature and temperature in PRINCETON dataset at location Chayu station.

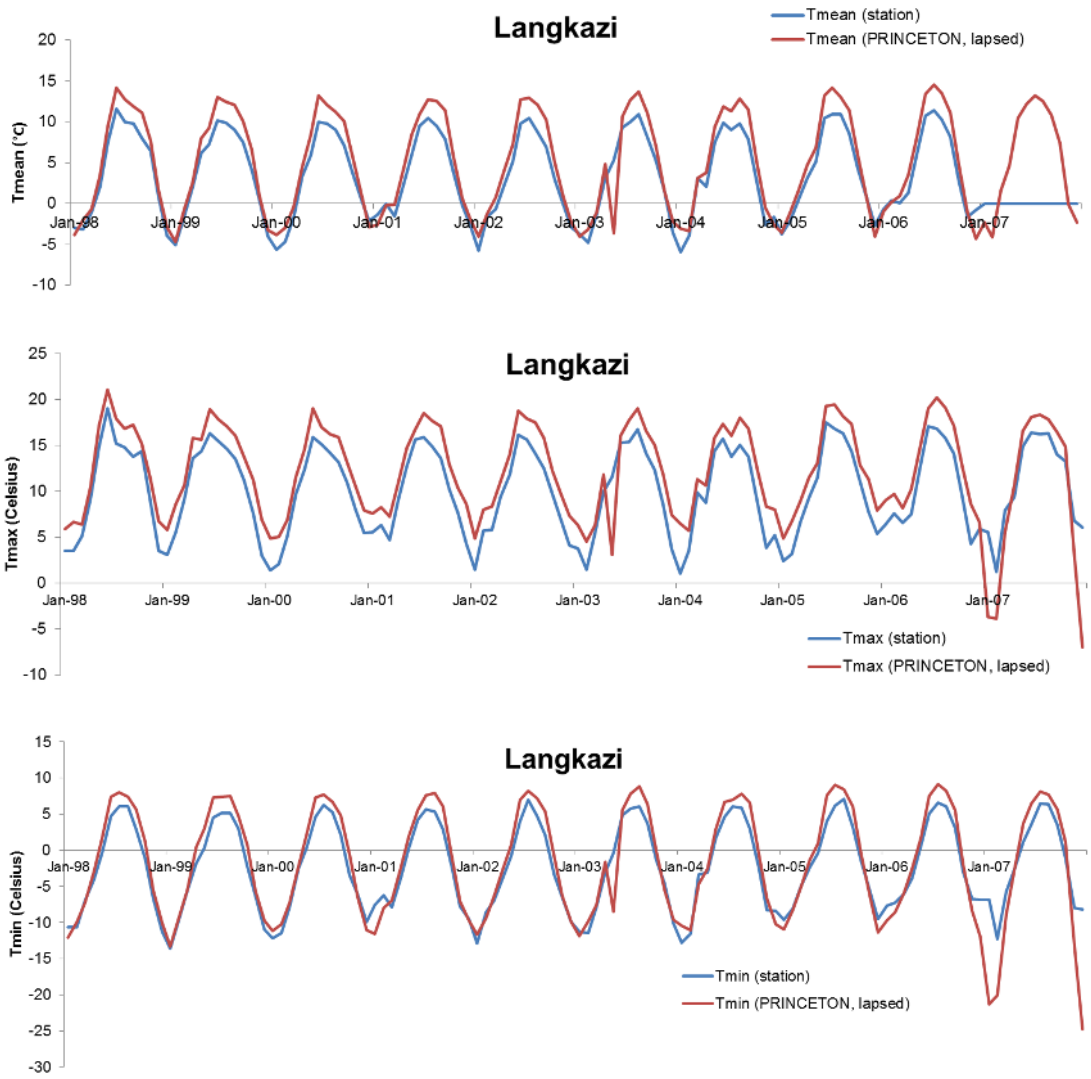

Figure 16: Observed temperature and temperature in PRINCETON dataset at location Langkazi station.

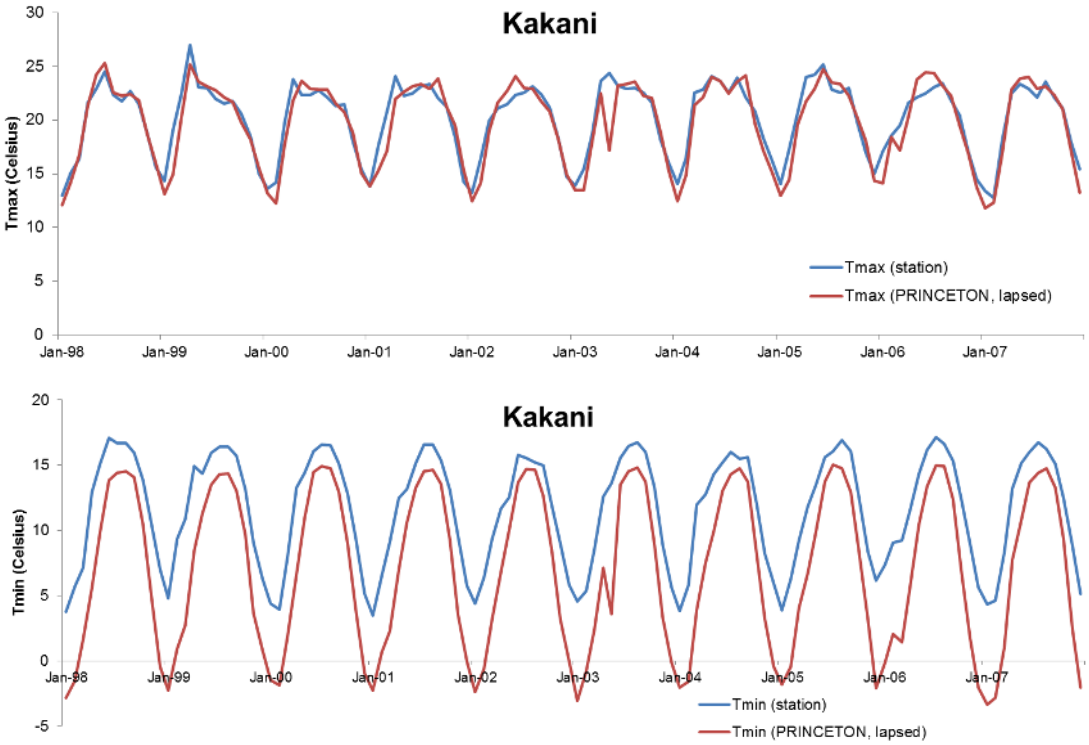

Figure 17: Observed temperature and temperature in PRINCETON dataset at location Kakani station.

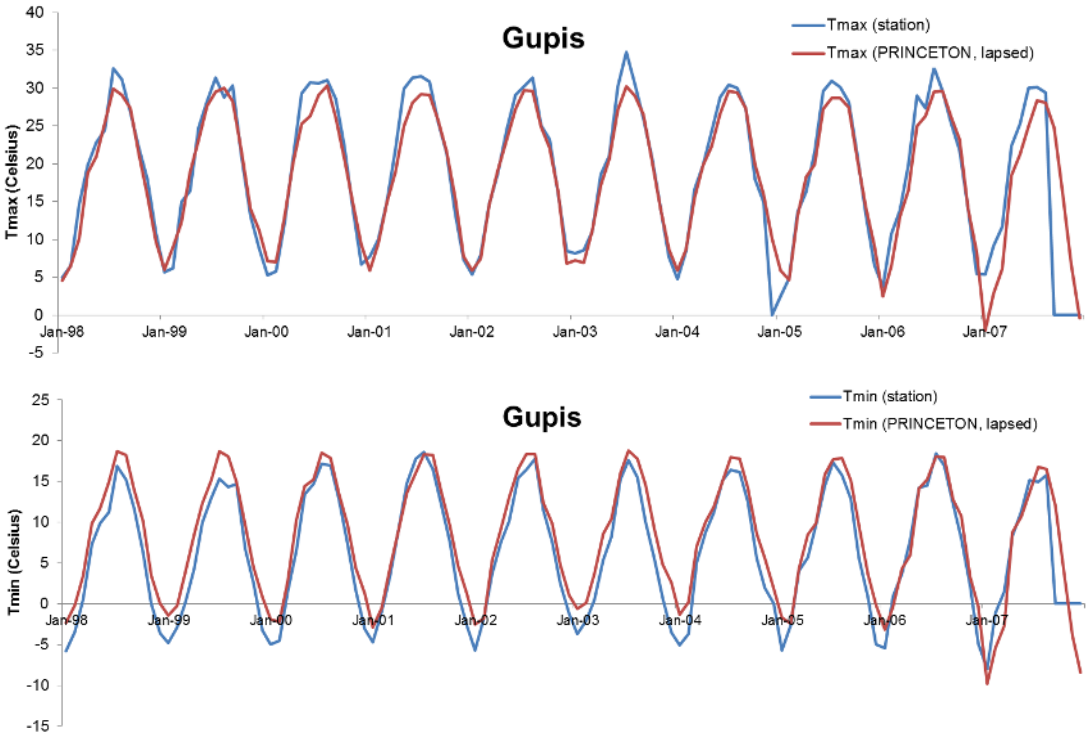

Figure 18: Observed temperature and temperature in PRINCETON dataset at location Gupis station.

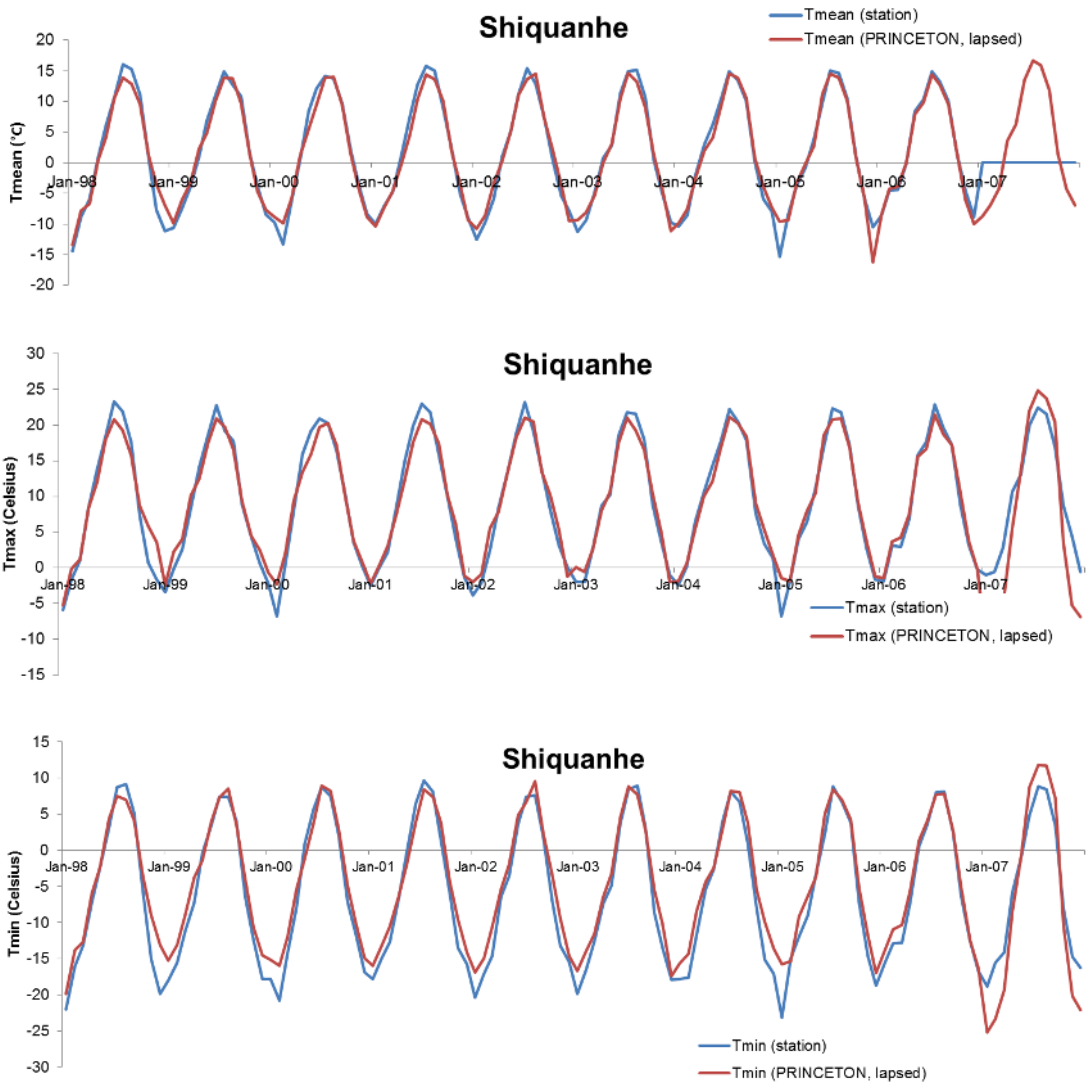

Figure 19: Observed temperature and temperature in PRINCETON dataset at location Shiquanhe station.

It is apparent from the figures that the correlation between PRINCETON temperature and measured temperature differs from station to station. Overall we conclude that the dataset has sufficient accuracy to be used for this modelling study.

4.4 Glacier outlines

The outlines of all debris covered and clean ice glaciers are an input dataset to the model. ICIMOD has recently completed a comprehensive glacier inventory [*Bajracharya and Shrestha*, 2011] and this dataset is used as the initial glacier extent (Figure 20). The glacier polygons are overlayed with the model grid and for each grid cell the fraction of debris and clean ice glacier is determined.

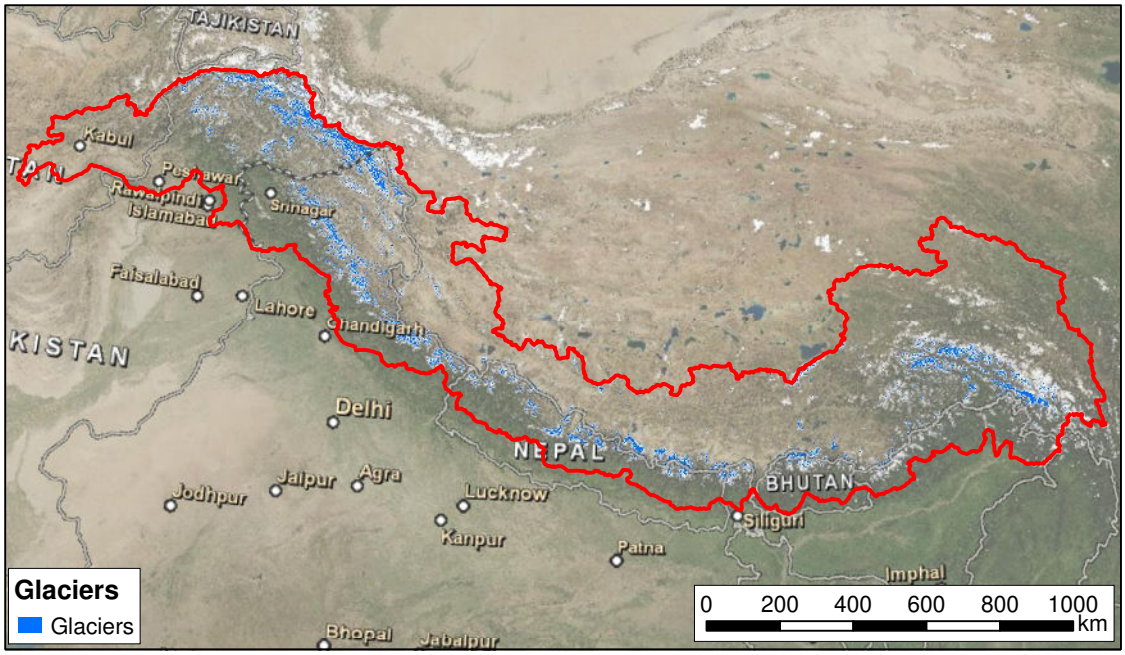

Figure 20: Glacier polygons ICIMOD glacier inventory.

The distinction between clean ice glaciers and debris covered glaciers is made based on elevation and slope. Debris covered glaciers are mostly present in lower regions and have relatively gradual incline. Based on visual analysis an elevation threshold at 4100 m a.s.l. was determined. The slope threshold was set at 24° according to [*Paul et al.*, 2004].
Following this definition, glaciers below 4100 m a.s.l., and with a slope smaller than 24° are defined as debris covered glaciers and other glaciers are defined as clean ice glaciers. Figure 21 shows the fractional glacier cover for debris covered and clean ice glaciers.

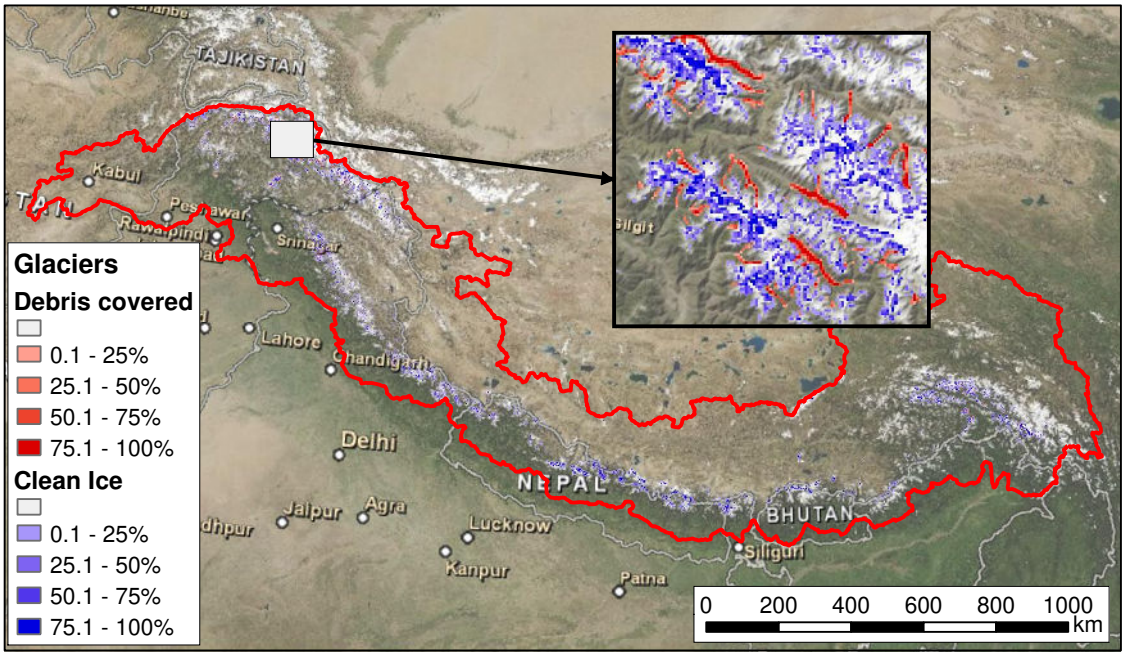

Figure 21: Fractional debris covered and clean ice glacier cover.

4.5 Soil type and land use type

The FAO global soil map is used to distinguish different soil types. Using pedotransfer functions, quantitative soil properties are derived to be used in the model (section 3.3). The soil map is much more detailed for the Chinese part of the basins compared to the other parts of the basins.

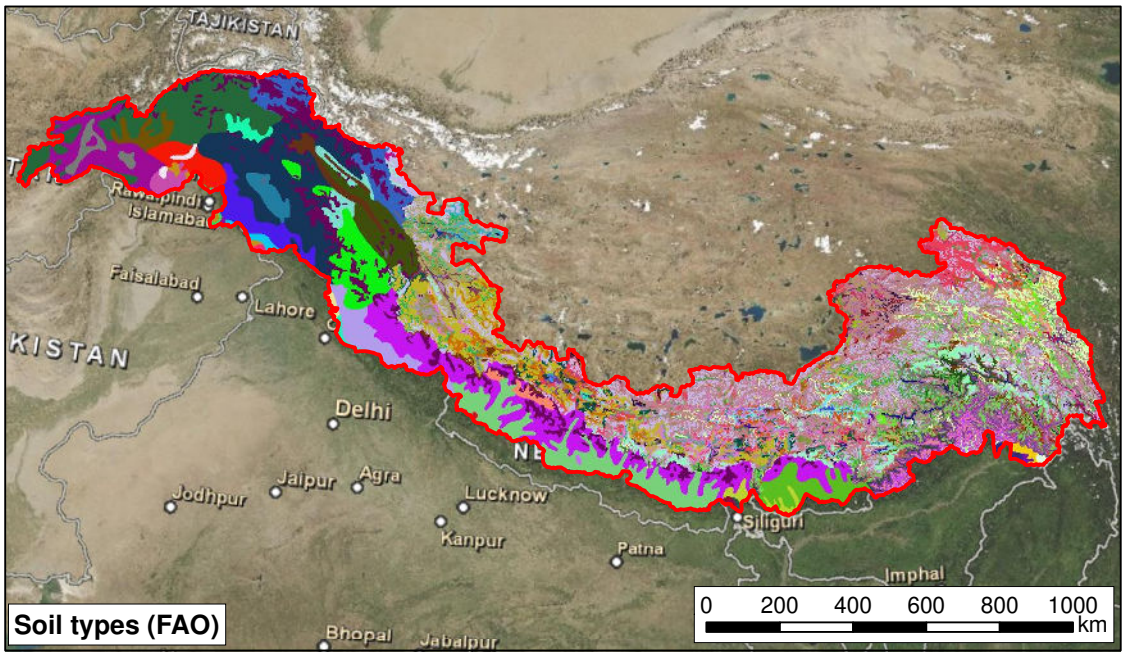

Figure 22: FAO soil map for model domain.

The MERIS GlobCover product is used to define different land use types. Each land use type is assigned a K_c factor used to calculate potential evapotranspiration. Table 2 shows the land use classes occurring in the model domain and the assigned values for the K_c factor.

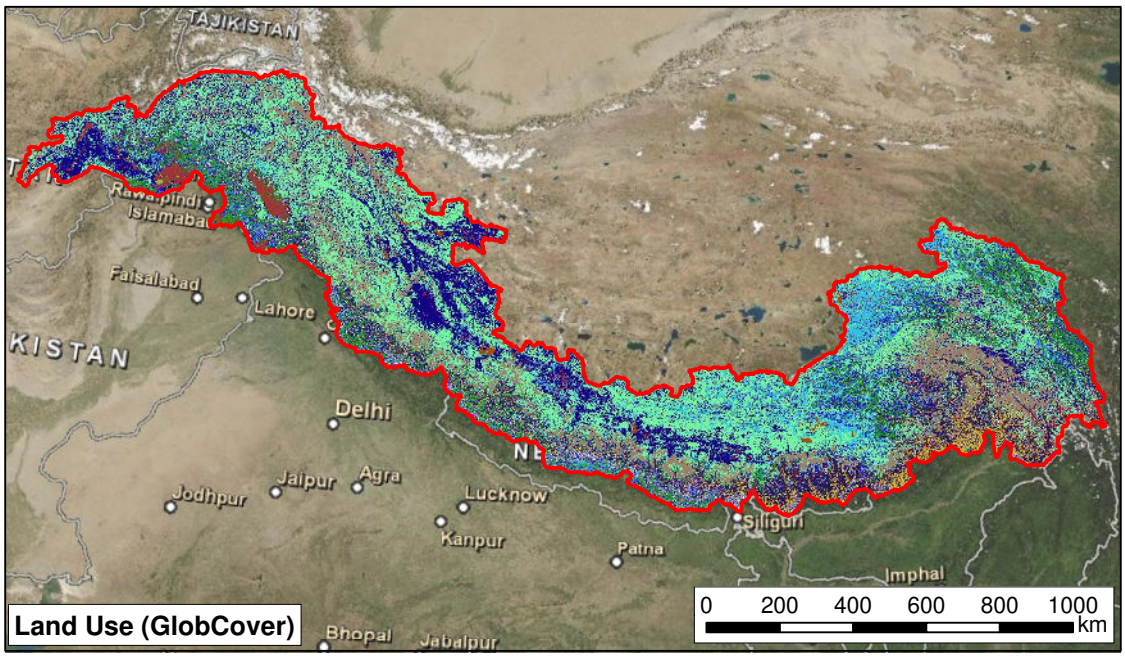

Figure 23: GlobCover land use classes for model domain.

Table 2: Land use classes in model domain with assigned Kc factors.

Land use class	Kc
Post-flooding or irrigated croplands (or aquatic)	0.6
Rainfed croplands	0.6
Mosaic cropland (50-70%) / vegetation (grassland/shrubland/forest) (20-50%)	0.6
Mosaic vegetation (grassland/shrubland/forest) (50-70%) / cropland (20-50%)	0.6
Closed to open (>15%) broadleaved evergreen or semi-deciduous forest (>5m)	0.6
Closed (>40%) broadleaved deciduous forest (>5m)	0.6
Open (15-40%) broadleaved deciduous forest/woodland (>5m)	0.6
Closed (>40%) needleleaved evergreen forest (>5m)	0.6
Closed to open (>15%) mixed broadleaved and needleleaved forest (>5m)	0.6
Mosaic forest or shrubland (50-70%) / grassland (20-50%)	0.6
Mosaic grassland (50-70%) / forest or shrubland (20-50%)	0.6
Closed to open (>15%) (broadleaved or needleleaved, evergreen or deciduous) shrubland (<5m)	0.6
Closed to open (>15%) herbaceous vegetation (grassland, savannas or lichens/mosses)	0.5
Sparse (<15%) vegetation	0.4
Closed to open (>15%) grassland or woody vegetation on regularly flooded or waterlogged soil - Fresh, brackish or saline water	0.6
Artificial surfaces and associated areas (Urban areas >50%)	0.7
Bare areas	0.6
Water bodies	0.5
Permanent snow and ice	0.2

4.6 River flow

River flow data are used to calibrate the HI-SPHY model for the reference period. River flow data were provided by ICIMOD and by IWMI Pakistan. Not all flow records (Table 3) cover the entire reference period. Tarbela inflow, Turkeghat and Chatara, are used as calibration sites for the HI-SPHY model.

Table 3: Locations with measured discharge time series

SITE	BASIN	COUNTRY	LATITUDE	LONGITUDE	ELEVATION (masl)
Turkeghat	Ganges	Nepal	27.33	87.18	414
Barhbise	Ganges	Nepal	27.79	85.88	840
Pachuwarghat	Ganges	Nepal	27.56	85.75	589
Khurkot	Ganges	Nepal	27.33	86.00	455
Rabuwa Bazar	Ganges	Nepal	27.27	86.65	460
Mulghat	Ganges	Nepal	26.93	87.32	276
Chatara	Ganges	Nepal	26.87	87.15	140
Dainyor bridge	Indus	Pakistan	35.93	74.37	1450
Besham Qila	Indus	Pakistan	34.92	72.88	580
Tarbela Inflow	Indus	Pakistan	34.38	72.87	430
Mangla inflow	Indus	Pakistan	33.20	73.65	335
Marala inflow	Indus	Pakistan	32.67	74.46	243

5 Calibration and validation

The model is calibrated to observed runoff at three stations (Tarbela inflow, Turkeghat and Chatara), for the entire reference period (1998-2007) at a daily time step. These locations were chosen because they have complete flow records for the reference period, represent a variety of catchment sizes and represent both climatological regimes (the monsoon dominated eastern and southern Himalayas and the upper Indus basin where the climate is influenced by westerlies in addition to the monsoon). Figure 24 shows the locations used for calibration and validation as well as the locations where flow projections are made. Tarbela is location 4, Turkeghat is location 10 and Chatara is location 11 in the figure.

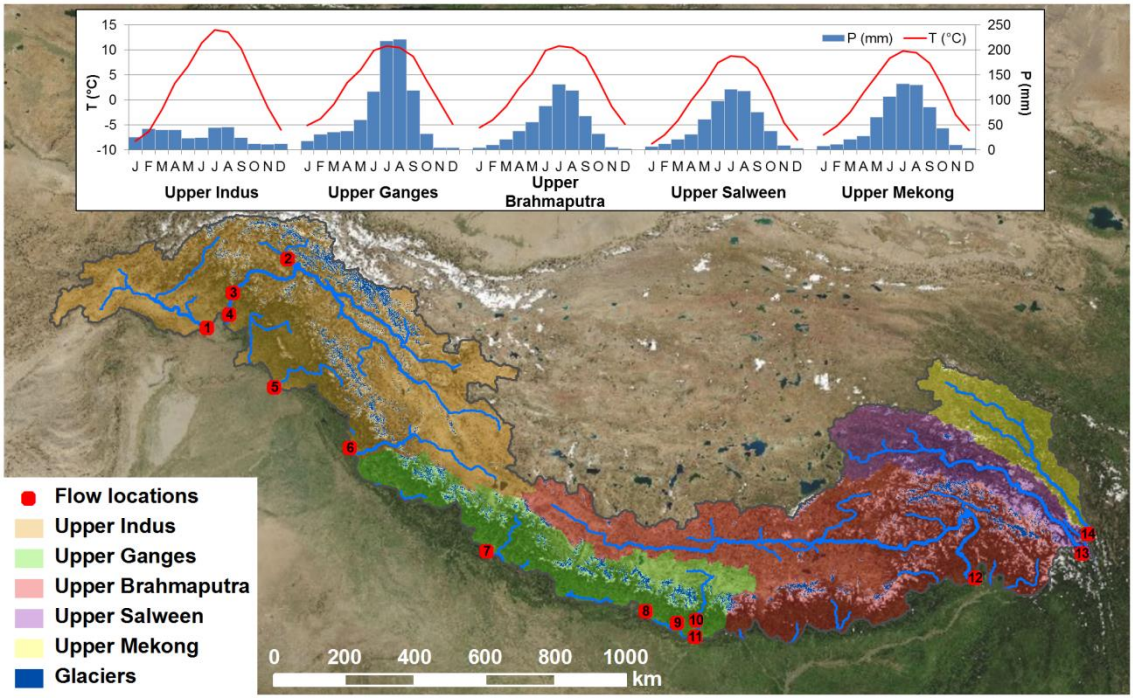

Figure 24: Map with locations of flow stations used for calibration and validation. Flow locations are listed in Table 4.

Table 4: Flow locations (partly used for calibration and validation of the model).

ID in Figure 24	Station name	River	Basin	Catchment area (km^2)	Calibration / Validation	Average observed discharge (m^3s^{-1})	Observation interval
4	Tarbela inflow	Indus	Indus	203142	C	2307	10 days
10	Turkeghat	Arun River	Ganges	28178	C	506	1 day
11	Chatara	Saptakoshi River	Ganges	54326	C	1498	1 day
2	Dainyor Bridge	Gilgit	Indus	14147	V	310	1 day (2001-2003)
3	Besham Qila	Indus	Indus	198896	V	2320	1 day (2000-2005)
5	Marala inflow	Jhelam	Indus	29628	V	921	10 days
9	Rabuwa Bazar	Dudhkoshi river	Ganges	3858	V	230	1 day
8	Pachuwarghat	Sunkoshi River	Ganges	4920	V	201	1 day

The model is calibrated using the non-linear parameter estimation package PEST [*Doherty*, 2005] and the following parameters are calibrated: degree day factor clean ice, degree day

factor snow, degree day factor debris covered glacier, precipitation correction factor, storage capacity of snow, root depth, subsoil depth, drainage time, baseflow recession constant, and routing recession coefficient. Calibrated parameter values are listed in Table 5.

Table 5: HI-SPHY model calibrated parameters.

Symbol	Description	Calibrated value
DDFCI	Degree day factor for clean ice glaciers	6.0 mm $K^{-1}d^{-1}$
DDFDG	Degree day factor for debris covered glaciers	3.0 mm $K^{-1}d^{-1}$
DDFS	Degree day factor for snow	4.8 mm $K^{-1}d^{-1}$
PrecF	Correction factor for precipitation input	1.17
SnowSC	Water storage capacity of snow pack	0.5 mm mm^{-1}
RDepth	Depth of rooting zone for flat area	300 mm
SDepth	Depth of subsoil for flat area	700 mm
ΔGW	Drainage time	1.0 d
αGW	Baseflow recession constant	0.005
kx	Recession coefficient for routing	0.958895
SlopeF	Slope correction for soil	0.713601 standard deviations

Figure 25 to Figure 27 show the calibration results for the three stations.

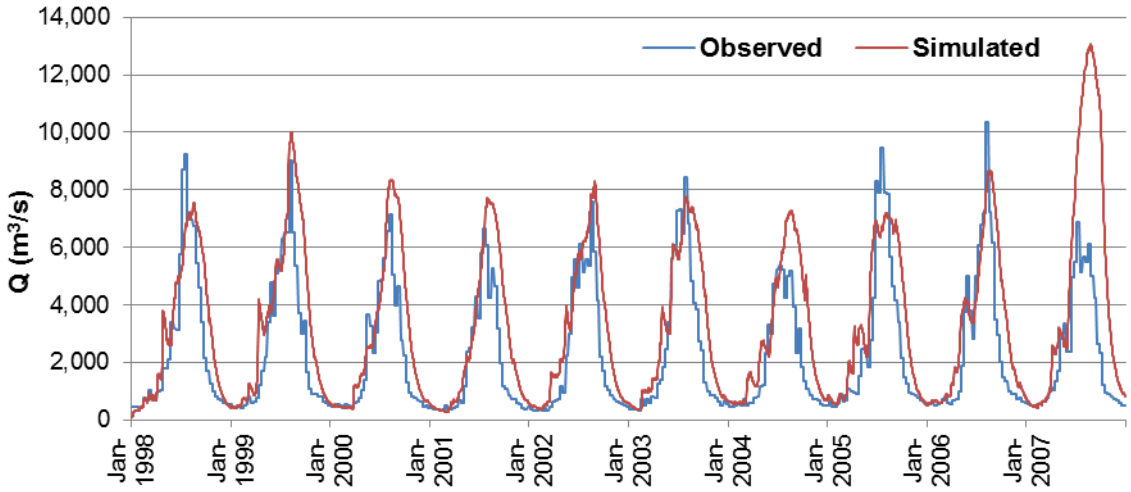

Figure 25: Daily observed and simulated discharge at Tarbela inflow (location 4 in Figure 24) 1998-2007. Note that the high simulated discharges in 2007 are due to errors in the PRINCETON temperature forcing in the Indus basin.

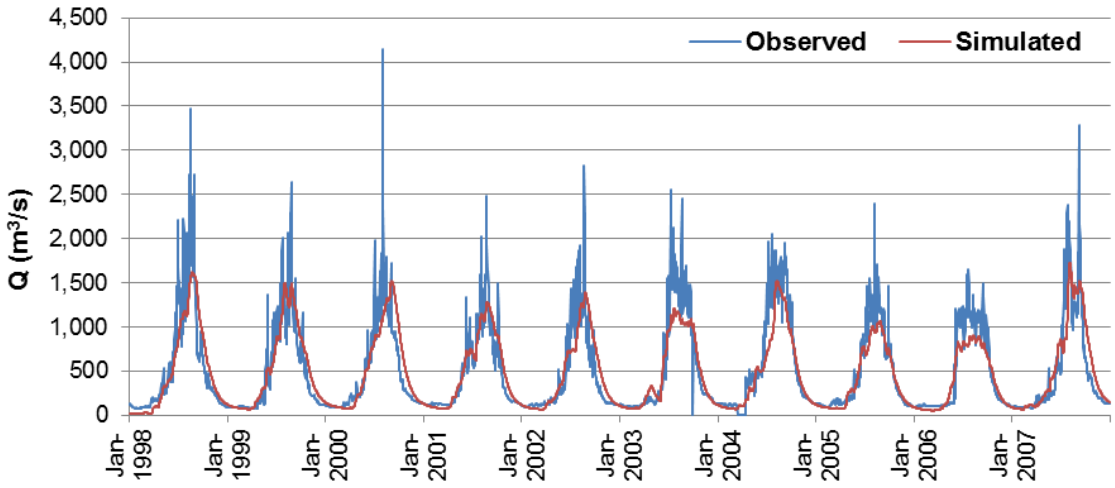

Figure 26: Daily observed and simulated discharge at Turkeghat (location 10 in Figure 24) 1998-2007.

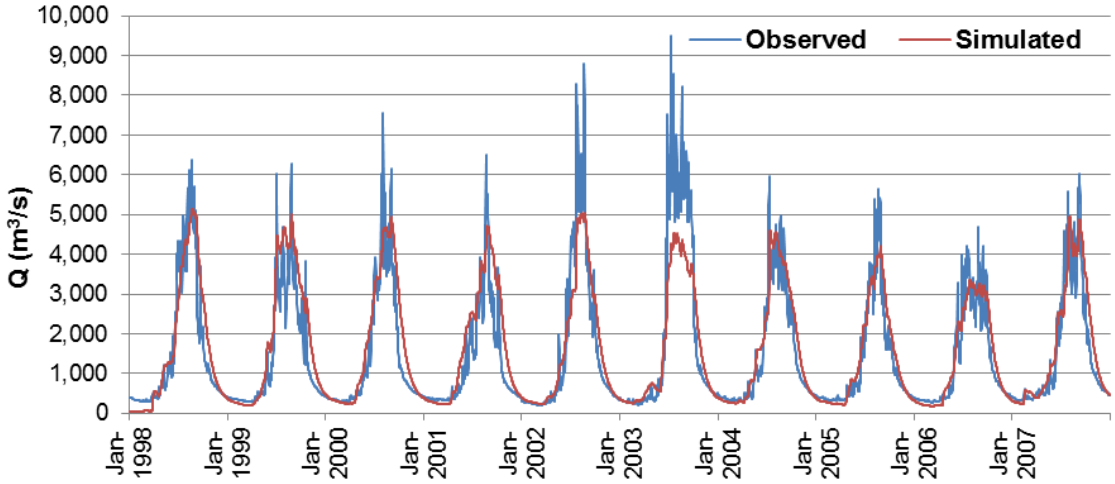

Figure 27: Daily observed and simulated discharge at Chatara (location 11 in Figure 24) 1998-2007.

The quality of the model performance can be expressed with different criteria for the correlation between the observed values and the simulated values. Figure 28 lists the values for three criteria describing the correlation between observed and simulated values at the three stations used for calibration. For Pearson's product-moment correlation coefficient, a perfect correlation, where simulated values equal to observed values, would yield a coefficient's value equal to +1 or -1. When no correlation exists, the coefficient's value is equal to 0. The simulation is unbiased when the bias is equal to 0. A positive value for bias indicates overestimation in the simulation, whereas a negative value for bias indicates underestimation in the simulation. The value for bias is given as percentages. The Nash-Sutcliffe model efficiency coefficient is used to assess the predictive power of hydrological models. The coefficient's value can range from $-\infty$ to +1. A value of 1 indicates a perfect correlation, where simulated values are equal to observed values. Coefficient value 0 indicates the simulated values are as accurate as the mean of the observed data. For a coefficient value smaller than 0, the mean of the observed data is a better predictor than the model.

We used five other stations in the model domain to validate the model performance for the same period. In Figure 28, the same correlation criteria are listed for the validation stations as

well as for the calibration stations. There are a number of uncertainties in the model, causing impediments in predicting the actual runoff. First, there are considerable uncertainties in the temperature and precipitation input data. As the PRINCETON and APHRODITE datasets are global and continental datasets respectively, with original spatial resolutions of 0.5° and 0.25°, they have biases when applied at the 1 km scale. Besides, the processes described in the model are simplified with respect to what happens in the real world. Assumptions are made in different stages of the modelling process adding to uncertainty. The largest bias between simulated and observed flow is for locations in the upper Indus basin. This is directly related to the underestimate in high altitude precipitation in the APHRODITE precipitation dataset.

We conclude that calibration results are satisfactory considering the complexity and heterogeneity of mountain hydrology, the large areas that have been modeled and the fact that we have used primarily public domain datasets. Moreover, it has been proven that relative model accuracy (= difference between current situation and scenario) is always much higher than relative model inaccuracy (difference between model output and observations) [*Droogers et al.*, 2008]. This is exactly why this modeling activity is undertaken: compare current climate with future climates.

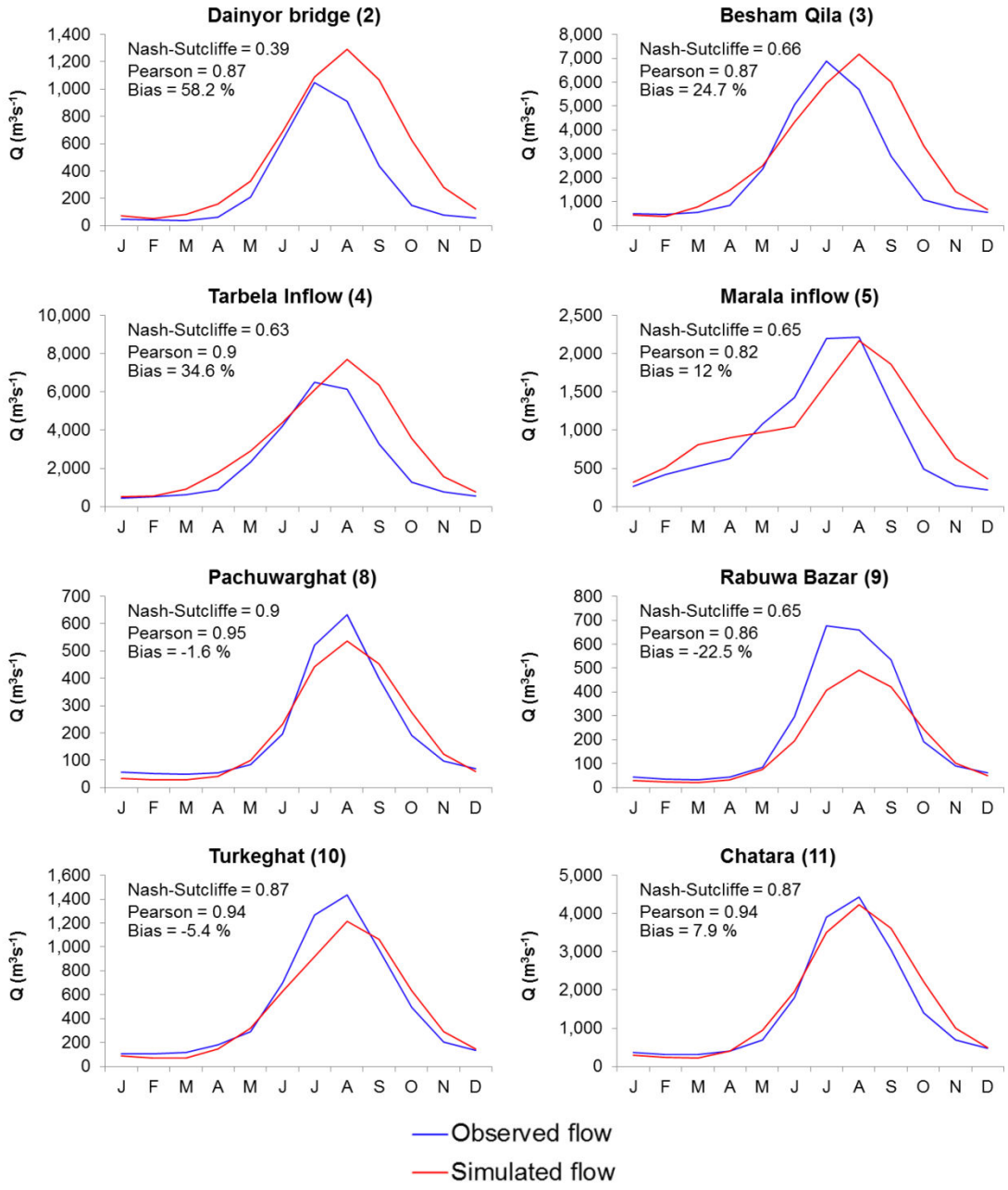

Figure 28: Calibration and validation results. IDs in parentheses behind the station name indicate the location in Figure 24. Correlation coefficients are calculated on a monthly basis.

6 Current hydrological regime

As the HI-SPHY model makes a distinction in the sources of the flow in different contributors (glacier melt, snow melt, rainfall-runoff and base flow), the calibrated and validated model is used to characterize the current hydrological regime. The distinction of flow in different components is summarized in Table 6, Figure 30, and the spatial distribution of flow composition is illustrated in Figure 29.

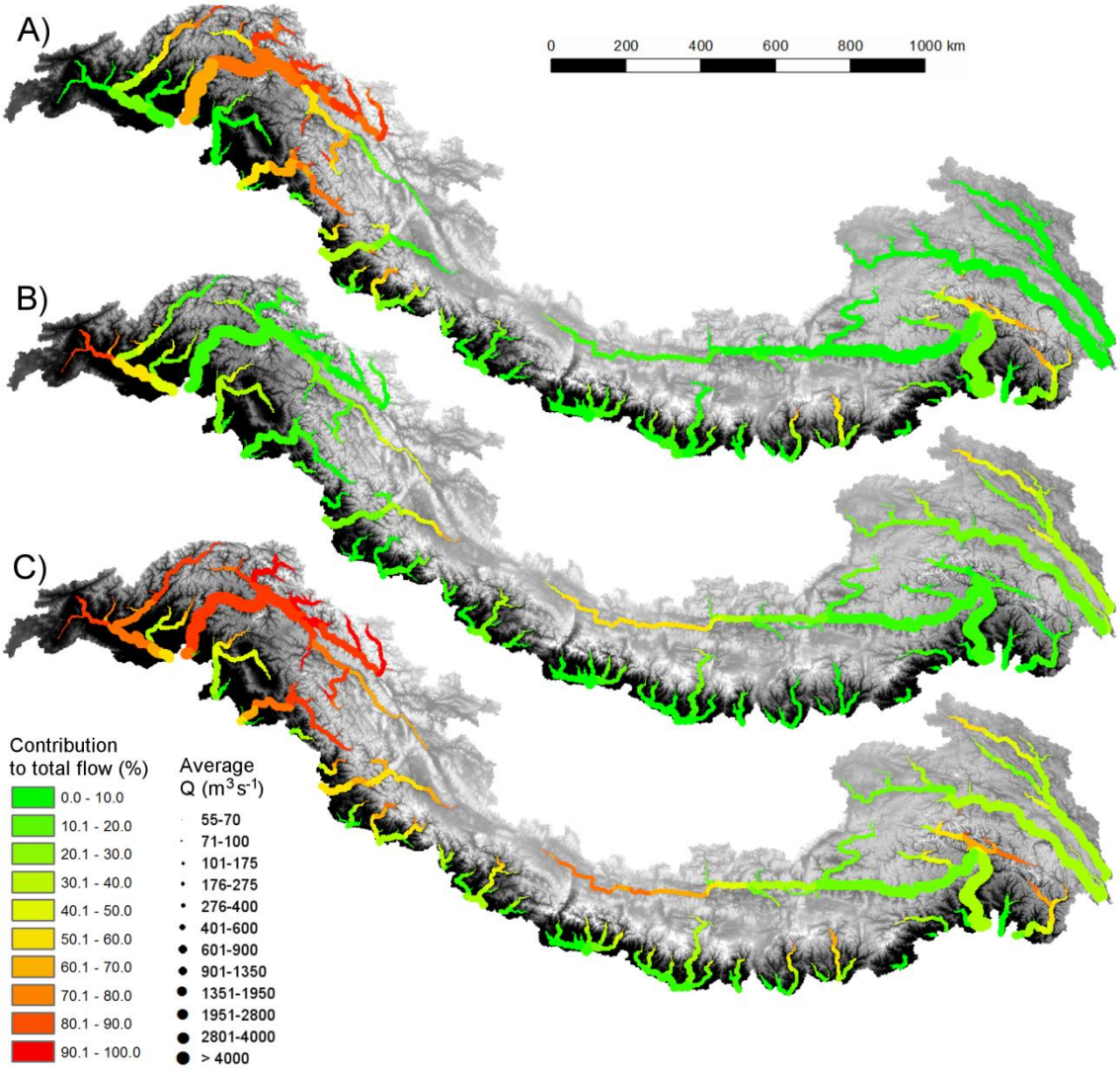

Figure 29: Average contribution of glacier melt (A), snow melt (B), glacier and snow melt combined (C) to total flow during and the average discharge at different stages in major streams in the model domain (all panels) during 1998-2007.

As is clear from the figure and table glacier melt has highest importance in the upper Indus basin, while the contribution of glacier melt to total flow is very small in the upper Salween. The upper Ganges and upper Brahmaputra are dominated by rainfall-runoff, although the glacier melt water contributes significantly. In the upper Salween and upper Mekong, rainfall runoff is also the most important, but the importance of snow melt is also substantial. As can be seen in Figure 29, the contribution of the glacier melt is highest in the most upstream parts of the basins, near the glaciers. More downstream, other components get higher contributions. Glacier melt is very important in the Indus basin and in rivers toward the interior of the Tibetan Plateau.

Table 6: Hydrological characteristics for each basin during the reference period (1998-2007)

Basin	Annual precipitation (mm)	Glacierized area (%)	Annual runoff (mm)	Contribution to total runoff (%)			
				Glacier melt	Snow melt	Rainfall-runoff	Base flow
Upper Indus	346	4.9	574	40.6	21.8	26.8	10.8
Upper Ganges	900	5.4	1088	11.5	8.6	66.0	13.9
Upper Brahmaputra	573	3.1	691	15.9	9.0	58.9	16.2
Upper Salween	595	1.3	480	8.3	27.5	42.0	22.2
Upper Mekong	642	0.2	464	0.9	32.5	43.9	22.8

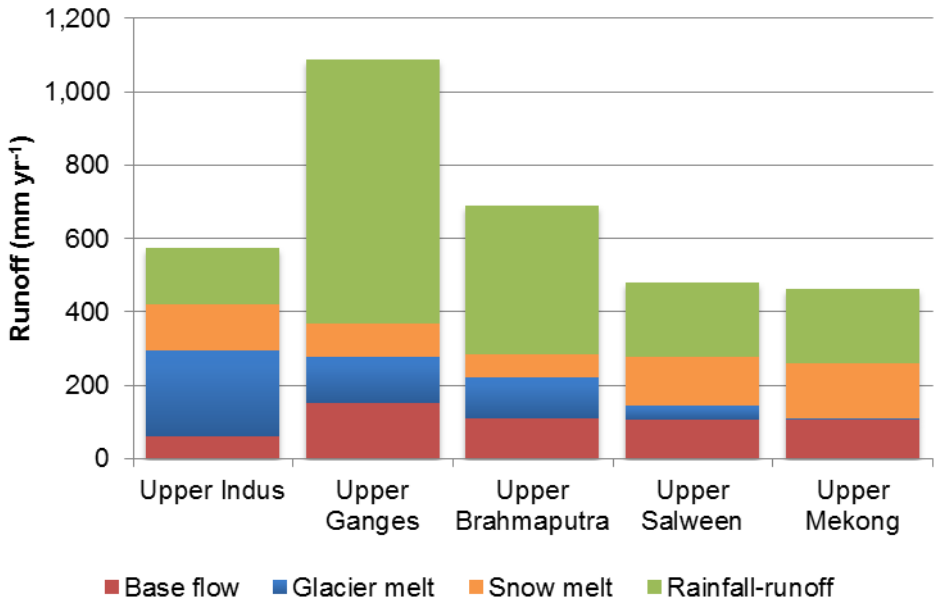

Figure 30: Hydrological regime 1998-2007 in the upper river basins.

7 Climate change scenarios

7.1 Precipitation and temperature

7.1.1 New approach to climate change projections

There is great variability in the projections in precipitation and temperature between different RCMs and GCMs and this variability is taken into account by forcing the model with a range of different models. Currently the IPCC is preparing the 5th assessment report (AR5) and the new climate model results that will be used for AR5 are used in this project. There has been a fundamental change from AR4 to AR5 in the way that the IPCC is dealing with climate change scenarios [*Moss et al.*, 2008].

Past scenario development has been conducted in a mainly sequential form, with socioeconomic and emissions scenarios developed first and climate change projections based on those scenarios carried out next. In contrast with the previous linear process, the parallel approach of AR5 should provide better integration, consistency, and consideration of feedbacks, and more time to assess impacts and responses (Figure 31). The parallel process is initiated with the identification of the Representative Concentration Pathways (RCPs), which will enable the climate modeling (CM) community to proceed with new climate change projections at the same time that new work is carried out in the integrated impact assessment (IAM) and impact and adaptation (IAV) communities (Figure 31). While the RCPs will enable CM scenario development that explores and characterizes future climate change, they do not constrain future work by the IAM community, which, in its portion of the parallel process, will simultaneously develop a range of completely new socioeconomic and emissions scenarios. IAM teams will have complete freedom to develop new scenarios across the full range of possibilities. IAM teams will also explore alternative technological, socioeconomic, and policy futures including both reference (without explicit climate policy intervention) and climate policy scenarios. This approach seems both promising and important given the interest of decision makers in exploring how to attain different stabilization levels.

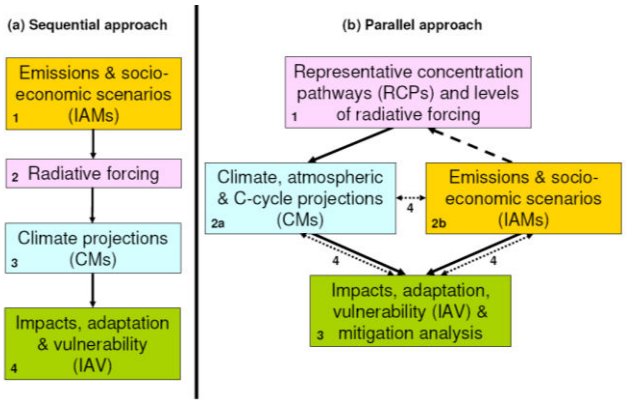

Figure 31 Approaches to the development of global scenarios: (a) previous sequential approach used in AR4; (b) parallel approach used in AR5.

7.1.2 Projection and models used

In this project we make projections for two RCPs: one rather extreme RCP that assumes that the radiative forcing will stabilize at 8.5 W/m^2 in 2100 and one less extreme that assumes stabilizations at 4.5 W/m^2 in 2100.

The upstream models are forced by both precipitation and air temperature outputs of a regional climate model and a selection of global climate models:

- The Bjerknes Centre for Climate Research is partner in the HICAP and outputs from their RCM simulations for RCP8.5 and RCP4.5 until 2050 are used to force the model.
- GCM AR5 data are downloaded from the CMIP5 model archive[1] for the same RCPs. Four are selected per RCP that span the entire range of possible futures: dry and cold, dry and warm, wet and cold, wet and warm.

In total the hydrological model is thus forced by 10 sets of climate change projections (2 RCPs x 5 models) using a daily time step from 2008 until 2050.

7.1.3 Downscaling

A simple delta change approach is used to downscale the climate change scenarios and the following steps are taken for both precipitation and temperature:

- For each year between 2011 and 2050 a random year from the reference period 1998 to 2007 is selected
- For each climate model the monthly change in precipitation and air temperature from 2008 to 2050 relative to the monthly average of the reference period is determined
- These changes are spatially interpolated to the model resolution of 1km
- The interpolated changes are added to the selected random year from 2008 to 2050

The GCM's used to force the model are listed in Table 7. For more information on the downscaling procedures and detailed spatial grids on temperature and precipitation change in the upstream and downstream basins we refer to the additional report on downscaling of GCM's [*Immerzeel and Lutz*, 2012], prepared for HICAP component 1: Climate change scenarios. Note that the selection of GCMs is based on the averaged climate change signal over the entire upstream and downstream HICAP domain. As the GCM outputs differ spatially, the dP and dT values mentioned in Table 7 can differ for the individual basins and within basins.

Table 7: Model selection based on 10th and 90th percentile values of projected changes in P and T from 1961-1990 to 2021-2050.

Description	RCP	dP (%)	dT (K)	Selected Model
DRY, COLD	RCP45	-1.8	1.4	GISS-E2-R-r4i1p1_rcp45
DRY, WARM	RCP45	-1.8	2.3	IPSL-CM5A-LR-r4i1p1_rcp45
WET, COLD	RCP45	8.9	1.4	CCSM4-r5i1p1_rcp45
WET, WARM	RCP45	8.9	2.3	CanESM2-r4i1p1_rcp45
DRY, COLD	RCP85	-1.1	1.7	GFDL-ESM2G-r1i1p1_rcp85
DRY, WARM	RCP85	-1.1	2.7	IPSL-CM5A-LR-r4i1p1_rcp85
WET, COLD	RCP85	12.1	1.7	CSIRO-Mk3-6-0-r3i1p1_rcp85
WET, WARM	RCP85	12.1	2.7	CanESM2-r4i1p1_rcp85

[1] http://cmip-pcmdi.llnl.gov/cmip5/

7.2 Projections for glacier area change

For each climate change projection a separate projection for glacier extent is made for the entire time series until 2050 based on a recently developed approach [*Lutz et al.*, 2012]. As dynamic ice flow cannot be simulated at the 1 km grid scale, this parameterization becomes necessary. We apply this method to each of the five basins separately. To derive the glacier extent first a hypsometric curve is derived using the present glacier fraction and the elevation distribution within a 1 km cell (see also Figure 32). Based on this hypsometric curve and precipitation and air temperature data we derive the 0 °C isotherm and accumulation area ratio (AAR) for each month from 1997 to 2007. Subsequently, the monthly accumulation and melt are calculated and we compute an overall specific mass balance over the 1998 to 2007 period. We then optimize calibration parameters until the modeled mass balance matches an average observed specific mass balance representative for the region, as calculated with published mass balance records based on ICESAT measurements in the region [*Kääb et al.*, 2012]. The model is then forced by monthly future precipitation and temperature projections from 1998 to 2050 based on the 10 sets of climate change projections. For each climate projection the results for 25 different glacier size classes are integrated to derive an overall glacier area depletion curve. This depletion is then integrated in the model forcing to change the fractional glacier cover for each grid cell for each month.

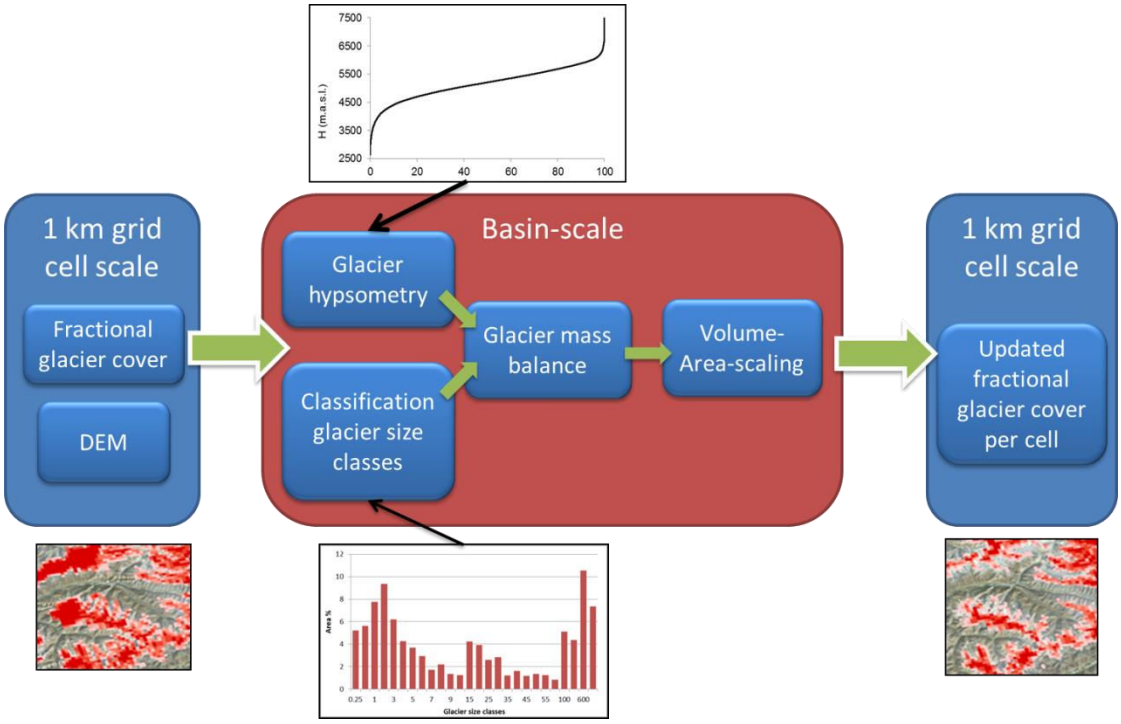

Figure 32: Schematic representation of approach to simulate changes in glacier cover at river basin scale.

8 Basin Scale Water Availability Scenarios

8.1 Future climate

As described in section 7.1, the future changes in precipitation and temperature are calculated using the “delta change” method for eight GCMs for RCP 4.5 and RCP 8.5 (4 GCMs per RCP). The delta change values averaged over the upper basins are shown in Figure 33. Delta change values are shown on annual basis (upper panel), for the monsoon months (middle panel), and winter months (lower panel) separately. As expected, ΔT values are always higher for RCP 8.5 compared to RCP 4.5 for each of the basins and each period. The variations regarding projected temperature changes in between the basins are small. Remarkably, the spread in temperature projections between the GCMs is especially large during the winter months and the spread is larger for RCP 8.5 than for RCP 4.5.

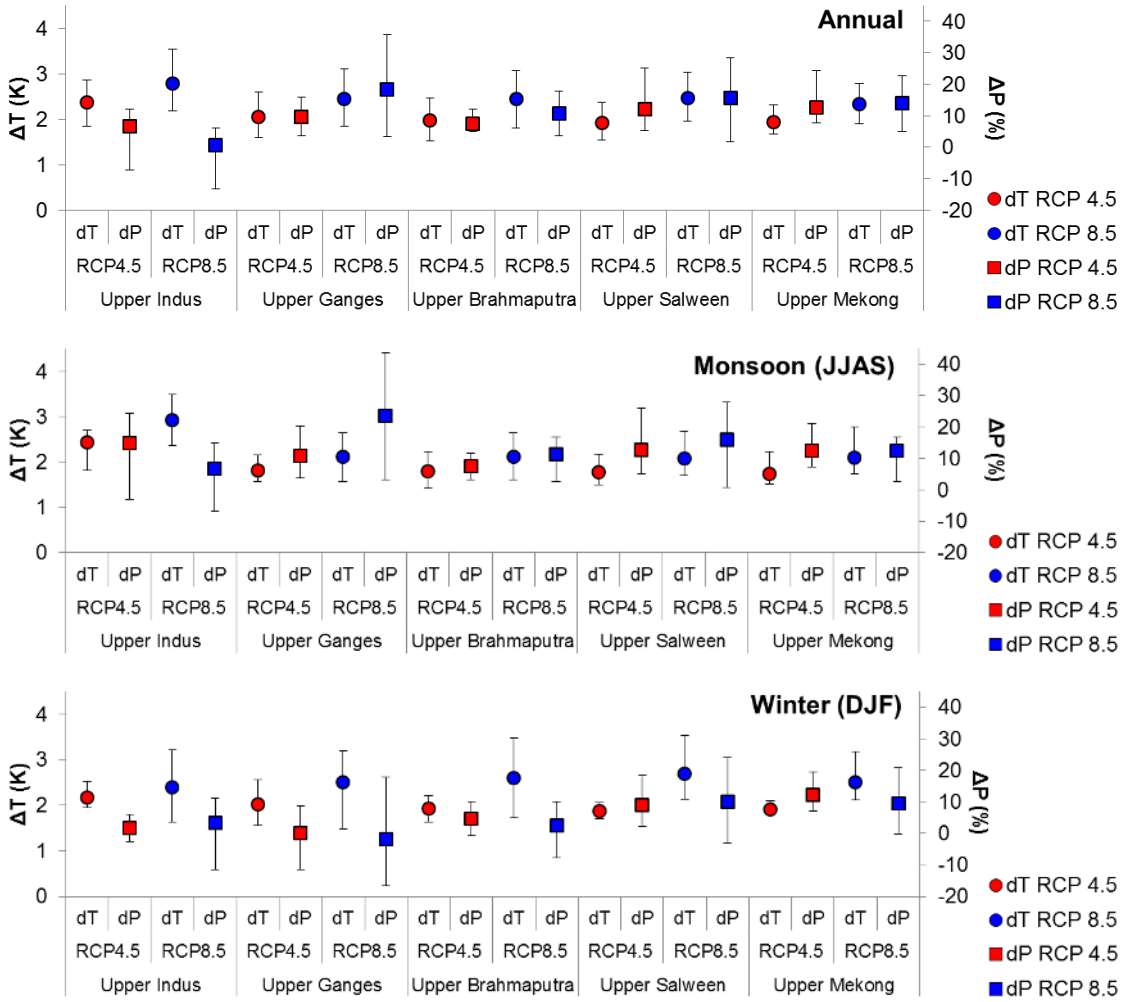

Figure 33: Changes in temperature (K) and precipitation (%) per basin. The values represent the change between 1961-1990 and 2021-2050, and thus change over 60 years. The changes are presented on annual basis (upper panel), for the monsoon months (JJAS, middle panel) and winter months (DJF, lower panel). The values are the average of 4 GCMs, whiskers show the maximum and minimum projection from the sample of 4 GCMs.

Projections for precipitation show more variation between GCMs, RCPs and basins. During the monsoon months, when the majority of the precipitation occurs, the spread in between GCMs is large, especially for RCP 8.5 (for the upper Ganges ranging between (0 to +40%). Between basins the variation is also apparent; see for example the difference between the RCP 8.5 mean projections for the upper Ganges (+20%) and upper Indus (+5%). There is also seasonal variation between projections; for example in the Upper Ganges the RCP 8.5 mean projection is +25% for the monsoon months and 0% during winter months.

8.2 Future glacier extent

As described in section 7.2, we provide a basin scale projection of glacier extent with a monthly time step for 2008-2050. This means we make a separate projection for each of the five basins for each of the GCMs. The changing glacier extent is updated every month in the model for transient runs from 2008 until 2050 (Figure 34). As our approach requires calibration using the average mass balance during the climatic reference period (1998-2007) in a basin, this leads to a generalization of glacier changes in a particular basin. The response of individual glaciers to climate change is not simulated. As dynamic ice flow cannot be simulated at the 1 km grid scale, the parameterization becomes necessary. The parameterization is calibrated using basin scale mass balance signals as derived using ICESAT [*Kääb et al.*, 2012] (Table 8). Although the uncertainty in the ICESAT signal is large, it provides a better estimate of basin-scale glacier mass balance compared to sparse field-observed glacier mass balance records, which are biased towards smaller, easily accessible glaciers. For example, when calculating a basin scale glacier mass balance for the upper Indus basin using field-observed mass balance records [*Bolch et al.*, 2012] -0.69 m w.e. is obtained for the reference period, whereas ICESAT observations indicate -0.15 m w.e. as glacier mass balance for the same period in the same basin.

Table 8: Basin scale mass balance signals used for calibration of the glacier area change parameterization.

	Indus	Ganges	Brahmaputra	Salween	Mekong
Mass balance 2003-2008 (m w.e. yr^{-1})	-0.15	-0.32	-0.30	-0.30	-0.30
Remaining glacier area 2050 (%)	72-80	52-64	55-69	33-56	32-61

The projected changes in temperature are the more important driver for future changes in glacier area compared to the projected changes in precipitation and intra-annual variability in climate change signals has to be considered because of the seasonality in glacier accumulation and ablation [*Lutz et al.*, 2012]. In general, the RCP 4.5 projections show the smaller decreases in the projected glacier decrease range. However, as the projected changes in temperature and precipitation partly overlap for the two RCPs (Figure 33), this is also true for the glacier change projections. Strongest relative decreases in glacier area are expected for the Salween and Mekong basins (-33% - -56% and -32% - -61% respectively), since their current glacier areas are smallest. For the Indus basin a decrease in glacier extent ranging from -20% to -28% is projected based on the 8 selected GCMs. The Indus shows the smallest decrease, because it has the largest glacier area, although it has the highest projected increases in temperature and smallest increase (or decrease) in precipitation. Changes in glacier area in the Ganges and Brahmaputra show similar trends. The range of projections in these two basins is also similar as they have a similar range of changes in future temperature. Although the precipitation projections for the upper Ganges have a large spread, this does not result in a large spread in

glacier area projections, showing that changes in temperature are the most important drivers of glacier area change.

The necessary parameterization of glacier area change has the limitation that individual glaciers are not modeled and the same glacier mass balance is assumed for the entire basin. Thus, in the simulation all grid cells with glaciers have the same fractional glacier cover change in the future. In reality, variation in glacier change can be large within a basin. For example in the Indus basin, glaciers have been advancing in recent decades, while glacier retreat was observed in other parts [*Hewitt*, 2005].

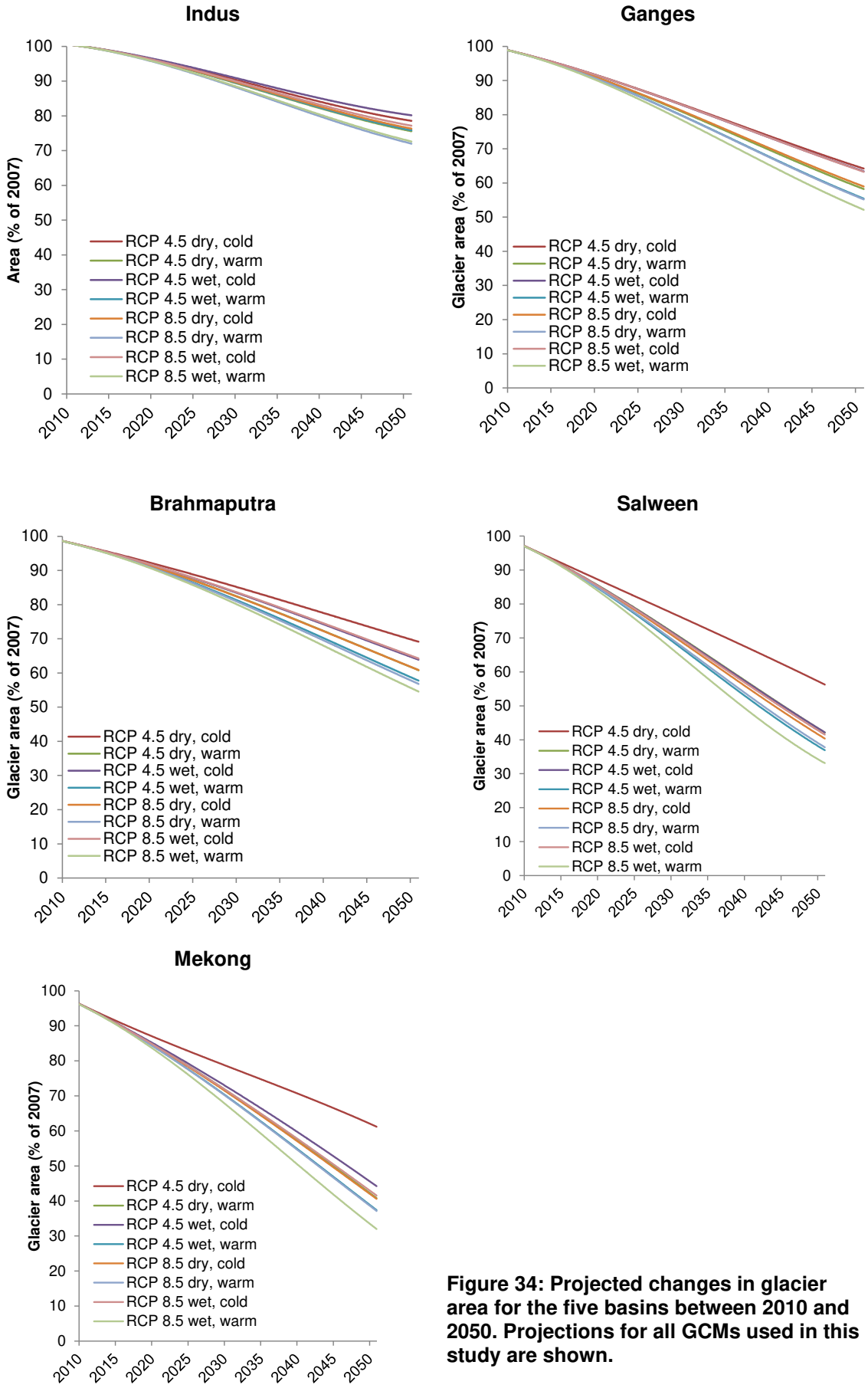

Figure 34: Projected changes in glacier area for the five basins between 2010 and 2050. Projections for all GCMs used in this study are shown.

8.3 Future water availability

To calculate the future water availability the calibrated and validated hydrological model is forced with climate change scenarios. For each year from 2008 until 2050 a random year is selected from the reference period. Subsequently the delta grids for temperature and precipitation are used to correct the high-resolution temperature and precipitation data from the randomly selected years from the reference period. Transient runs are done for two RCP's for the BCCR RCM and the four selected GCMs. In total 2 x 5 = 10 projections are made. In this paragraph, results for the runs with eight GCMs are discussed. Runs forced with the BCCR RCM are discussed in chapter 9.

As seen in Figure 35, for RCP 4.5 the flows for all basins increase slightly during the first decade (2011-2020). For the Salween and Mekong flows decrease in 2021-2030 but increase afterwards. For the Ganges and Brahmaputra the changes in terms of total discharge are minimal until 2040, but then increase. For the Indus, increases in flow are expected for all decades for most GCMs, although the spread is large, also showing the possibility of slightly decreasing flow. The projections have a large spread for the Indus, Salween and Mekong, while the spread is smaller for the Ganges and (in particular) Brahmaputra. For all basins, it is most likely that flows in 2041-2050 have increased with respect to 1998-2007.

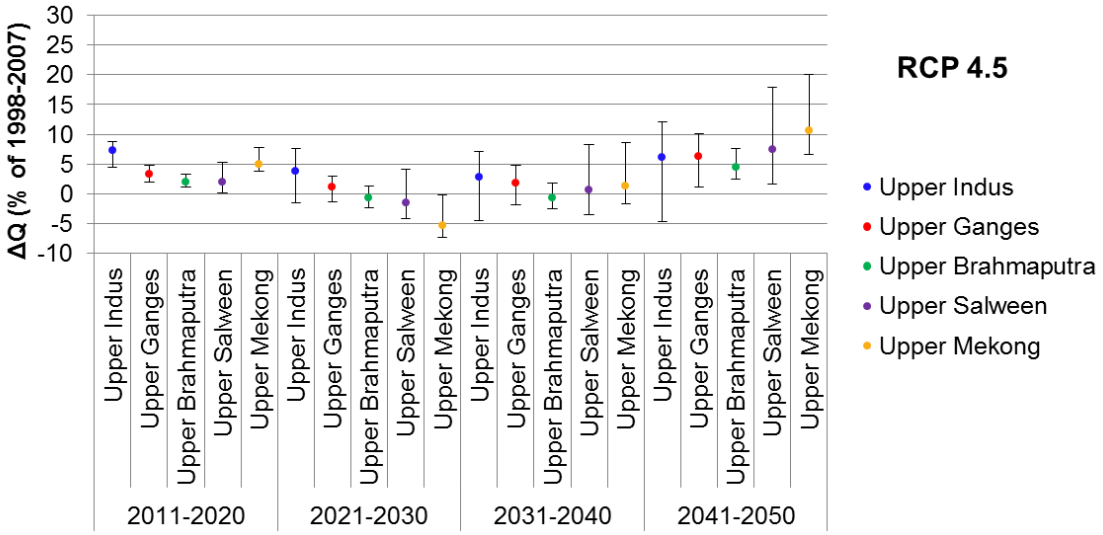

Figure 35: Changes in discharge per basin for four time intervals with respect to the reference period. The plot shows model results for RCP 4.5. The dots are the average output of four GCMs. The whiskers indicate the maximum and minimum projection based on four GCMs.

For RCP 8.5 (Figure 36), the trends are similar as for RCP 4.5. For the Ganges and Brahmaputra however, the RCP 8.5 mean projection shows a stronger increase in discharge in 2041-2050, compared to the same period for RCP 4.5. However, the spread in projections is large, especially for the Ganges. For the Indus the projected decrease in discharge is somewhat smaller for RCP 8.5 compared to RCP 4.5. Note that the spread of projections in rain-dominated basins is larger for RCP 8.5 compared to RCP 4.5. This is mainly due to the larger spread in precipitation projections in the GCMs used for RCP 8.5 compared to the GCMs used for RCP 4.5 (as seen in Figure 33)

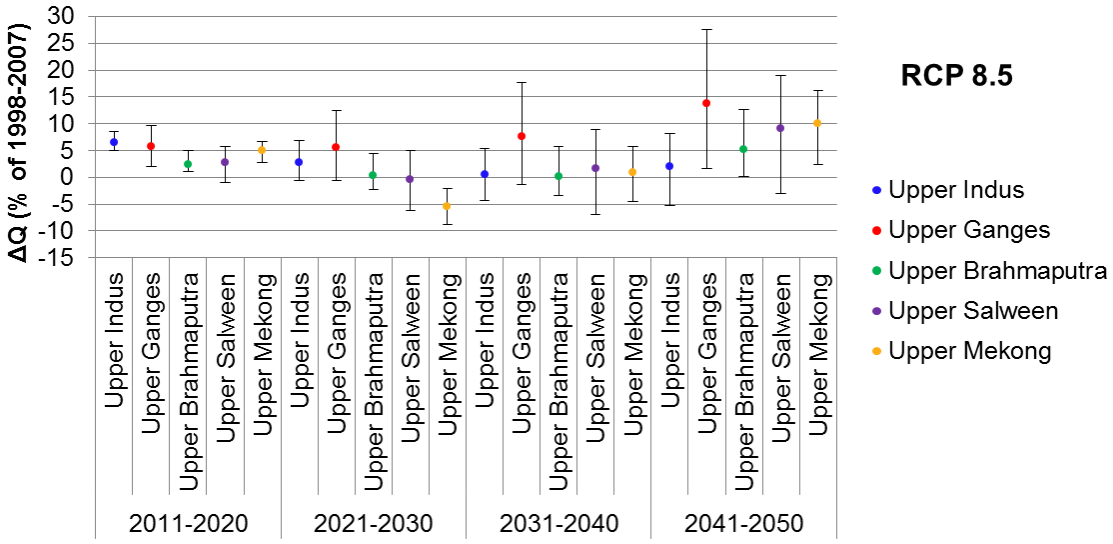

Figure 36: Changes in discharge per basin for four time intervals with respect to the reference period. The plot shows model results for RCP 8.5. The dots are the average output of four GCMs. The whiskers indicate the maximum and minimum projection based on four GCMs.

Looking at the changes in discharge between 1998-2007 and 2041-2050 for major rivers in the basins (Figure 37), little change in discharge for the rivers in the Indus basin is observed. The glacier melt component is very important for total flow of these rivers. Although the glacier area is decreasing, total flow does not decrease because the amount of melt water generated per surface unit of ice is increasing with increasing temperatures. For the rivers in the Ganges basin, the discharge changes very little for RCP 4.5. For RCP 8.5 however, increased flows are observed during the flow peak in the monsoon season. The spread in projections for RCP 8.5 is relatively large, in particular for the Ghaghara river, where a large spread is observed for precipitation projections. For the Brahmaputra, the changes in flow are small for both RCPs, but a slight shift in the flow peak is expected in RCP 8.5 to later in the year. For the Salween and Mekong increased flows are expected for August-May, while decreasing flows are expected in June and July. During 2041-2050, the peak in flow is expected to be in September and is expected to be higher than the current peak flow in July. In general, the projections have a larger spread for RCP 8.5 compared to RCP 4.5.

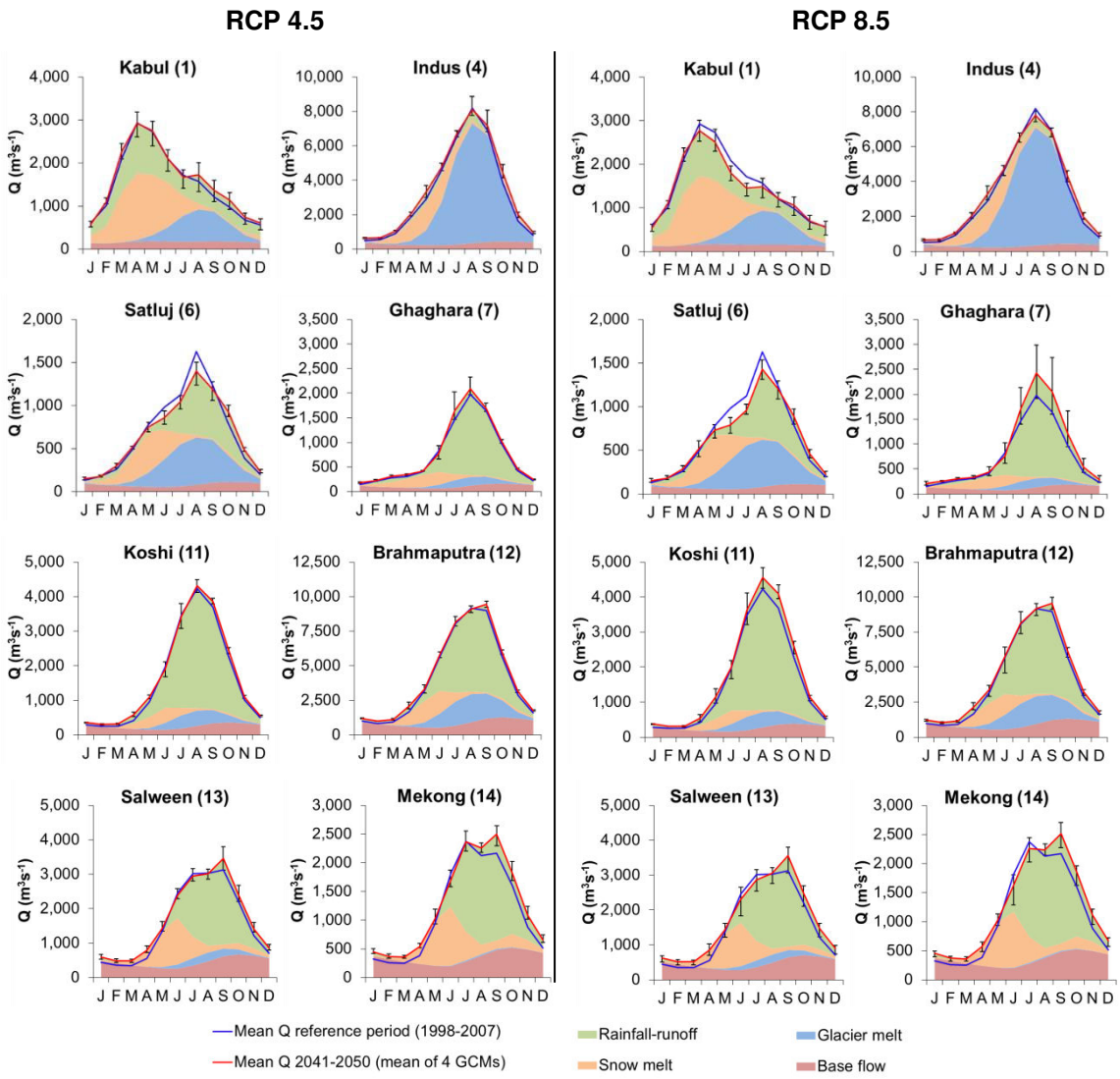

Figure 37: Changes in discharge for major rivers in the basins. Red lines are the average discharge in 2041-2050 based on four GCMs; the whiskers indicate the maximum and minimum projection based on four GCMs. The blue lines are the average simulated flow for 1998-2007.

Table 9 and Figure 38 show the changes in hydrological regime for the two most extreme scenarios when the total HICAP domain is considered (RCP 4.5 cold & wet case, RCP 8.5 warm and dry case). Note that these don't have to be the most extreme cases for each particular basin. The total range of projections per basin is discussed in section 8.3. For the RCP 4.5 cold & wet case, total annual runoff increases slightly for all basins (2-7%). For the RCP 8.5 warm and dry case, total runoff decreases in the upper Indus (-5%) and stays the same in the upper Brahmaputra. For the upper Ganges, Salween and Mekong the total runoff increases by 5-14%. In the Indus basin RCP 4.5 cold and wet case, the amount of generated water increases for all components except snow melt. In the RCP 8.5 warm and dry case, only the amount of glacier melt water increases, while the other components decrease. The amount of glacier melt water decreases in both cases for all basins except the Indus basin. In both cases, the amount of rainfall-runoff increases for all basins (except the Indus basin in the RCP 8.5 warm, dry case), while the amount of snow melt decreases.

In Figure 39 and Figure 40, the hydrological regime in 2041-2050 is displayed for major streams, for both cases. Comparing to the reference situation (Figure 29), the decline in glacier melt and snow melt contribution for all basins except Indus is clear in both figures, indicating the transition from melt water dominated rivers towards rain water dominated rivers for many major streams.

Table 9: Hydrological characteristics for the five basins in 2041-2050. Results for the two extreme projections are listed (RCP 4.5 cold, wet case and RCP 8.5 warm, dry case).

	RCP 4.5 cold, wet case (ΔT Q10, ΔP Q90)					RCP 8.5 warm, dry case (ΔT Q90, ΔP Q10)				
	Total annual runoff (mm (*% of reference*))	Glacier melt (mm (*% of reference*))	Snow melt (mm (*% of reference*))	Rainfall runoff (mm (*% of reference*))	Baseflow (mm (% of reference))	Total annual runoff (mm, (*% of reference*))	Glacier melt (mm (*% of reference*))	Snow melt (mm (*% of reference*))	Rainfall runoff (mm (*% of reference*))	Baseflow (mm (*% of reference*))
Upper Indus	614 (107)	237 (102)	121 (97)	186 (121)	71 (115)	544 (95)	255 (109)	92 (74)	137 (89)	60 (97)
Upper Ganges	1146 (105)	113 (90)	90 (96)	775 (108)	169 (112)	1237 (114)	120 (96)	62 (66)	870 (121)	185 (122)
Upper Brahmaputra	726 (105)	98 (89)	58 (93)	445 (109)	125 (112)	692 (100)	100 (91)	39 (63)	428 (105)	124 (111)
Upper Salween	488 (102)	26 (65)	116 (88)	224 (111)	122 (114)	502 (105)	26 (65)	87 (66)	246 (122)	144 (135)
Upper Mekong	494 (106)	3 (72)	125 (83)	237 (116)	129 (122)	507 (109)	3 (72)	99 (66)	257 (126)	149 (141)

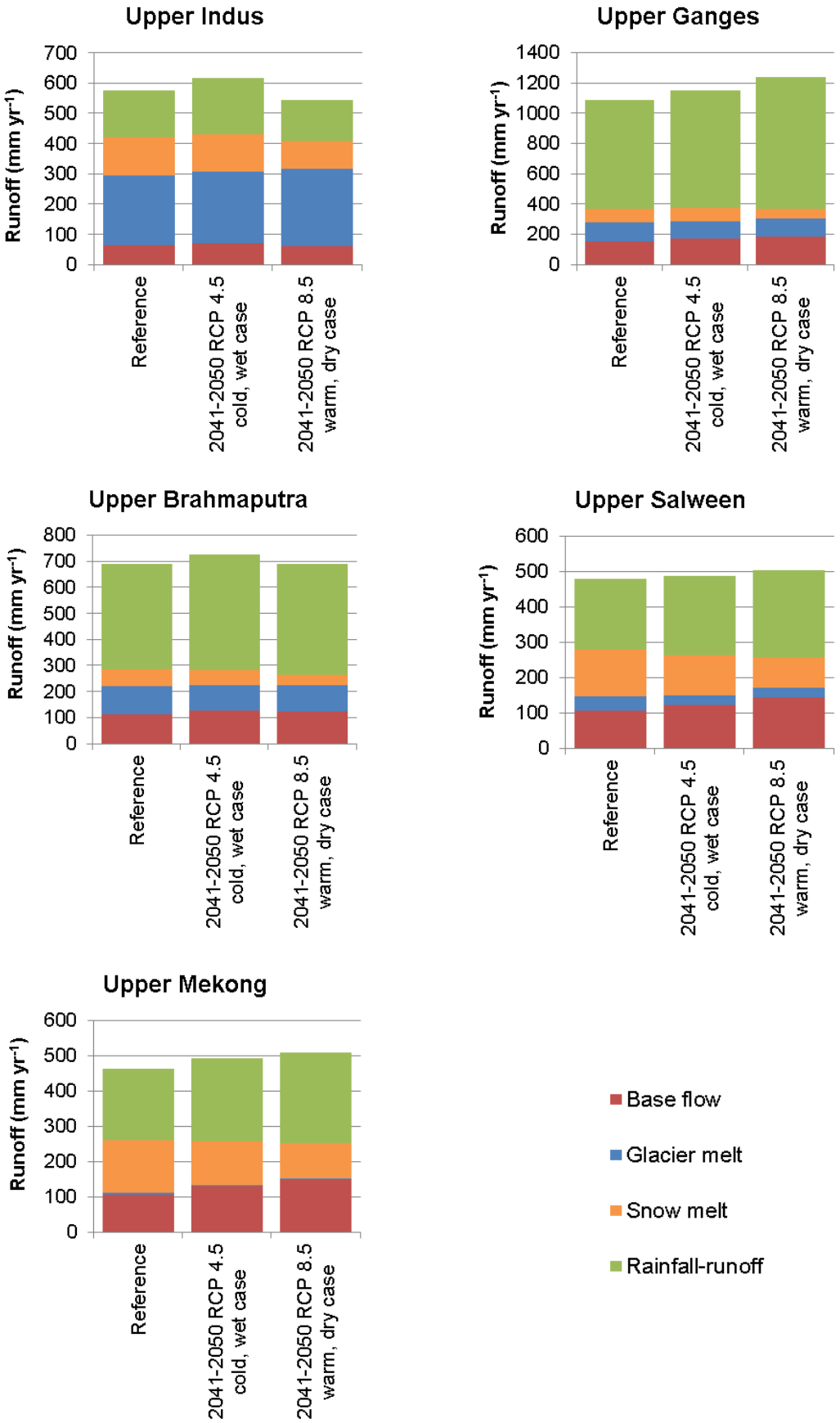
Upper Indus
Runoff (mm yr-1)
700
600
500
400
300
200
100
0
Reference
2041-2050 RCP 4.5 cold, wet case
2041-2050 RCP 8.5 warm, dry case
Upper Ganges
Runoff (mm yr-1)
1400
1200
1000
800
600
400
200
0
Reference
2041-2050 RCP 4.5 cold, wet case
2041-2050 RCP 8.5 warm, dry case
Upper Brahmaputra
Runoff (mm yr-1)
800
700
600
500
400
300
200
100
0
Reference
2041-2050 RCP 4.5 cold, wet case
2041-2050 RCP 8.5 warm, dry case
Upper Salween
Runoff (mm yr-1)
600
500
400
300
200
100
0
Reference
2041-2050 RCP 4.5 cold, wet case
2041-2050 RCP 8.5 warm, dry case
Upper Mekong
Runoff (mm yr-1)
600
500
400
300
200
100
0
Reference
2041-2050 RCP 4.5 cold, wet case
2041-2050 RCP 8.5 warm, dry case
Base flow
Glacier melt
Snow melt
Rainfall-runoff

Figure 38: Contribution to total runoff specified for runoff contributors at basin scale. Plots show the reference situation (1998-2007) and the situation in 2041-2050 for RCP 4.5 cold, wet case and RCP 8.5 warm, dry case.

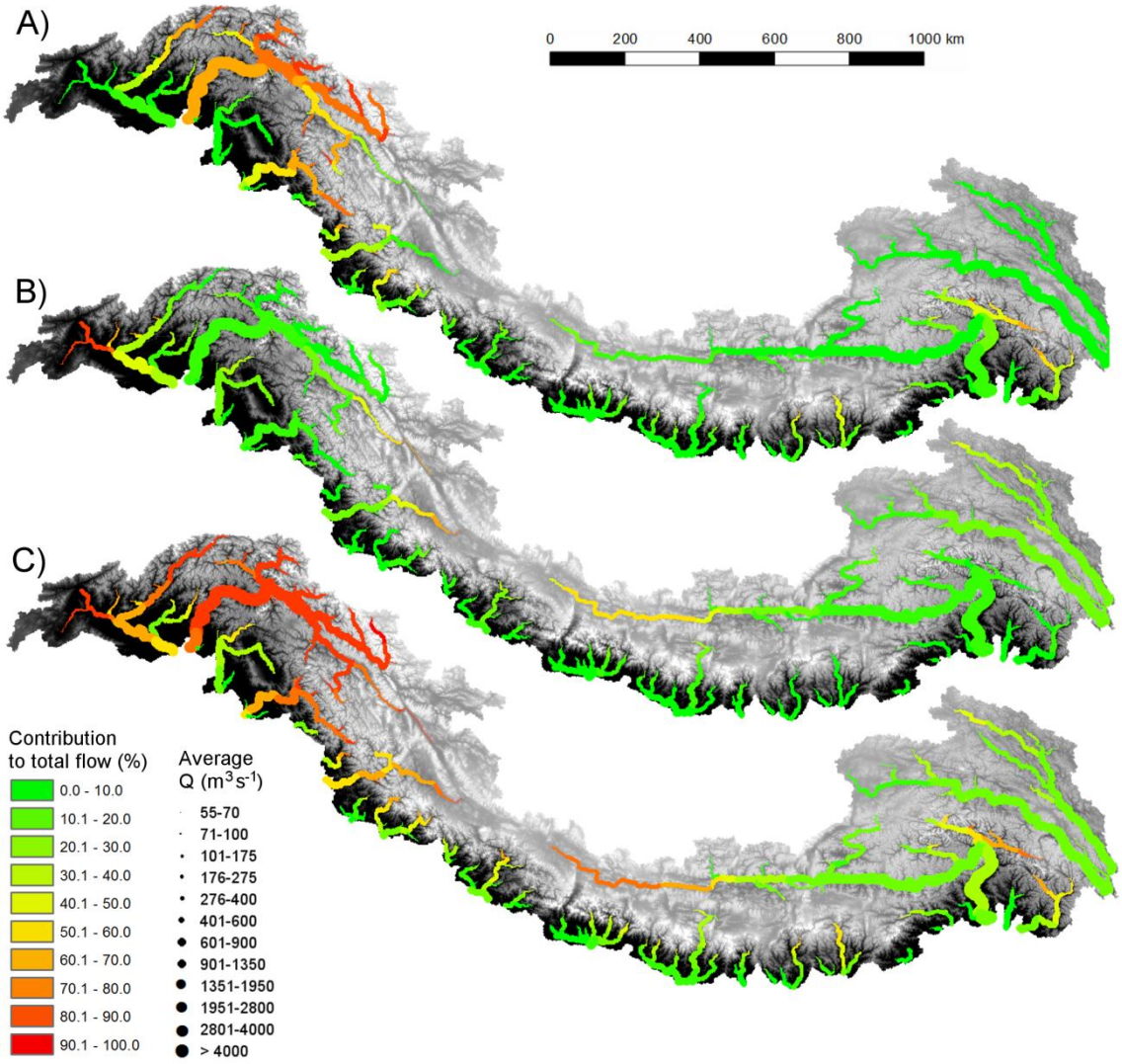

Figure 39: Average contribution of glacier melt (A), snow melt (B), glacier and snow melt combined (C) to total flow and average discharge during 2041-2050 in major streams in the model domain (all panels) Results are for HI-SPHY model forced with RCP 4.5 CCSM4-r5i1p1 GCM (cold, wet) case.

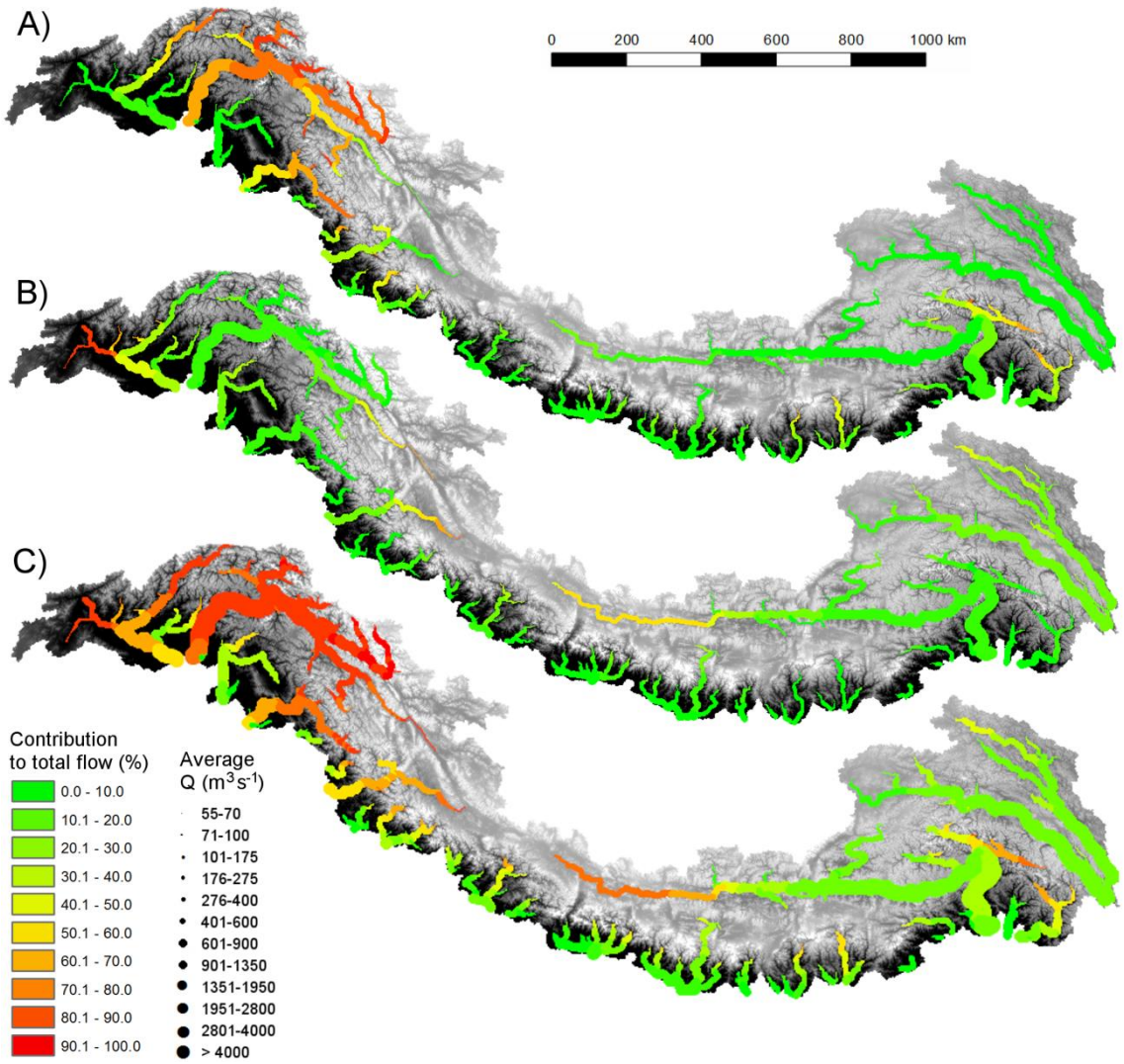

Figure 40: Average contribution of glacier melt (A), snow melt (B), glacier and snow melt combined (C) to total flow and average discharge during 2041-2050 in major streams in the model domain (all panels) Results are for HI-SPHY model forced with RCP 8.5 IPSL-CM5A-LR-r4i1p1 GCM (dry, warm case).

9 Model runs forced with BCCR RCM data

9.1 Bjerknes Centre for Climate Research Regional Circulation Model

The BCCR RCM data has a nominal resolution of 0.12° x 0.12°. These data where projected in the model projection and downscaled to model resolution using a DEM at 1x1 km resolution. Comparing the BCCR RCM data to the gridded air temperature (PRINCETON) and precipitation data (APHRODITE) yields the following conclusions:

- Maximum air temperature generated with the BCCR model is generally colder than the PRINCETON based reference dataset
- Minimum air temperature generated with the BCCR model is colder in the north, but warmer in the south (where most glaciers are)
- Precipitation at high altitude is unrealistically high for the BCCR dataset

The observed biases in precipitation and air temperature for the BCCR dataset compared to PRINCETON and APHRODITE logically results in an overestimation of simulated runoff. This is very considerable (~factor 3 for Brahmaputra and ~factor 2 for Indus, Ganges). Because of this, the analysis of results for future runoff focuses on changes in runoff between the reference period and the future period, rather than absolute numbers for projected runoff. Because parts of the Salween and Mekong river basins are not included in the BCCR RCM model domain, these river basins are not included in the analysis.

The HI-SPHY model, including the parameterization for changes in future glacier extent, is run for the reference period (1998-2007) forced with the BCCR RCM reference period data. For the future, two runs are done: One run forced with the BCCR RCM RCP 4.5 data from 2008 until 2050 and a second run forced with the BCCR RCM RCP 8.5 data from 2008 until 2050. For the parameterization of future glacier extent a correction is applied to the precipitation input (precipitation * 0.5), to yield realistic changes in glacier area.

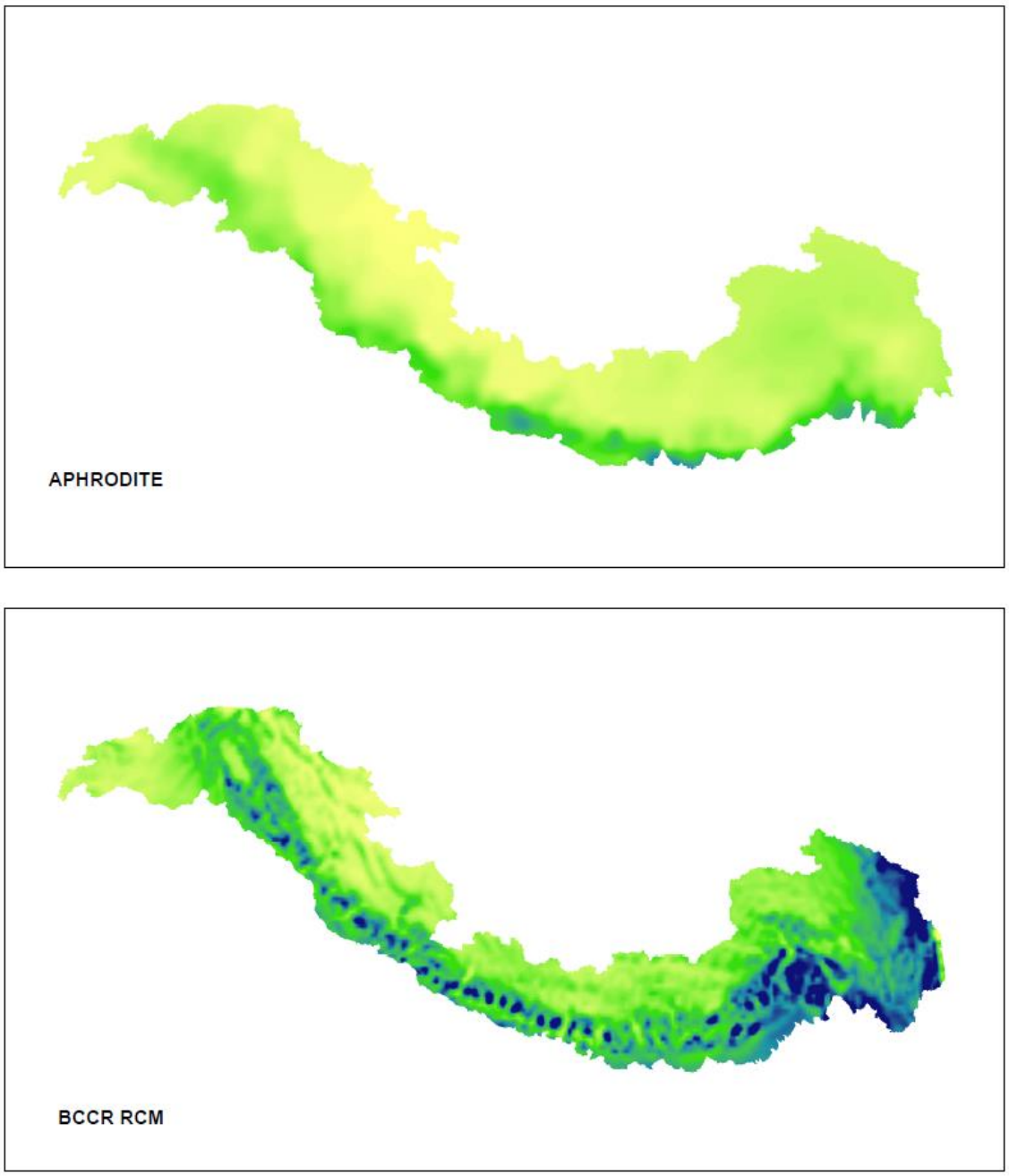

Figure 41: Annual average precipitation in model domain for 1998-2005 according to APHRODITE (upper panel) and BCCR RCM (lower panel).

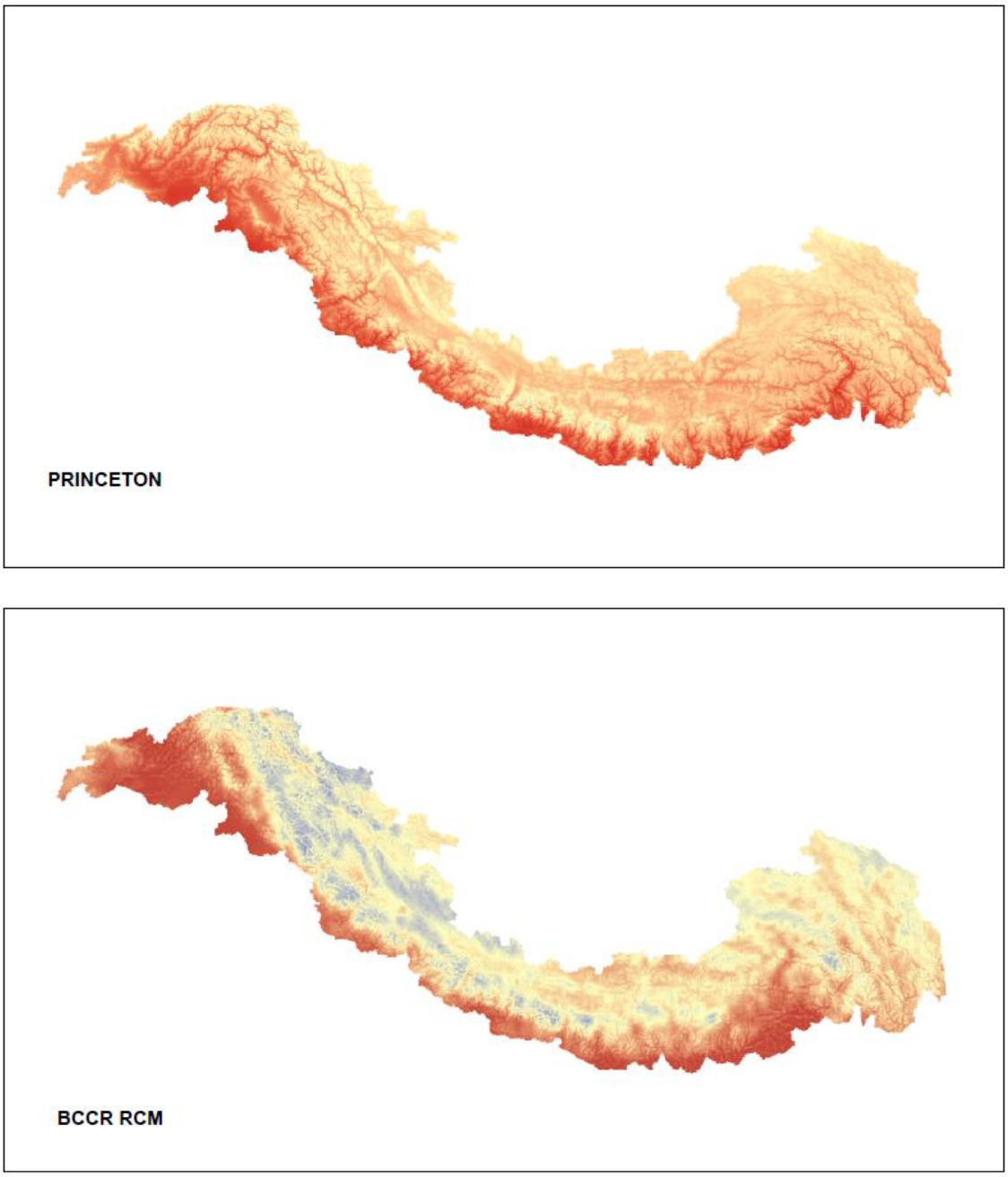

Figure 42: Average maximum air temperature in model domain for 1998-2005 according to PRINCETON (upper panel) and BCCR RCM (lower panel).

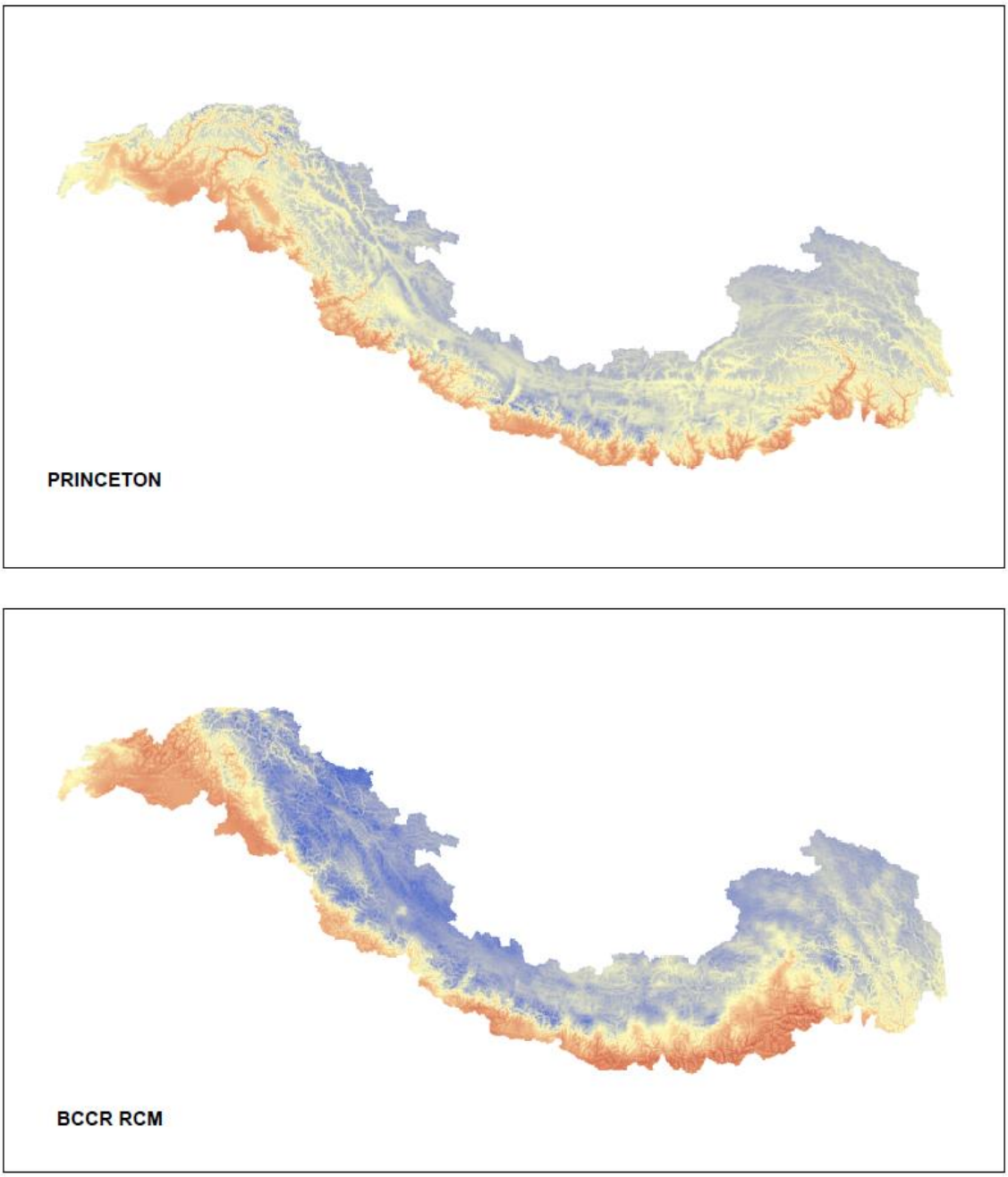

Figure 43: Average minimum air temperature in model domain for 1998-2005 according to PRINCETON (upper panel) and BCCR RCM (lower panel).

9.2 Changes in hydrological regime

Figure 44 shows the average annual hydrograph for the reference period (1998-2007) for major river outlets from the model domain. Note that the simulated runoff is very unrealistic due to biases in precipitation and air temperature as described in section 9.1. See for comparison the simulated flows for the reference period when forced with the PRINCETON/APHRODITE climate data (red line) in the figure.

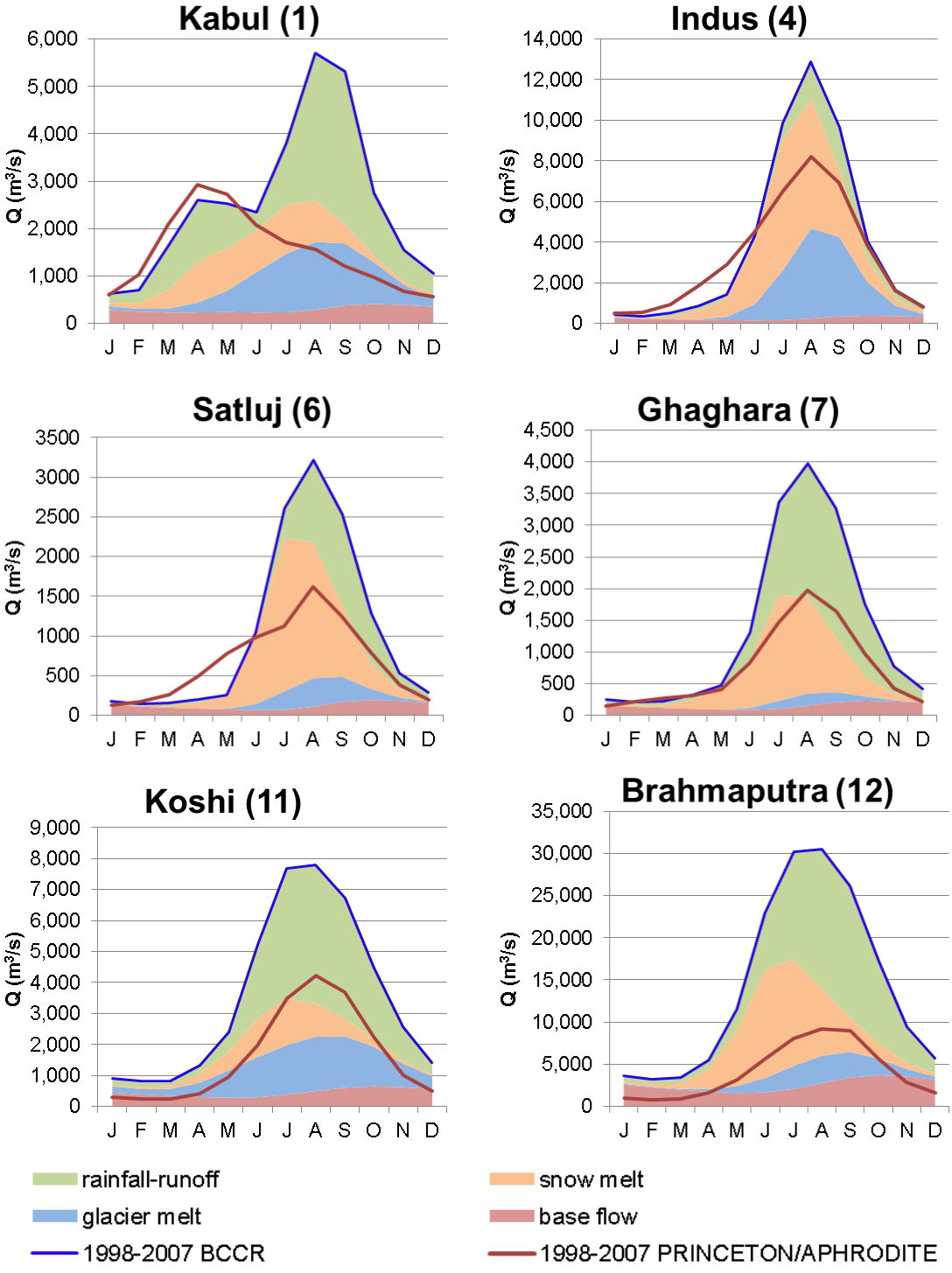

Figure 44: Average annual hydrographs with specification of runoff contributors for major rivers in the basins for BCCR RCM reference (1998-2007). The hydrograph for the

model forced with PRINCETON/APHRODITE forcing is shown in red. Numbers in parentheses refer to locations in Figure 24.

Since the simulated flow during the reference period is unrealistic we analyse the relative changes between the reference period and future period. According to model forced with the BCCR RCM, a decrease in total flow is expected for the upper Indus, and parts of upper Ganges (Ghaghara) by the year 2050 (Figure 45). For the Brahmaputra and Koshi changes are small. For the Koshi a slight increase in flow is projected. The projected changes in the hydrological regime are very similar for RCP 4.5 and RCP 8.5.

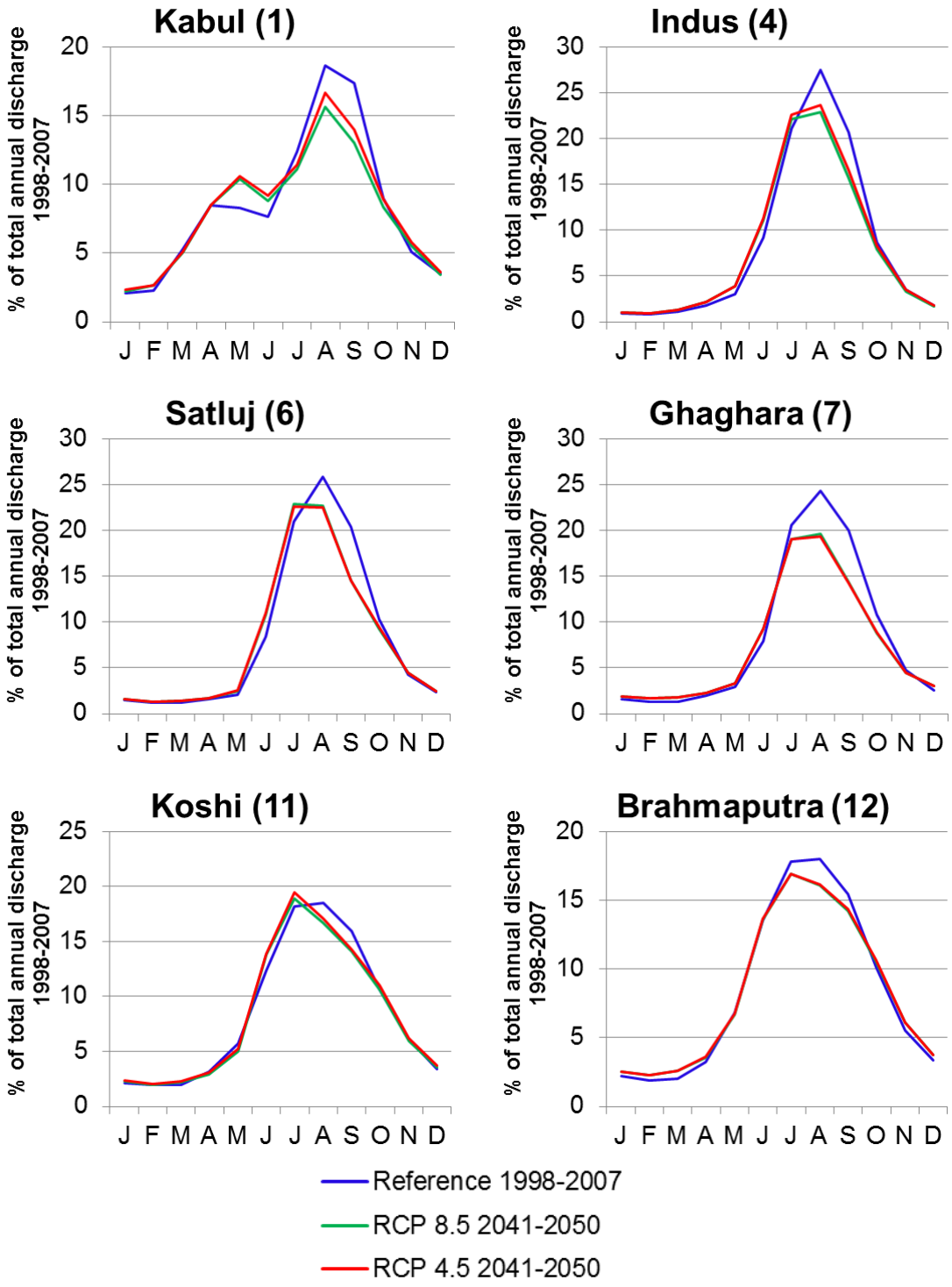

Figure 45: Hydrographs for major rivers in the basins for BCCR RCM reference, RCP 4.5 and RCP 8.5. The numbers represent the monthly share of the average total annual discharge during 1998-2007. Numbers in parentheses refer to locations in Figure 24.

Looking at the seasonal changes per month (Figure 46, Figure 47), the general observation for the upper Indus is a strong projected decrease in flow for the second half of the year (July-December), while increases in flow are projected for May and June. For Satluj river increases are projected for the entire first half of the year. In the upper Brahmaputra basin, decreases in flow are projected for the monsoon months, while flow is projected to increase for the rest of the

year. In the major rivers in the upper Ganges basin the changes differ locally due to very regional difference in projected precipitation changes.

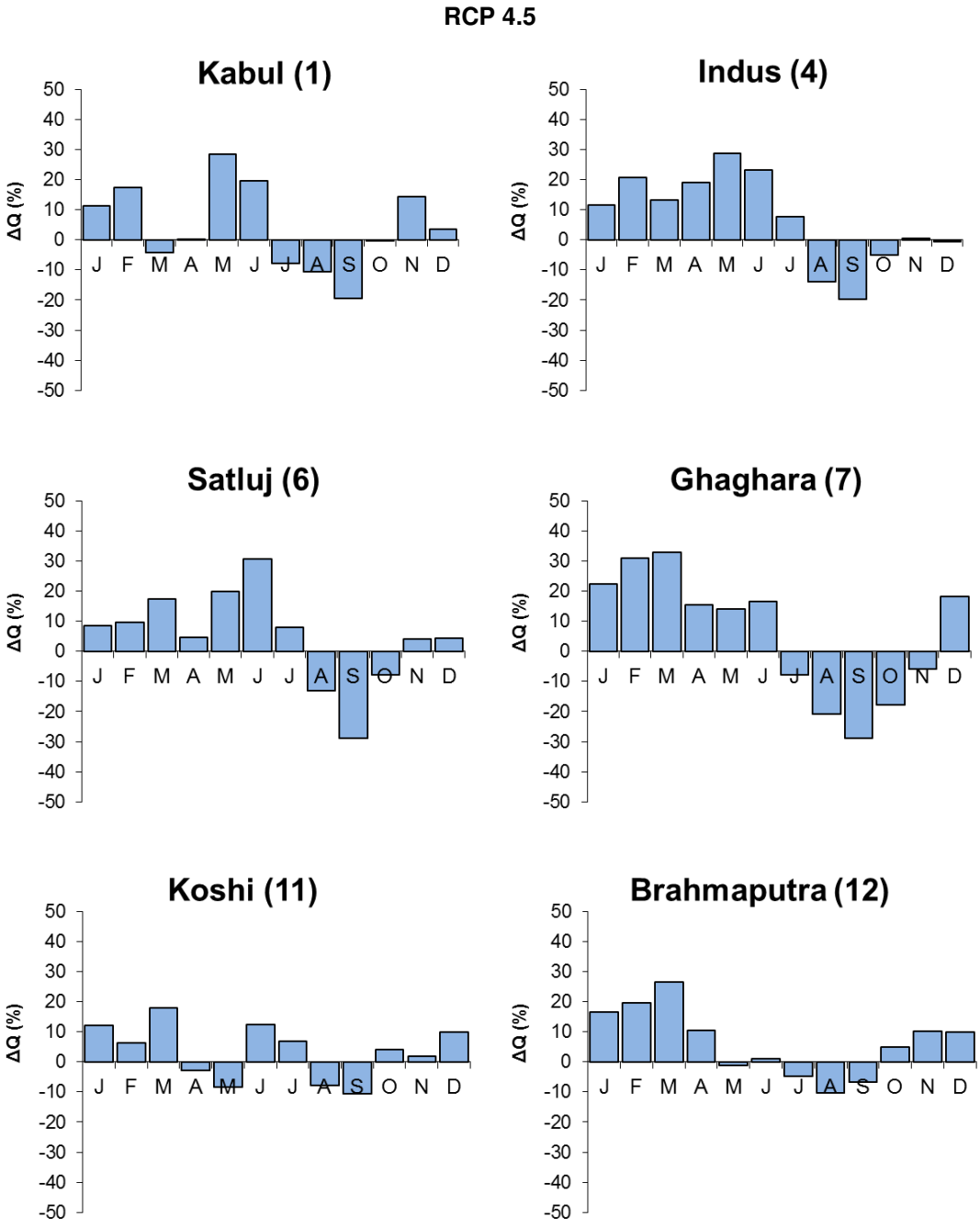

Figure 46: Changes in discharge for major rivers in the basins for BCCR run RCP 4.5. The changes represent changes for 2041-2050 with respect to 1998-2007. Numbers in parentheses refer to locations in Figure 24.

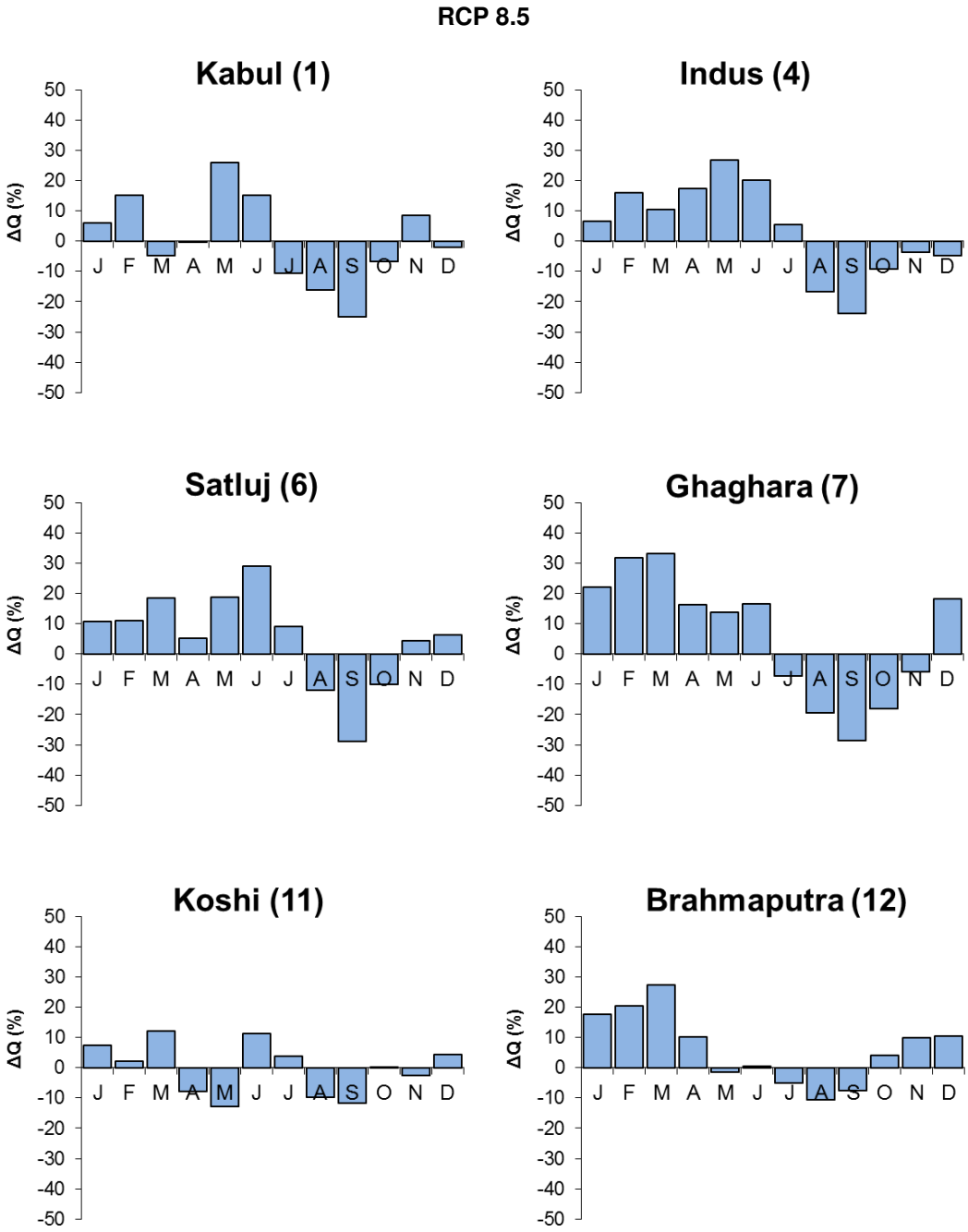

Figure 47: Changes in discharge for major rivers in the basins for BCCR run RCP 4.5. The changes represent changes for 2041-2050 with respect to 1998-2007. Numbers in parentheses refer to locations in Figure 24.

10 Pilot catchments

For three pilot catchments a detailed analysis is conducted (Figure 2). This analysis focuses on two components. First of all an uncertainty analysis is conducted to analyze the impact of climate model uncertainty at a monthly timescale and per flow component using the HI-SPHY model. Secondly we focus on assessing changes in hydropower potential using the Water Evaluation and Planning system (WEAP). The analyses for the pilot catchments are performed only done for the model runs forced by the downscaled GCMs.

10.1 Uncertainty analysis

Hawkins and Sutton (2009, 2010) identified three main sources of uncertainty in future climate projections: i) model uncertainty due to the structural differences among GCMs, by which different models produce different projections for the same radiative forcing; ii) scenarios uncertainty due to different radiative forcing; and iii) uncertainty due to the natural climate variability. They showed that the first source of uncertainty is the larger throughout the century for both temperature and precipitation. Besides uncertainty in future runoff as a result of the uncertainty in the climate change projections, the simulated runoff changes are subject to other uncertainties. These include parametric uncertainty, uncertainty in climate evolution, uncertainty in climatic forcing for the reference period, uncertainty in discharge time series used for calibration and uncertainties stemming from simplifications and assumptions applied to the model. However, since the uncertainty in future runoff projections as a result of the uncertainty in future climate as projected by different GCMs is the largest source of uncertainty, we make a detailed analysis of this uncertainty for the projections used for 2041-2050 for the four pilot catchments.

10.1.1 Projected changes in runoff

The projected changes in flow for 2041-2050 at the pilot catchment's outlets are displayed in Figure 48 (RCP 4.5) and Figure 49 (RCP 8.5). For the Chitral catchment in RCP 4.5 a slight decrease in flow is projected for April-June, whereas a slight increase in flow is projected for August-December. RCP 8.5 shows the same trend but the projected decrease and increase are somewhat larger. Besides, the range of projections is larger. For the Lhasa catchment, only small changes in flow are projected for RCP 4.5. For RCP 8.5, the mean projection indicates little change, but the uncertainty is larger than for RCP 4.5. For both RCPs flows start to increase earlier in the season due to earlier snow melt. For the Dudh Koshi and Tama Koshi catchments, the projected changes in flow are rather small. In general, for RCP 4.5 a slight decrease in flow is projected, while a slight increase is projected for RCP 8.5. The range of projections according to the different GCMs shows that a slight decrease in flow as well as a slight increase in flow can be expected for both RCPs.

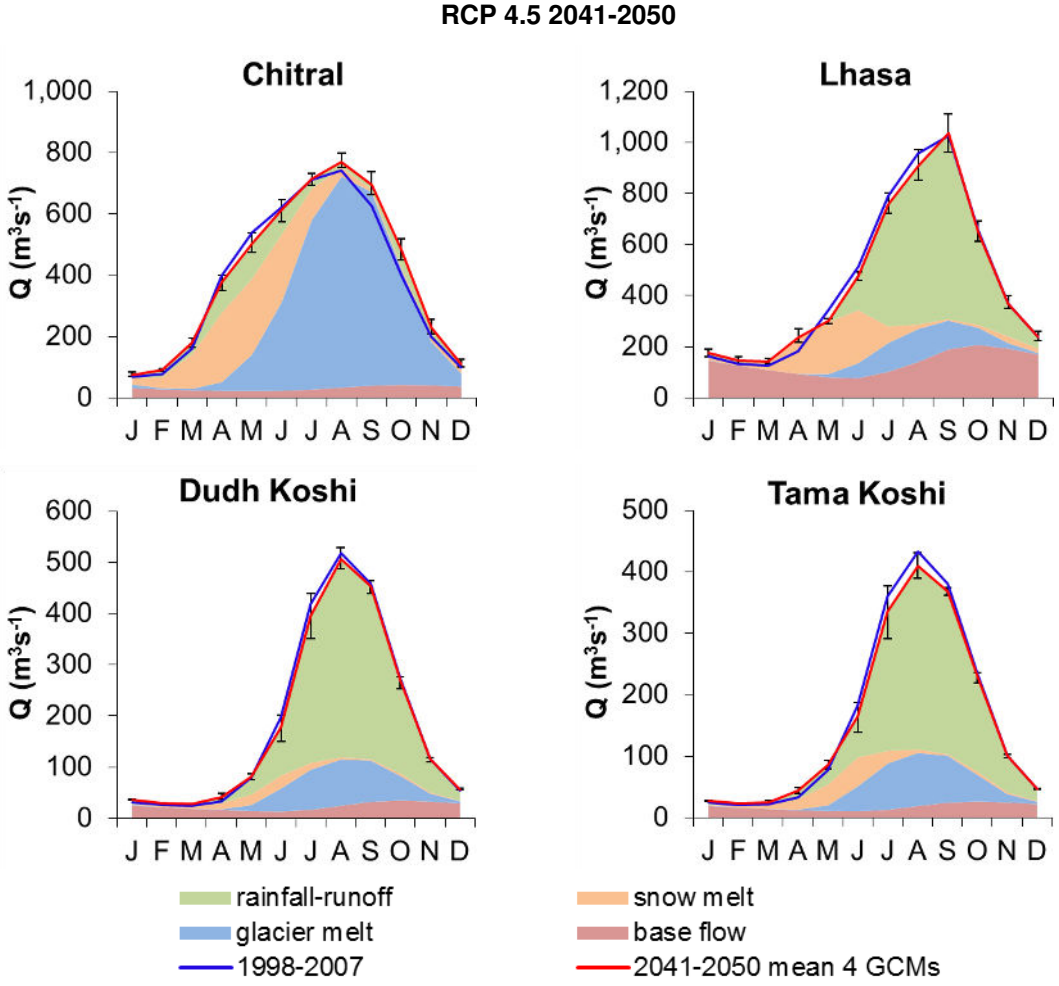

Figure 48: Changes in discharge for the outlets of the four pilot catchments for RCP 4.5. Red lines are the average discharge in 2041-2050 based on four GCMs; the whiskers indicate the maximum and minimum projection based on four GCMs. The blue lines are the average simulated flow for 1998-2007.

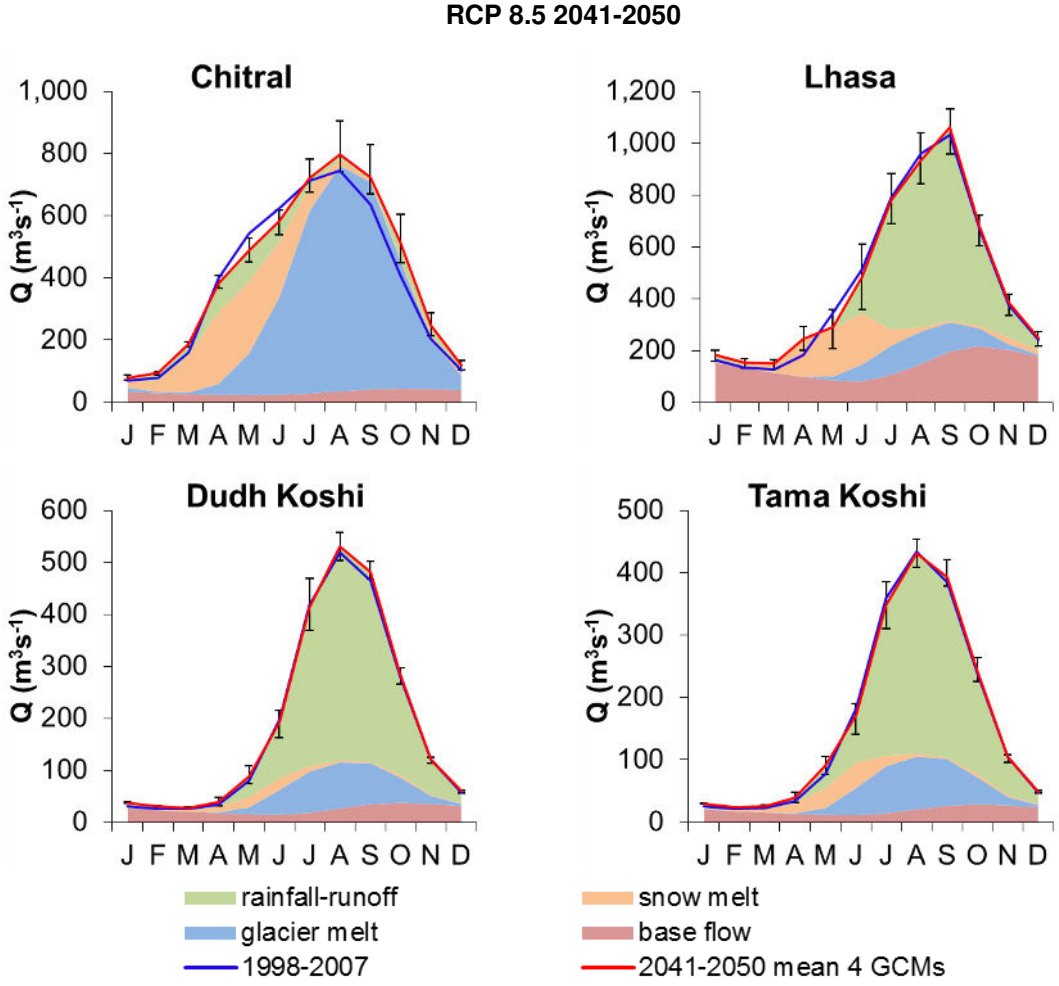

Figure 49: Changes in discharge for the outlets of the four pilot catchments for RCP 8.5. Red lines are the average discharge in 2041-2050 based on four GCMs; the whiskers indicate the maximum and minimum projection based on four GCMs. The blue lines are the average simulated flow for 1998-2007.

10.1.2 Uncertainty in flow projections

The uncertainty in future runoff projections as a result of the uncertainty in future climate as projected by different GCMs is quantified at a monthly scale for both RCPs and all four pilot catchments. The uncertainty for each month is calculated according to the following steps:

- For each of the four GCMs within the RCP a mean flow is calculated for January to December during 2041-2050.
- A mean projection is calculated by averaging the four projections.
- A positive bias is defined as the difference between the mean projection and the maximum projection from the four GCMs
- A negative bias is defined as the difference between the mean projection and the minimum projection from the four GCMs
- The minimum bias and maximum bias are averaged
- The uncertainty is defined as the relative share of the average bias with respect to the projected flow.

For the Chitral catchment, the uncertainty in the total flow projection is largest in the late autumn and winter months (October-January) (Figure 50, Figure 51). For Lhasa, Dudh Koshi and Tama Koshi the uncertainty is large during April, May and June for RCP 8.5. For Dudh Koshi and Tama Koshi for RCP 4.5 the uncertainty is large during April, June and July. For RCP 8.5 the uncertainty for these three catchments is clearly highest during April, May and June. For RCP 4.5 the uncertainty is more homogenous throughout the year for Dudh Koshi, Tama Koshi and Lhasa. On the whole, the uncertainty for Chitral is largest during winter, whereas the uncertainty for the other three catchments is highest in spring. Largest uncertainty has the Lhasa catchment for RCP 8.5, during spring. In general, Chitral has the smallest uncertainty. This is because Chitral is dominated by glacier melt and the uncertainty in glacier melt is mostly related to change in temperature, which has a smaller spread than the projected precipitation change. The three other catchments are dominated by rainfall-runoff, with higher uncertainty due to the large spread in precipitation projections.

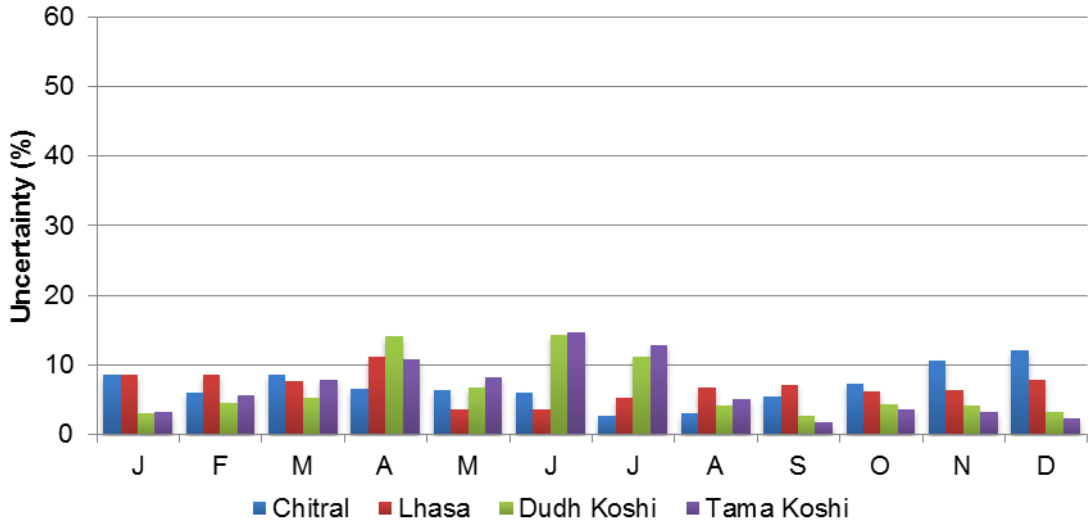

Figure 50: Uncertainty in total runoff RCP 4.5

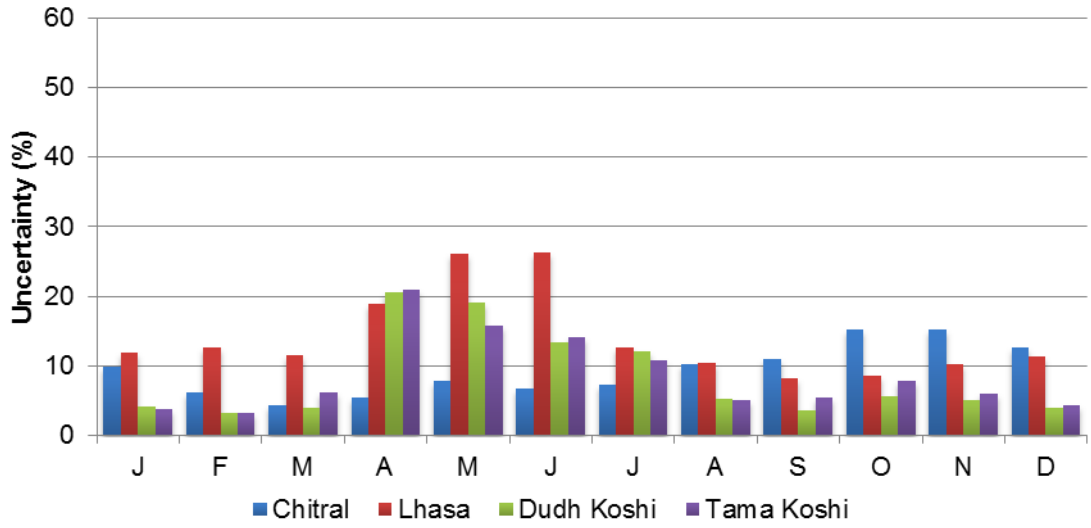

Figure 51: Uncertainty in total runoff RCP 8.5

10.1.3 Uncertainty in flow projection specified per runoff component

Besides assessing the uncertainty in total runoff, the uncertainty can be specified for each runoff component in the same way. For RCP 4.5 the uncertainty of glacier melt runoff is largest for the Lhasa catchment (Figure 52). In April and May the uncertainty gets as high as +/- 46%. For the Tama Koshi and Dudh Koshi catchments, the uncertainty is highest in May. For Chitral, the uncertainty of glacier melt projections is quite small, with maximum 19% in March, due to a small range in temperature projections in the catchment.

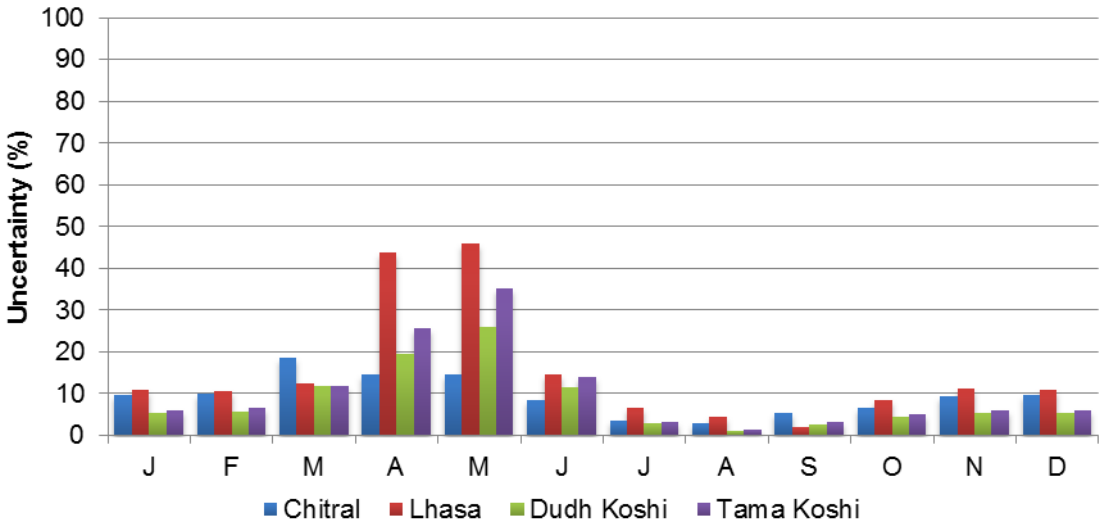

Figure 52: Uncertainty in glacier melt runoff RCP 4.5

For RCP 8.5, the uncertainty in glacier melt runoff for the Chitral catchment is slightly larger than for RCP 4.5, especially during October to February. The uncertainty for Lhasa is very high in April (+/- 88%, Figure 53). For Dudh Koshi and Tama Koshi the uncertainty in April and May is also higher for RCP 8.5 compared to RCP 4.5. For Lhasa, Dudh Koshi and Tama Koshi the uncertainty during other months is similar for RCP 4.5 and RCP 8.5.

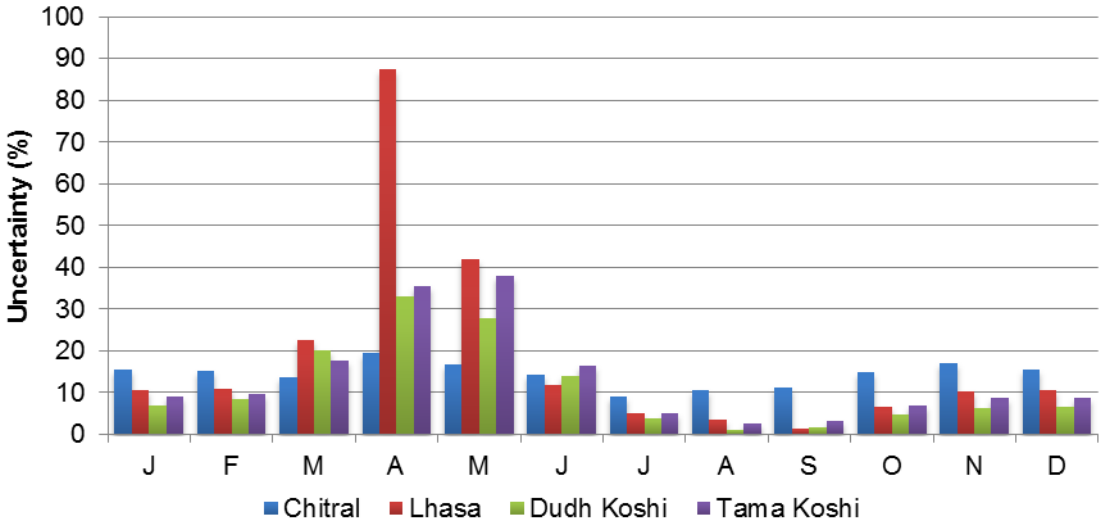

Figure 53: Uncertainty in glacier melt runoff RCP 8.5

The uncertainty in snow melt runoff is in general larger for RCP 8.5 compared to RCP 4.5 (Figure 54, Figure 55). For Chitral, Dudh Koshi and Tama Koshi the uncertainty is highest

during July, August and September. For Lhasa, the uncertainty is large in particular for RCP 8.5, during April to October.

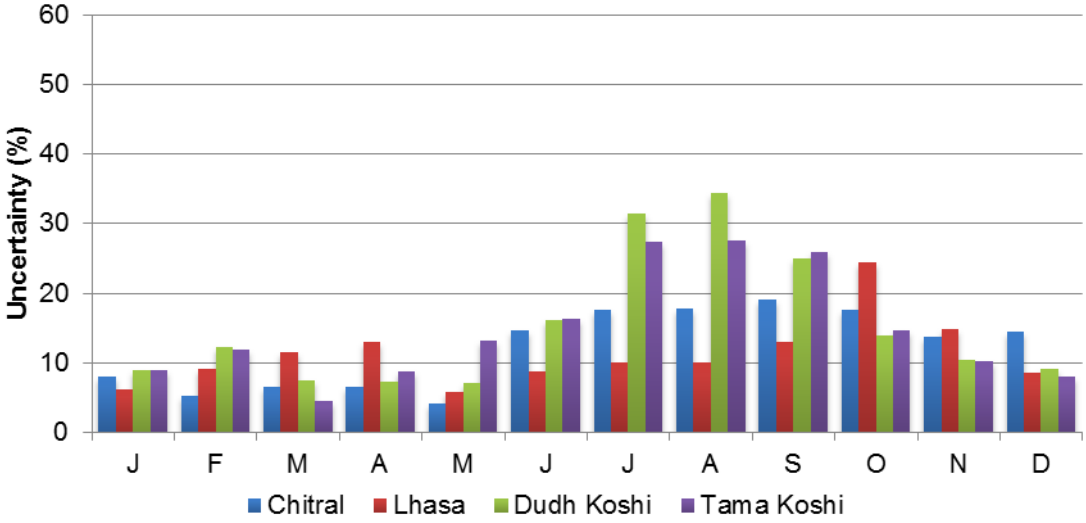

Figure 54: Uncertainty in snow melt runoff RCP 4.5

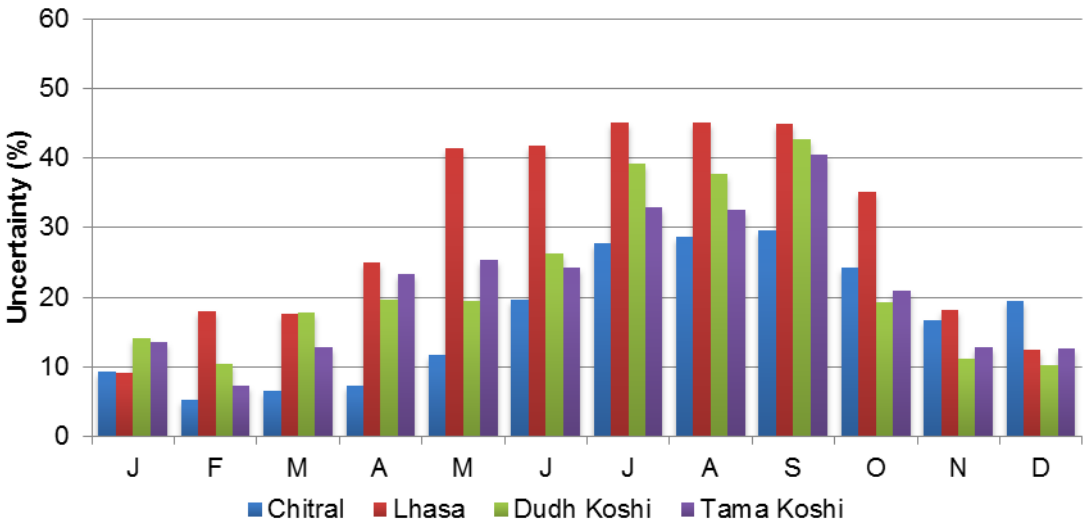

Figure 55: Uncertainty in snow melt runoff RCP 8.5

The uncertainty of rainfall-runoff for Chitral is largest during August to December (Figure 56, Figure 57). For Dudh Koshi and Tama Koshi the uncertainty is highest (up to +/- 85%) in March and April. For Lhasa catchment the uncertainty is highest during May and June. The uncertainty is larger for RCP 8.5 compared to RCP 4.5. The uncertainty in rainfall-runoff is directly related to the uncertainty in projected precipitation change which differs strongly in space and over the seasons.

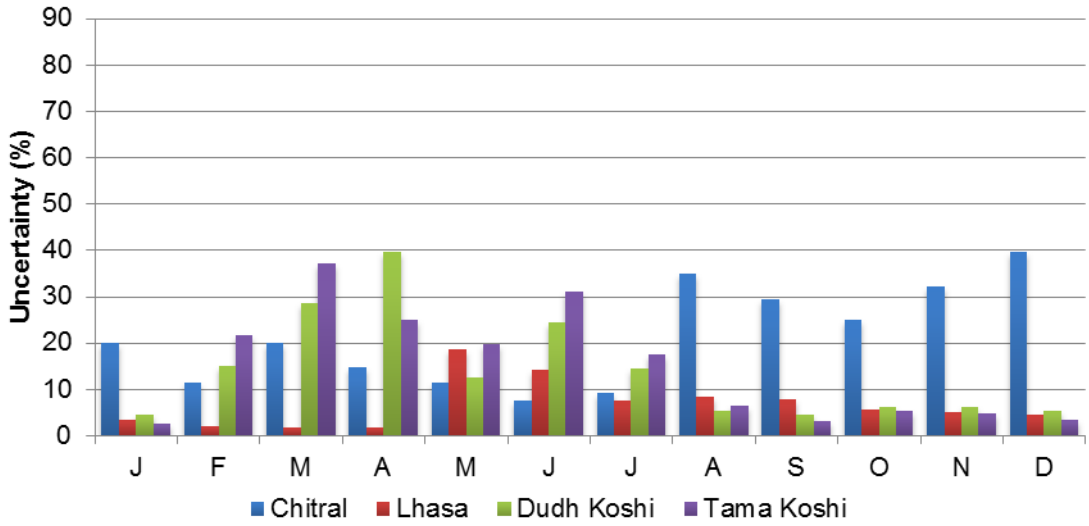

Figure 56: Uncertainty in rainfall-runoff RCP 4.5

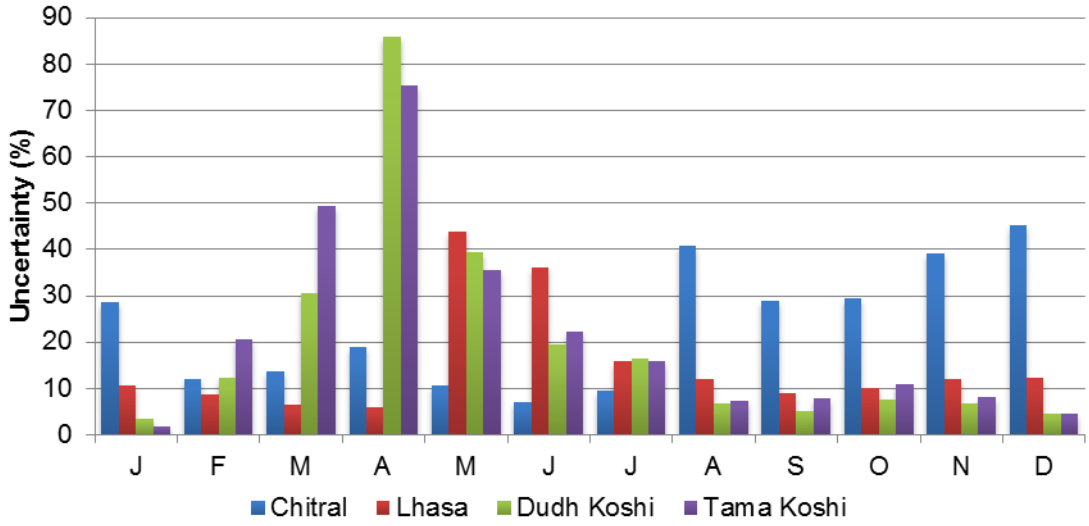

Figure 57: Uncertainty in rainfall-runoff RCP 8.5

10.2 Hydropower potential

To assess the hydropower potential in the pilot catchments, we use the Water Evaluation and Planning system (WEAP). WEAP is a well-known software tool that takes an integrated approach to water resources planning. WEAP is developed by the Stockholm Environment Institute's U.S. Center. WEAP was originally developed for simulating water balances, evaluating water management strategies including hydropower components in the Aral Sea region [*Raskin et al.*, 1992]. This makes WEAP a very suitable tool to conduct hydropower related assignments.

10.2.1 Hydropower in the study area

To provide basic knowledge on the role of hydropower in the study area, we list a number of key figures for hydropower in Nepal in 2011 [*NEA*, 2012].

- About 90% of all electricity in Nepal is generated by hydropower
- A total of 2122 GWh was generated by NEA hydropower facilities in Nepal with a total installed capacity of 469.29 MW. NEA is the state-owned hydropower company with the largest capacity in the country. Additionally there are private hydropower companies and numerous hydropower stations are under construction or planned to be constructed.
- To supply the total electricity demand, additional 746 GWh was imported from India.
- Future electricity demand is expected to increase rapidly (Figure 58).
- Most energy in Nepal is supplied by fuelwood (about 68%).

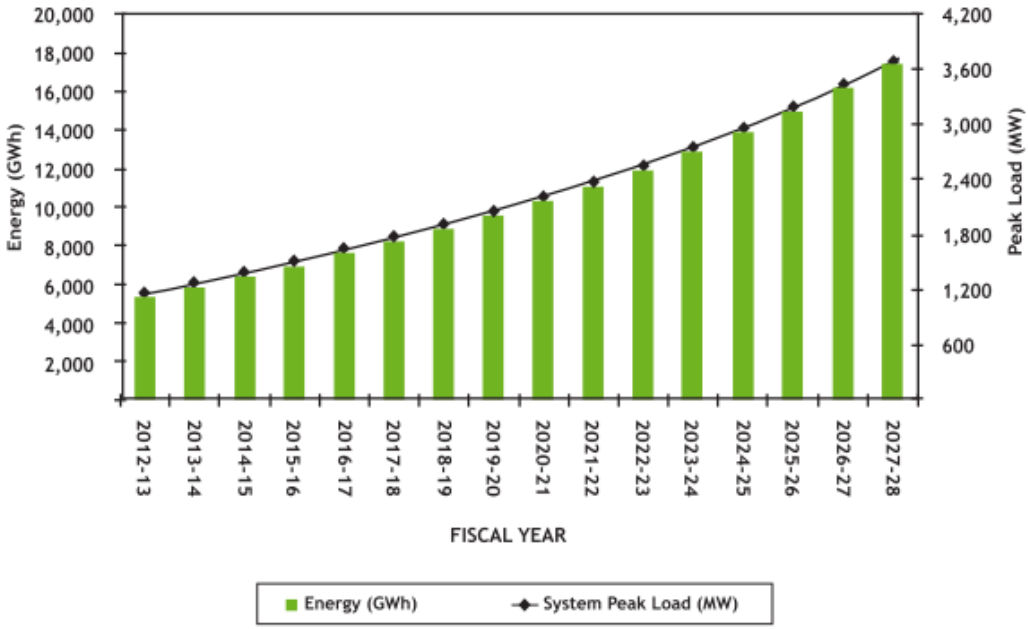

Figure 58: Expected increase in Nepalese energy demand and peak load [*NEA*, 2012]**.**

10.2.2 Model setup

In WEAP one hypothetical reservoir with hydropower facilities is simulated at the outlet of each pilot catchment. The flow at the catchment outlets as calculated in HI-SPHY for the reference period (1998-2007) is used in the reference scenario. For each of the RCP's and each of the GCMs a future scenario is calculated for 2041-2050, using the simulated flow at the catchments outlets as calculated in HI-SPHY. This means in total 2 RCPs x 4 GCMs = 8 scenarios are calculated and compared. To assess the hydropower potential, a number of assumptions are made for the hypothetical reservoirs:

- Reservoir storage capacity is assumed to be half the annual inflow during the reference period (1998-2007).
- Reservoir initial storage is assumed to be 80% of the total storage capacity.
- A volume-elevation curve typical for reservoirs in high mountain areas is assumed.
- Losses through evaporation and infiltration to groundwater are neglected.
- A top of buffer is assumed to be 50% of the total storage capacity. Below this level reservoir releases are constrained by a buffer coefficient which is assumed to be 50%.
- The hydropower generation is assumed to be not constrained by a maximum turbine flow.

- The hydrologic head for power generation is assumed to be 100 meter.
- A flow requirement downstream of the reservoir is incorporated to simulate downstream water demands.
- Hydropower electricity net revenue is assumed to be $ 0.023 per kWh, based on figures in the Nepal Electricity Authority Annual report for fiscal year 2012 [*NEA*, 2012]. The net revenue is assumed to be linearly related to the production.

For the reference period, the model is forced with the average simulated monthly flow of 1998-2007 from the HI-SPHY model. For future scenarios the model is forced with the average simulated monthly flow of 2041-2050.

10.2.3 Reference situation 1998-2007

Table 10 lists the assumed reservoir capacity, simulated inflow from the HI-SPHY model and the hydropower potential for each basin during the reference period.

Table 10: For each pilot catchment: assumed reservoir capacity, average inflow 1998-2007 from HI-SPHY model, potential hydropower 1998-2007.

Catchment	Assumed reservoir storage capacity (million m^3)	Average inflow 1998-2007 (m^3/s)	Potential hydropower 1998 – 2007 (GWh/yr)
Chitral	6099	390	2364
Lhasa	7221	460	2673
Dudh Koshi	2929	185	1064
Tama Koshi	2516	160	919

The Chitral and Lhasa catchments, with highest inflow, have the highest hydropower potential, when the same hydrologic head is assumed for each hypothetical reservoir. However, the hydrologic head is a very important parameter in assessing the hydropower potential and is very susceptible to dam height and reservoir morphology. Hydropower potential and potential revenues for the reference period are visualized in Figure 59. In the model, revenues are linearly related to the generated hydropower.

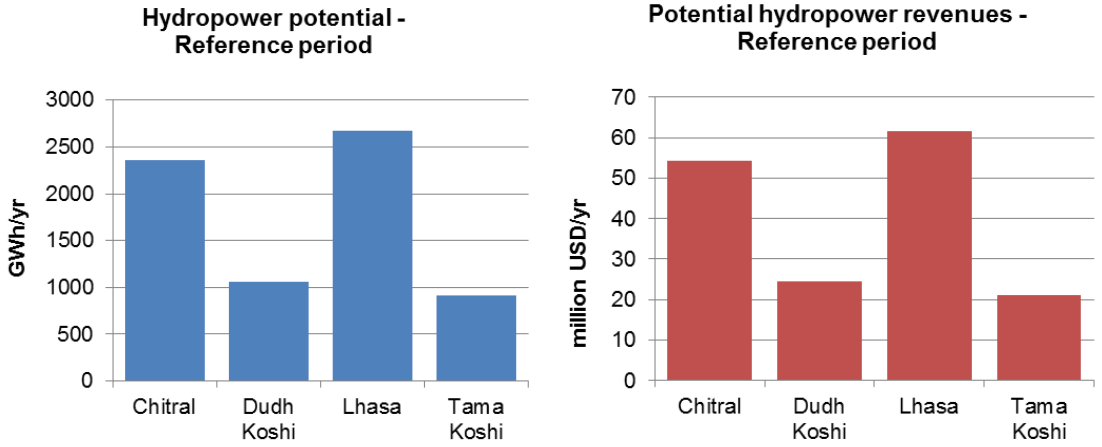

Figure 59: Hydropower potential and potential revenues for reference period (1998-2007)

Since the flows in the catchments have a high seasonal variablility due to the monsoonal climate and dependence on glacier melt and snow melt, the hydropower potential varies

strongly during the year and per catchment. Figure 60 shows the hydropower potential per month, per catchment. Note that the flow peak in the Lhasa catchment is later in the year (October) than the other catchments. For Chitral the flow peak lasts longest (May-November), whereas the flow peak in the Koshi basins is shorter (July-November).

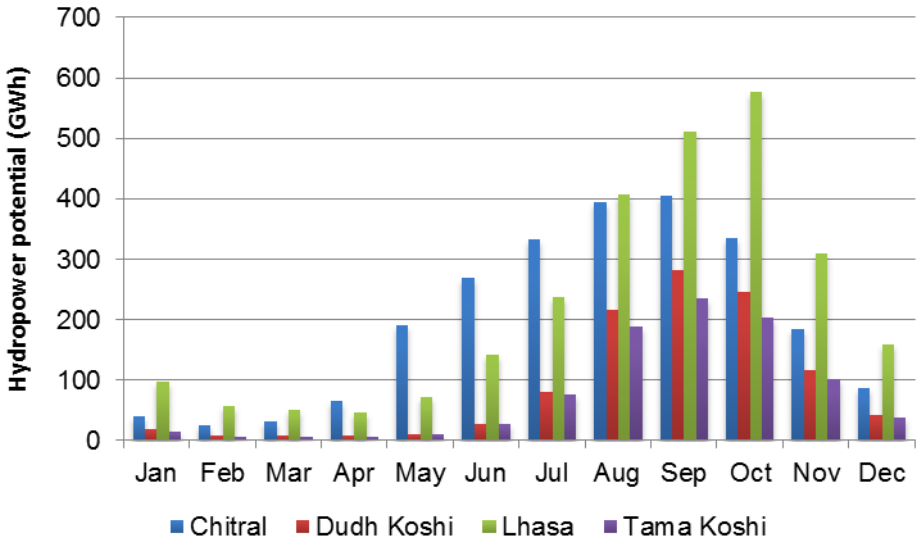

Figure 60: Hydropower potential per basin per month for reference period (1998-2007).

10.2.4 Future situation 2041-2050

The future hydropower potential is calculated with the changed flow, which is output from the HI-SPHY model forced with eight different GCMs (4 GCMs x 2 RCPs). The resulting hydropower potential for 2041-2050 is plotted in Figure 61 to Figure 64, with the reference situation for comparison. The implications of climate change for hydropower potential differ strongly between the RCPs, GCMs and catchments.

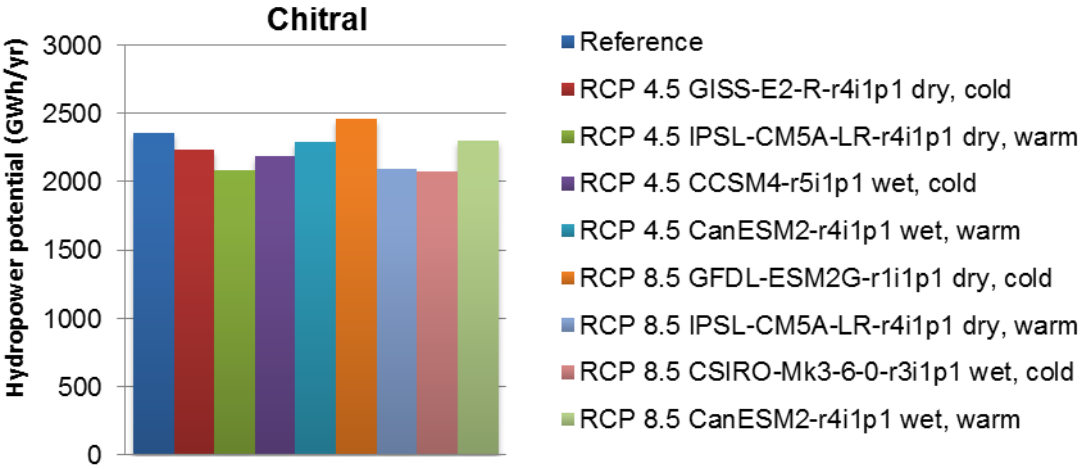

Figure 61: Hydropower potential for Chitral catchment for reference situation (1998-2007) and future according to 8 climate change scenarios (2041-2050).

For the Chitral catchment, hydropower potential increases or decreases slightly as an effect of changing stream flow in the future. This projection is applicable for both RCPs and all GCMs.

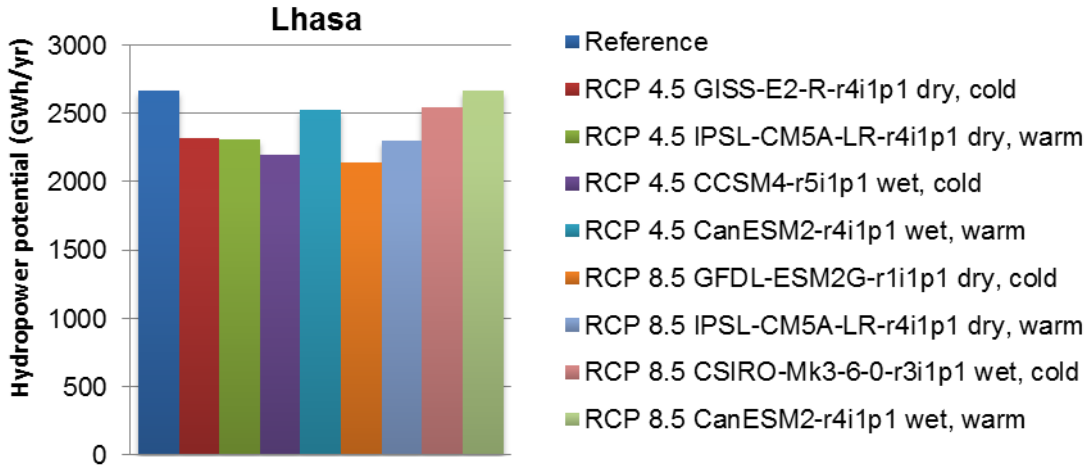

Figure 62: Hydropower potential for Lhasa catchment for reference situation (1998-2007) and future according to 8 climate change scenarios (2041-2050).

For Lhasa catchment, a decrease in hydropower potential is projected by all of the GCMs in both RCPs. Strongest decreases are projected by the dry, cold projection for RCP 8.5, whereas the decrease is minimal for the wet, warm projection in RCP 8.5.

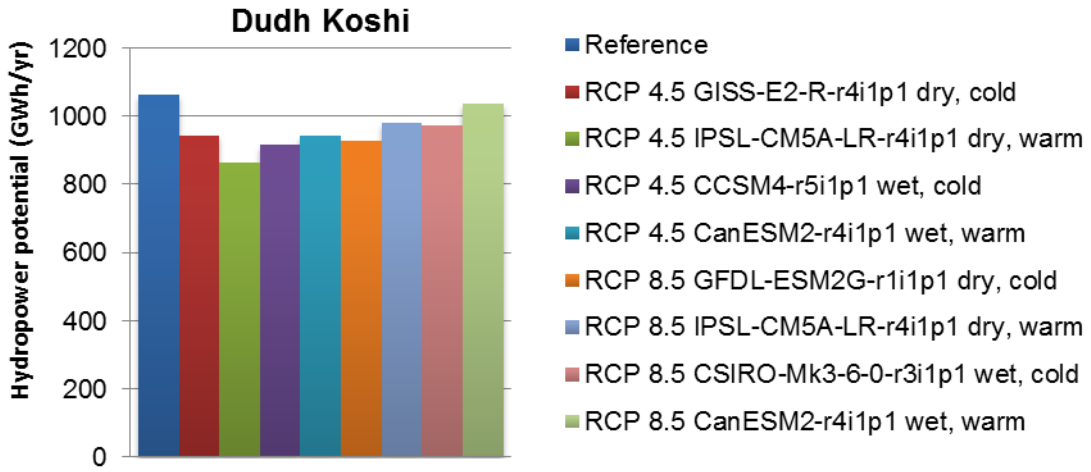

Figure 63: Hydropower potential for Dudh Koshi catchment for reference situation (1998-2007) and future according to 8 climate change scenarios (2041-2050).

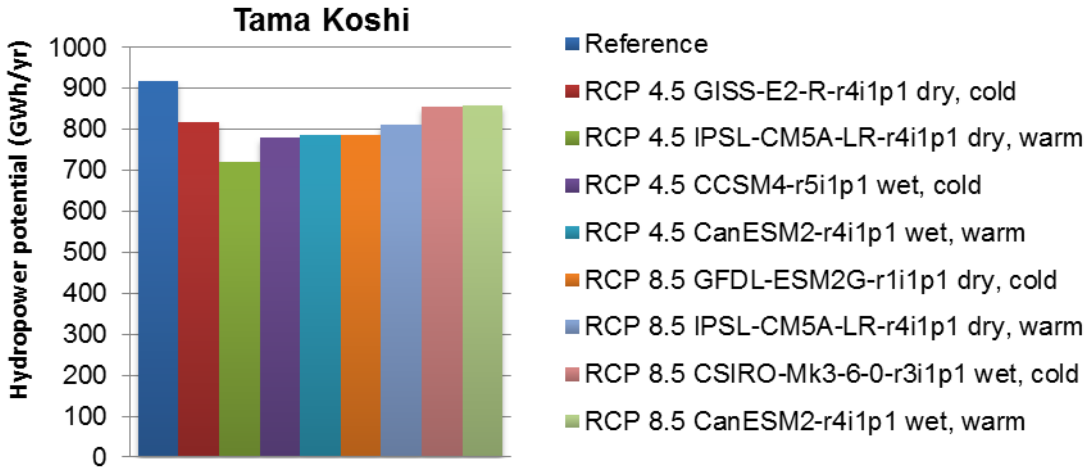

Figure 64: Hydropower potential for Tama Koshi catchment for reference situation (1998-2007) and future according to 8 climate change scenarios (2041-2050).

The projections for Dudh Koshi and Tama Koshi are similar. All scenarios project a decrease in hydropower potential with respect to the reference situation. The dry, warm projection in RCP 4.5 projects the strongest decrease in hydropower potential, while the smallest decrease is projected by the wet, warm projection in RCP 8.5.

10.2.5 Flow duration curves

For hydropower production, the distribution of flow throughout the year is of particular interest. Flow duration curves indicate the percentage of time a particular discharge is equaled or exceeded. Comparing flow duration curves for different periods in time provides information for changes in flow strength. Here we list the flow duration curves for the four pilot basins for the reference period and each projection in both RCPs (Figure 65 to Figure 68). Note that the flow duration curves have a logarithmic scale on the vertical axis.

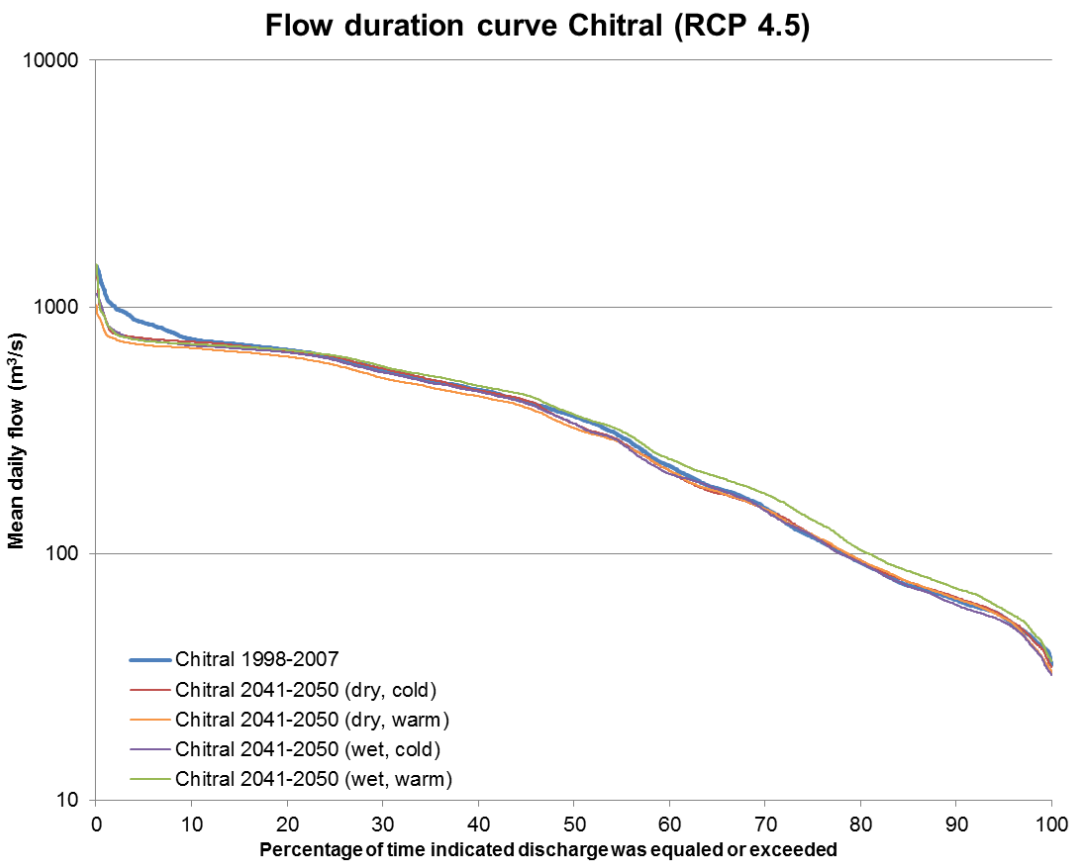

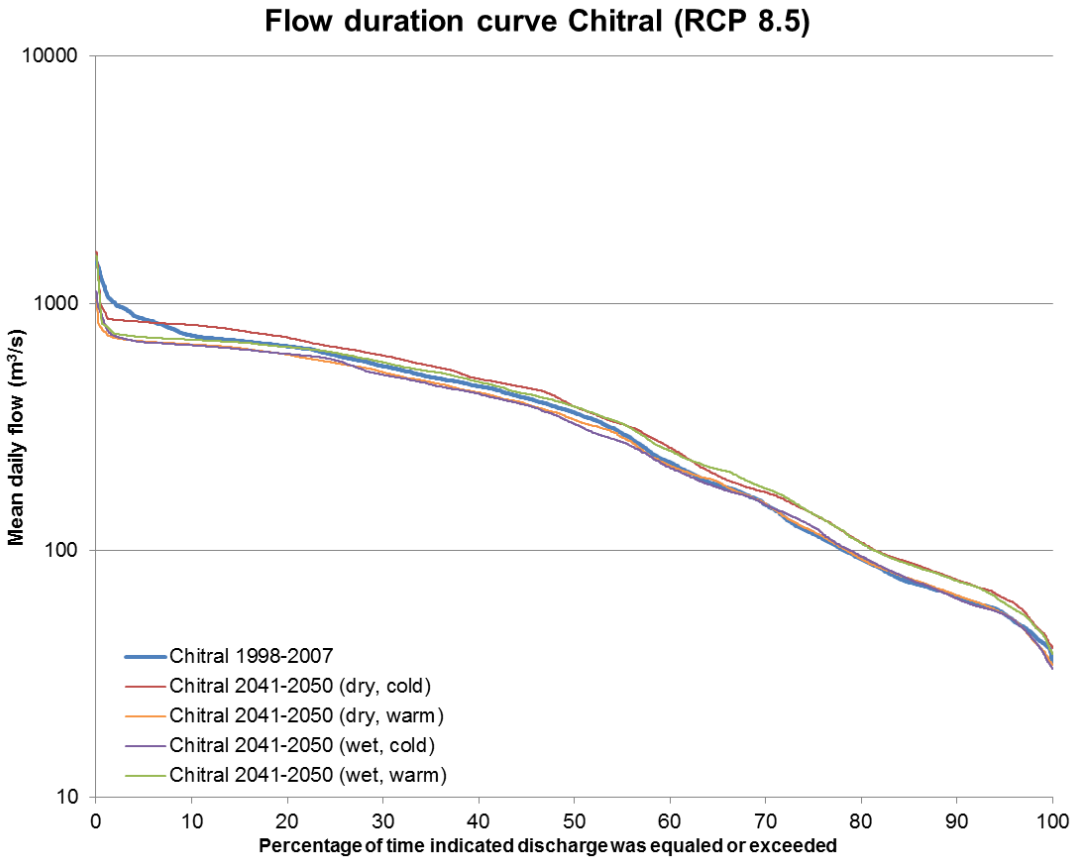

Figure 65: Flow duration curves for the Chitral basin for the reference period and 2041-2050 projections for RCP 4.5 (upper panel) and RCP 8.5 (lower panel).

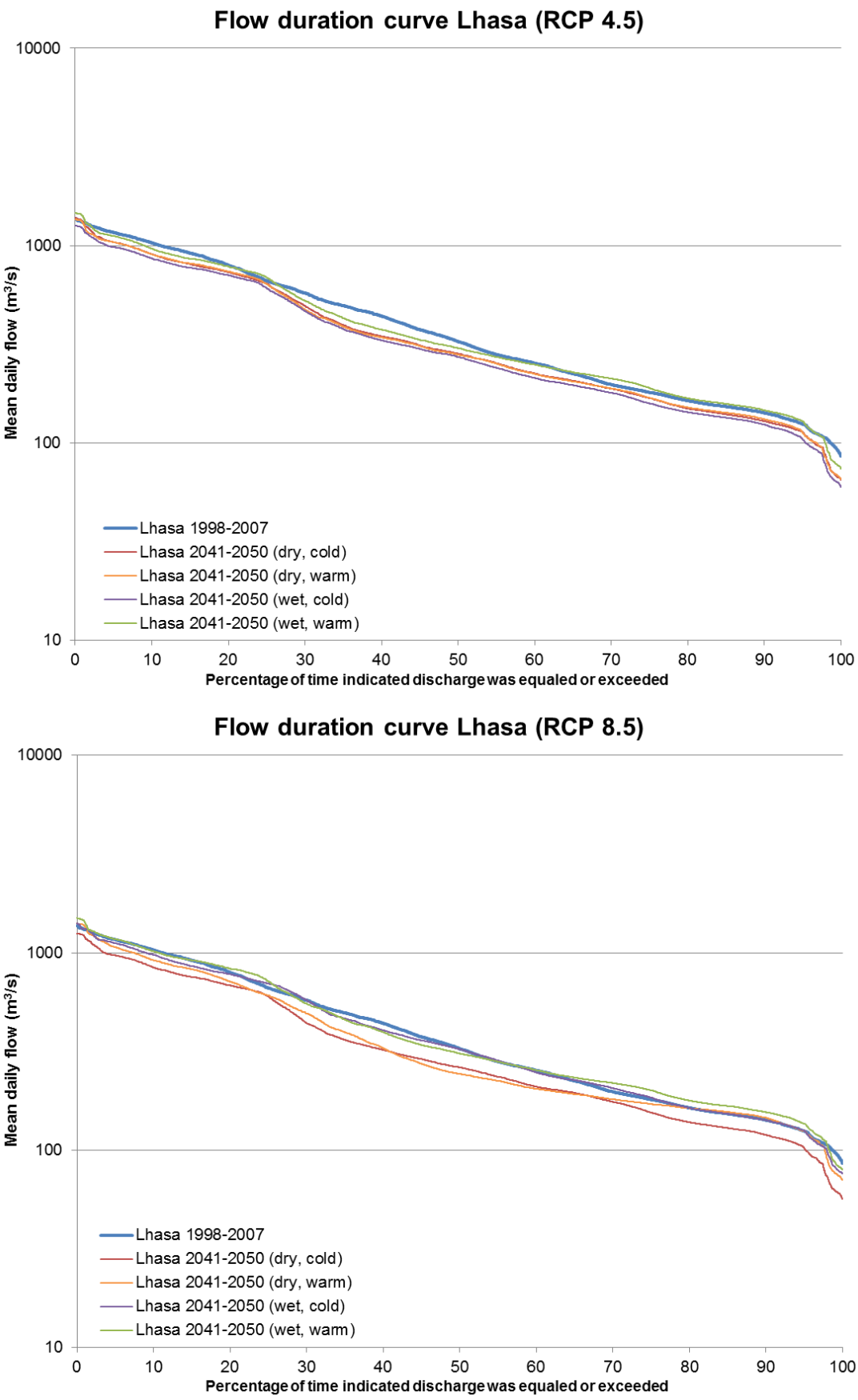

Figure 66: Flow duration curves for the Lhasa basin for the reference period and 2041-2050 projections for RCP 4.5 (upper panel) and RCP 8.5 (lower panel).

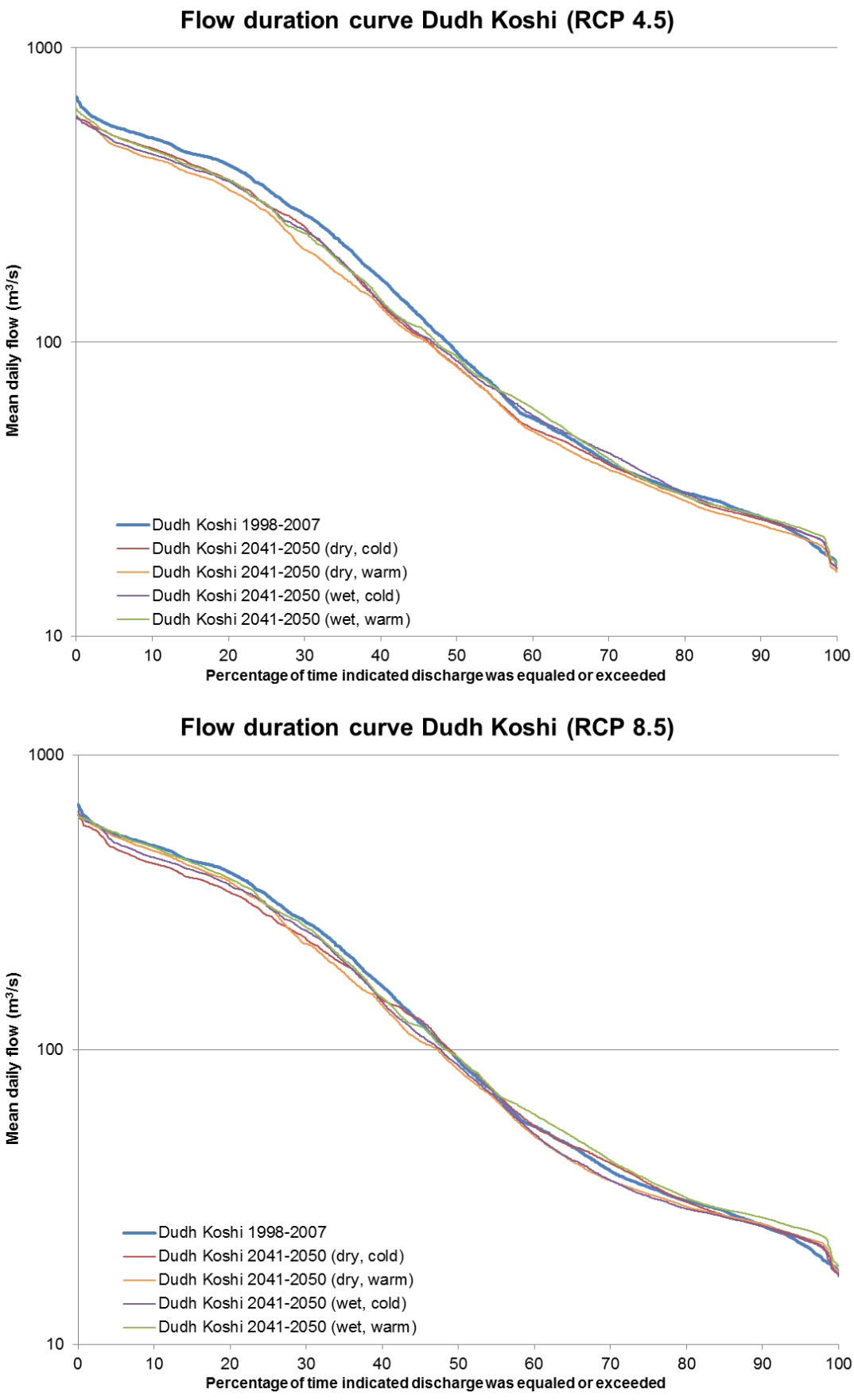

Figure 67: Flow duration curves for the Dudh Koshi basin for the reference period and 2041-2050 projections for RCP 4.5 (upper panel) and RCP 8.5 (lower panel).

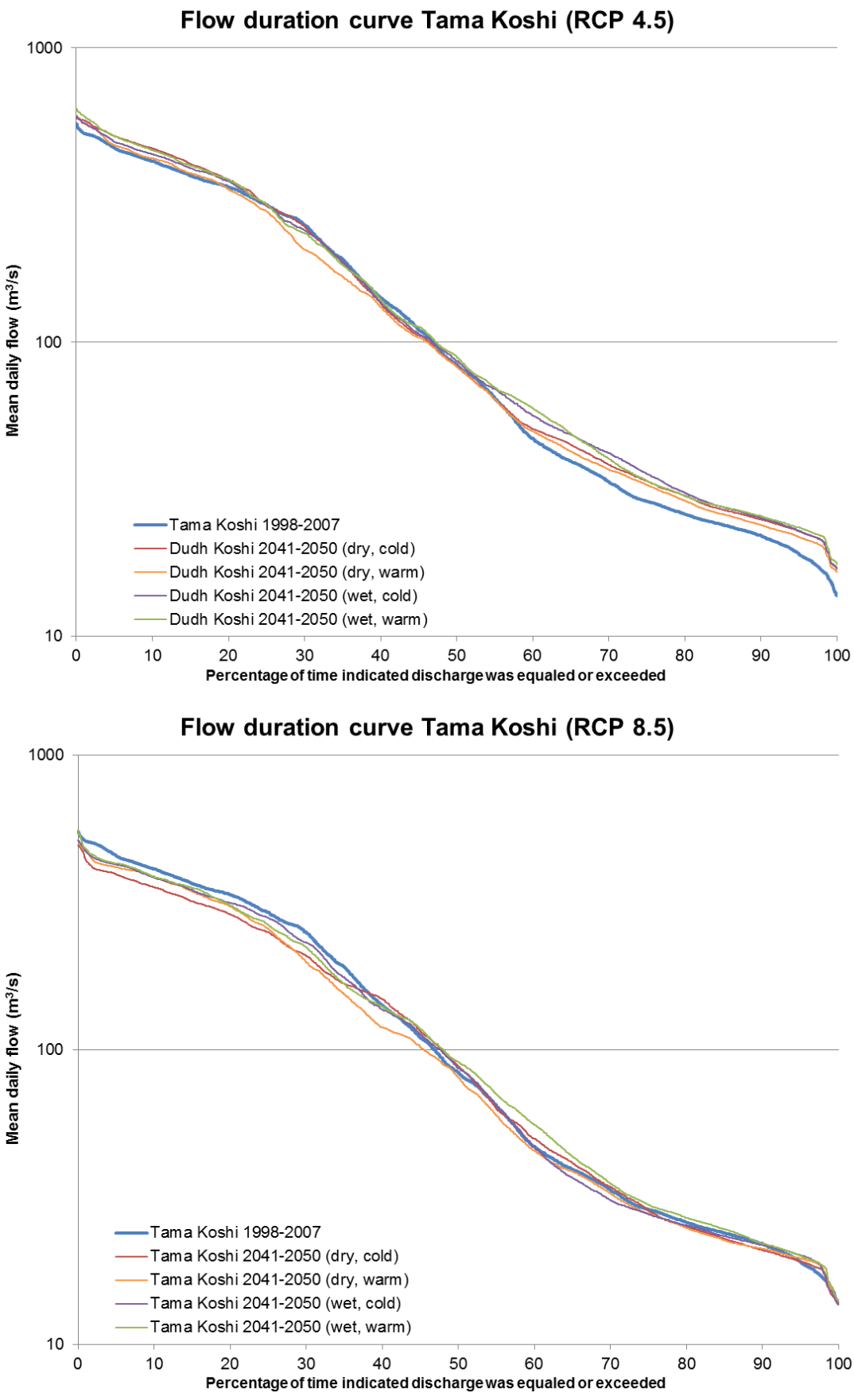

Figure 68: Flow duration curves for the Tama Koshi basin for the reference period and 2041-2050 projections for RCP 4.5 (upper panel) and RCP 8.5 (lower panel).

10.2.6 Limitations and recommendations

This analysis is a first order assessment of hydropower potential in the three pilot catchments. A more detailed analysis is recommended to assess the hydropower potential for each valley in the catchments. Future improvements could include:

- Assessment of hydropower potential per subcatchment
- Include multiple potential dam heights and storage volumes, or assessment of possible reservoir morphology and possible dam height
- Include flow projections until 2100
- Include detailed economic analysis

11 Conclusions

This report is part of ICIMOD's Himalayan Climate Change Adaptation Programme component 2: Water availability and demand scenarios.

The objectives of FutureWater's assignment discussed in this report are:

- Assess climate change scenarios and develop water availability scenarios corresponding to base and future climate scenarios at sub-basin and catchment scales in the Indus, Ganges, Brahmaputra, Salween and Mekong river basins;
- Improve understanding of the partitioning of runoff contribution from different natural sources (snow, glacier, rainfall and base flow);
- Detailed analysis of uncertainty of water availability scenarios and assessment of hydropower potential for four pilot catchments.

Based on local and public domain datasets a distributed cryospheric-hydrological model has been developed for the upstream basins of the five mentioned rivers. This is one of the first models that covers the entire upstream parts of these basins and includes all processes related to glacier and snow melt, rainfall-runoff and base flow.

The key findings regarding runoff composition and future runoff (per basin) are:

- In the upper Indus, stream flow is dominated by glacier melt (~41%) and snow melt (~22%). Rainfall-runoff has minor importance (~27%). Total runoff is likely to change by -5% to +12% by 2050. The share of melt water stays the same, and the changes in total runoff are directly related to changes in precipitation.
- In the upper Ganges, stream flow is dominated by rainfall-runoff (~66%), with ~20% of stream flow contributed by melt water. It is likely that total runoff increases by ~1-27% by 2050. The share of melt water is decreasing and the share of rainfall-runoff in total runoff is increasing.
- The stream flow in the upper Brahmaputra is dominated rainfall-runoff (~59%), and melt water contributes ~25% to total runoff. It is likely that total runoff increases by 2050 (0% to +13%). The share of melt water is decreasing while the share of rainfall-runoff increases.
- In the upper Salween, runoff is dominated by rainfall runoff (~42%), but snow melt is also important (~28%). Glacier melt contributes ~8% to total runoff. It is likely that total runoff changes by -3% to +19% by 2050. The share of glacier melt and snow melt is likely to decrease, while the share rainfall-runoff increases.
- The runoff in the upper Mekong is dominated by rainfall-runoff (44%). Snow melt contributes ~33% and glacier melt contributes ~1% to total runoff. It is likely that the total runoff increases ~2-20% by 2050. The share of melt water is decreasing while the share of rainfall-runoff increases.

A first order assessment of the hydropower potential in the Chitral, Lhasa, Dudh Koshi and Tama Koshi catchments leads to the following conclusions:

- The Chitral catchment has a hydropower potential of ~2350 GWh/yr in the current situation. A projected change to ~2100-2450 GWh/yr is projected for 2041-2050.

- The Lhasa catchment has ~2650 GWh/yr hydropower potential in the current situation. This is expected to stay the same or decrease to ~2650-2150 GWh/yr by 2041-2050.
- The Dudh Koshi and Tama Koshi catchments currently have a hydropower potential of ~1000 GWh/yr each. Future projections suggest that this might decrease by ~0-10% until 2050.

Recommendations for future work:

- Given the uncertainty in the used precipitation forcing for precipitation at high altitudes a further improvement of this forcing is highly recommended to lower the uncertainty in future runoff projections. This is especially valid for the upper Indus basin, where the uncertainty in precipitation estimates is largest.
- The hydropower potential assessment is a first order indication and should be extended since more detail should be considered (inclusion of subcatchments, multiple reservoir designs, detailed economic analysis).

12 References

Bajracharya, S. R., and A. B. Shrestha (2011), *The Status of Glaciers in the Hindu Kush-Himalayan Region*, Kathmandu.

Bolch, T. et al. (2012), The State and Fate of Himalayan Glaciers, *Science*, *336*, 310–314, doi:10.1126/science.1215828.

Cheema, M. J. M., and W. G. M. Bastiaanssen (2012), Local calibration of remotely sensed rainfall from the TRMM satellite for different periods and spatial scales in the Indus Basin, *International Journal of Remote Sensing*, *33*(8), 2603–2627, doi:10.1080/01431161.2011.617397.

Doherty, J. (2005), *PEST: Model Independent Parameter Estimation - Fifth Edition of User Manual*, Brisbane.

Droogers, P., and R. G. Allen (2002), Estimating reference evapotranspiration under inaccurate data conditions, *Irrigation and Drainage Systems*, *16*, 33–45.

Droogers, P., A. Van Loon, and W. W. Immerzeel (2008), Quantifying the impact of model inaccuracy in climate change impact assessment studies using an agro-hydrological model, *Hydrology and Earth System Sciences*, *12*, 669–678.

Duncan, J. M. a., and E. M. Biggs (2012), Assessing the accuracy and applied use of satellite-derived precipitation estimates over Nepal, *Applied Geography*, *34*, 626–638, doi:10.1016/j.apgeog.2012.04.001.

Hawkins, E., and R. Sutton (2009), The Potential to Narrow Uncertainty in Regional Climate Predictions, *Bulletin of the American Meteorological Society*, *90*(8), 1095–1107, doi:10.1175/2009BAMS2607.1.

Hawkins, E., and R. Sutton (2010), The potential to narrow uncertainty in projections of regional precipitation change, *Climate Dynamics*, *37*(1-2), 407–418, doi:10.1007/s00382-010-0810-6.

Hewitt, K. (2005), The Karakoram Anomaly ? Glacier Expansion and the “Elevation Effect,” Karakoram Himalaya, *Mountain Research and Development*, *25*(4), 332 – 340.

Hock, R. (2005), Glacier melt: a review of processes and their modelling, *Progress in Physical Geography*, *29*(3), 362–391, doi:10.1191/0309133305pp453ra.

Immerzeel, W. W., L. P. . Van Beek, and M. F. P. Bierkens (2010), Climate change will affect the Asian water towers., *Science*, *328*(5984), 1382–5, doi:10.1126/science.1183188.

Immerzeel, W. W., and A. F. Lutz (2012), *Regional knowledge sharing on climate change scenario downscaling. FutureWater technical report 116.*, Wageningen, The Netherlands.

Kääb, A., E. Berthier, C. Nuth, J. Gardelle, and Y. Arnaud (2012), Contrasting patterns of early twenty-first-century glacier mass change in the Himalayas., *Nature*, *488*(7412), 495–8, doi:10.1038/nature11324.

Karssenberg, D., P. Burrough, R. Sluiter, and K. de Jong (2001), The PCRASTER software and course materials for teaching numerical modelling in the environmental sciences, *Transactions in GIS*, *5*, 99–110, doi:10.1111/1467-9671.00070.

Lutz, A. F., W. W. Immerzeel, A. Gobiet, F. Pellicciotti, and M. F. P. Bierkens (2012), New climate change scenarios reveal uncertain future for central Asian glaciers, *Hydrology and Earth System Sciences Discussions*, *9*, 12691–12727.

Moss, R., M. Babiker, S. Brinkman, and E. Calvo (2008), *Towards new scenarios for analysis of emissions, climate change, impacts, and response strategies*, Noordwijkerhout, The Netherlands.

NEA (2012), *Nepal Electricity Authority Annual Report*, Kathmandu.

Palazzi, E., J. Von Hardenberg, and A. Provenzale (2013), Precipitation in the Hindu-Kush Karakoram Himalaya : Observations and future scenarios, *Journal of Geophysical Research: Atmospheres*, *118*, 85–100, doi:10.1029/2012JD018697.

Paul, F., C. Huggel, and A. Kääb (2004), Combining satellite multispectral image data and a digital elevation model for mapping debris-covered glaciers, *Remote Sensing of Environment*, *89*(4), 510–518, doi:10.1016/j.rse.2003.11.007.

Raskin, P., E. Hansen, Z. Zhu, and M. Iwra (1992), Simulation of Water Supply and Demand in the Aral Sea Region, *Water International*, *17*, 55–67.

Sheffield, J., G. Goteti, and E. F. Wood (2006), Development of a 50-Year High-Resolution Global Dataset of Meteorological Forcings for Land Surface Modeling, *Journal of Climate*, *19*(13), 3088–3111, doi:10.1175/JCLI3790.1.

Winiger, M., M. Gumpert, and H. Yamout (2005), Karakorum-Hindukush-western Himalaya: assessing high-altitude water resources, *Hydrological Processes*, *19*(12), 2329–2338, doi:10.1002/hyp.5887.

Yatagai, A., N. Yasutomi, A. Hamada, A. Kitoh, K. Kamiguchi, and O. Arakawa (2012), APHRODITE: Constructing a Long-term Daily Gridded Precipitation Dataset for Asia Based on a Dense Network of Rain Gauges, *Geophysical Research Abstracts*, *14*.